Investigating the Effect of Applied Shear Stress on Cohesive Riverbank Erosion

by

Navid Kimiaghalam

A thesis submitted to the Faculty of Graduate Studies of
the University of Manitoba
in partial fulfillment of the requirements for the degree of

Doctor of Philosophy

Department of Civil Engineering
University of Manitoba
Winnipeg, Manitoba, Canada

Abstract

Morphological changes along several channels have raised concerns in the Province of Manitoba. This thesis presents a comprehensive study of fluvial morphological processes in open channels. Due to the recent concerns in the Province of Manitoba, the study mainly focused on the Red River in the city of Winnipeg, and two diversion channels in northern Manitoba. Morphodynamic conditions of these channels have become more complicated due to the cohesive nature of the channels bed and bank material and significant effects of subaerial processes. Several field measurement techniques, experimental setups, and numerical models were used to gain a better understanding of these complicated processes within the study reaches. Field measurements include soil sampling, water sampling, hydrometric surveys using an ADCP; the experimental setup includes several standard soil properties tests as well as an erosion measurement test; numerical modelling includes hydrodynamic and thermal modelling to quantify applied shear stress and seasonal freeze-thaw processes. Moreover, the effect of deposition processes on the final geomorphology of the study areas is discussed.

Acknowledgements

First I want to thank my advisor Dr. Shawn Clark. It has been an honor to be his first PhD student. I appreciate all his contributions of time, ideas, and funding to make my PhD experience productive and exciting.

Thank you also to the employees of the University of Manitoba (Mr. Alexander Wall and Kerry Lynch) and all our summer students involved in this project.

I greatly acknowledge the financial contributions from Manitoba Hydro and the Natural Science and Engineering Research Council of Canada which made this research project possible. Also, I would like to appreciate DHI Group for providing educational license for MIKE 21 software.

Lastly, I would like to thank my parents for all their love and support and for my loving, supportive wife Golnaz. Thank you all.

Table of Contents

List of Tables

List of Figures

Nomenclature

Symbol	Units	Description
τ_c	[Pa]	Critical shear stress
τ_s	[kPa]	Soil shear strength
PI	[-]	Plasticity index
C_p	[-]	Clay percentage
ρ_{dry}	[kg/m^3]	Dry density
ρ_s	[kg/m^3]	Sediment density
ρ_b	[kg/m^3]	Bulk density
E	[mm/h]	Erosion rate
k_d	[mm/(h.Pa)]	Material dependent coefficient
$SC\%$	[-]	Silt and clay fraction

C	[kPa]	Cohesion
$\emptyset_{cr}'$	[^{o}]	Friction angle
SAR	[-]	Sodium adsorption ratio
CEC	[meq/100g]	Cation exchange capacity
OG	[-]	Organic content
EC	[dS/cm]	Electrical conductivity
τ_a	[Pa]	Applied shear stress
ρ	[kg/m3]	Density of water
V	[m/s]	Streamwise mean velocity
ε/D	[-]	Relative roughness
E_h	[mm]	Erosion height
h_{ps}	[mm]	Total movement of piston
h_{ew}	[mm]	Equivalent water height between the sample surface and flume bottom
h_{rs}	[mm]	Equivalent height of the remaining sample
V_{er}	[mm^3]	Total volume of eroded material
e	[-]	Soil void ratio
V_s	[mm^3]	Soil particles volume

A_{ts}	[mm^2]	Testing tube surface area
W	[-]	Natural water content
VS	[lb/ft^2]	Vane shear value
D%	[-]	Percentage of maximum proctor density
LL	[-]	Liquid limit
Re	[-]	Reynolds number
D	[m]	Hydraulic diameter
μ	[Ns/m^2]	Dynamic viscosity
k_x	[W/(m.K)]	Thermal conductivity in the x-direction
k_y	[W/(m.K)]	Thermal conductivity in the y-direction
Q_T	[W/m^2]	Applied thermal boundary flux
T	[°C]	Soil temperature
λ	[j/(hg.K)]	Heat capacity
t	[s]	time
k_{uf}	[W/(m.K)]	Unfrozen thermal conductivity
k_f	[W/(m.K)]	Frozen thermal conductivity
θ	[m3/m3]	In-situ volumetric water content
k_f	[W/(m.K)]	Frozen thermal conductivity

c_{vf}	[MJ/(m^3°C)]	Frozen volumetric heat capacity
c_{vu}	[MJ/(m^3°C)]	Unfrozen volumetric heat capacity
T_s	[°C]	Temperature at the soil surface
T_a	[°C]	Air temperature
γ	[-]	Psychrometric constant
Q^*	[mm/day]	Net radiant energy available at the surface
$f(u)$	[-]	Wind function
$\tau_{a,c}$	[Pa]	Current applied shear stress
f_c	[-]	Current friction factor
h	[m]	Water depth
k_s	[m]	Bed roughness
n	[-]	Manning number
Q	[m^3/s]	Discharge
w_s	[m/s]	Fall velocity
w'	[m/s]	Vertical velocity fluctuation
C	[mg/L]	Average suspended sediment concentration
c_i	[m^3/m^3]	Depth-averaged volumetric sediment concentration
u	[m/s]	Streamwise depth-averaged velocity

v	[m/s]	Spanwise depth-averaged velocity
D_x	[m^2/s]	Streamwise dispersion coefficients
D_y	[m^2/s]	Spanwise dispersion coefficients
S	[m/s]	Sink and source term
A	[m^2]	Cross sectional area
u_*	[m/s]	Frictional velocity
S_f	[-]	Slope of the energy grade line
g	[m^2/s]	Gravitational acceleration
R	[m]	Hydraulic radius
H_{m0}	[m]	Significant wave height
MWD	[^{o}]	Mean wave direction
T_m	[s]	Mean wave period
DSD	[^{o}]	Directional standard deviation
$\tau_{a,max}$	[Pa]	Total maximum applied shear stress
$\tau_{w,c}$	[Pa]	Wave applied shear stress
$a', m, and\ l$	[-]	Consatants
f_w	[-]	Wave friction factor
U_b	[m/s]	Horizontal mean wave orbital velocity at the bed

Declaration of academic achievement

The outline of this thesis follows "sandwich format" whose guidelines are appointed by the Faculty of Graduate Studies, University of Manitoba. It merges four individual papers prepared for publication in peer-reviewed journals. Chapter 1 contains an introduction about the problem statement and the thesis contributions; Chapters 2 to 5 are manuscripts containing an abstract, introduction, methods, results and discussion; Chapter 6 provides the conclusions of the work and recommendations for future research direction.

Chapters 2 to 4 have been published as three journal papers and Chapter 5 has been prepared as a journal article for submission. The contributions of N. Kimiaghalam in all the papers are listed as following: developing the research idea, developing the numerical models, implementing the field works and experiments, data analysis, drawing the figures, writing all the manuscripts; submitting the manuscripts and responding to reviewer's comments. My co-authors contributed in developing the research idea, analyzing data, and editing the manuscripts for publication.

Copyright notices and Journal Papers Information

With kind permission from Elsevier:

Kimiaghalam, N., Goharrokhi, M., Clark, S. and Ahmari, H., 2015. *A comprehensive fluvial geomorphology study of riverbank erosion on the Red River in Winnipeg, Manitoba, Canada*. Journal of Hydrology, 529(3): 1488-1498. Doi: 10.1016/j.jhydrol.2015.08.033.

With kind permission from International Research and Training Centre on Erosion and Sedimentation/ the World Association for Sedimentation and Erosion Research and Elsevier:

Kimiaghalam, N., Clark, S. and Ahmari, H., 2016. *An experimental study on the effects of physical, mechanical, and electrochemical properties of natural cohesive soils on critical shear stress and erosion rate*. International Journal of Sediment Research, 31(1):1-15. Doi: 10.1016/j.ijsrc.2015.01.001.

With kind permission from NRC Research Press:

Kimiaghalam, N., Goharrokhi, and M., Clark, S., 2016. *Estimating cohesive sediment erosion and deposition rates in wide rivers*. Canadian Journal of Civil Engineering, 43(2): 164-172. Doi: 10.1139/cjce-2015-0361.

Canadian Water Resources Association and Tylor and Francis:

Kimiaghalam, N., Clark, S., Under Review. *Morphodynamics of diversion channels in northern Manitoba, Canada*. Canadian Water Resources Journal, MS ID: TCWR-2016-0018.

CHAPTER 1: INTRODUCTION

1.1 *Definition and Importance*

Riverbank erosion is the dynamic removal of soil from riverbanks. This process has physical, ecological, and socio-economic effects on fluvial environments. Riverbank erosion has two important consequences: (1) land loss during fluvial or slope failures that can cause economic or safety issues; and (2) impact on downstream water quality, such as increasing turbidity and sediment concentration which may be harmful for aquatic environments.

Many riverbank failures in Canada have occurred during flooding events, and governments have budgeted considerable money for erosion protection projects. The city of Calgary budgeted $12 million in 2013 for erosion protection and they estimated that the budget will be expanded in 2014 after the flood in 2013 (Dormer, 2013). In Winnipeg, Manitoba riverbank erosion has accelerated since the 1990s, particularly on the Red River due to a number of spring and summer floods and this has caused an increase of property-tax bills of up to $8,000 annually for riverbank property owners

(Jansen, 2012). Thus, protecting and restoring the river morphology requires a thorough understanding of erosion processes and the factors that affect this process.

The most important and the first step for starting erosion studies is to understand the nature of the riverbank material. Generally, two different kinds of soil exist: cohesive and non-cohesive. The term cohesion is related to the electrochemical forces acting on the particle surface. Therefore, the degree of cohesion depends on the ratio of particle surface area to particle weight. Studies show that 10% clay is enough to affect the soil behaviour (Debnath & Chaudhuri, 2010). Thus, based on the typical riverbank composition observations in Manitoba, research will be focused on studying erosion processes of cohesive soil. The field of cohesive soil erosion is still not fully understood, in large part due to the many soil parameters that affect cohesive soils. Unlike non-cohesive sediment, the behaviour of cohesive soils also depends on the electrochemical, mineral soil properties as well as the chemistry of the eroding fluid.

1.2 *Causes of Riverbank Failures*

Riverbank failures occur through three scenarios: 1) fluvial or hydraulic erosion due to the applied shear stress induced by flow or waves; 2) geotechnical instabilities due to the variation of effective shear stress and pore water pressure thorough the soil structure; 3) a combination of fluvial and geotechnical failure, which is especially common in composite banks.

1.2.1 *Fluvial Erosion Process*

Depending on the water velocity in rivers and the riverbank roughness, certain shear stresses are applied to the surface of the riverbanks. Waves can increase the total applied

shear stresses. Based on the riverbank properties and eroding water chemistry, riverbank soil will start to erode at a certain applied shear stress. This threshold of movement is called critical shear stress and with increasing the shear stress, the erosion rate increases. Many parameters may affect the critical shear stress and erosion rate of different riverbanks. The most important parameters are:

1) Physical and mechanical soil properties: Particle grain size distribution, plasticity, water content, bulk or dry density, friction angle, and cohesion.

2) Mineral and electrochemical properties of soil: Cation exchange capacity, electric conductivity, sodium adsorption ratio (salinity), and organic content.

3) Environment changes: Weathering process, freezing and thawing in cold regions like Canada.

4) Eroding fluid: Chemistry and solid particles in water, in particular water pH, sediment concentration, and water temperature.

1.2.2 *Geotechnical Failure Process*

The variation of water level causes changes in pore water pressure over time. This change in pore water pressure mainly depends on how fast the water level goes down, as well as the soil permeability and structure. With dissipating pore water pressure, effective stress increases and on the other hand hydrostatic resistance forces due to water level decreases, therefore the probability of failure increases.

1.2.3 *Composite Failure*

The most common cause of riverbank failure is a combination of geotechnical failure and fluvial erosion processes. This type of slope failure is common in composite riverbanks

with non-cohesive material at the bottom layers and cohesive soil at the top layers, which often results in a cantilever failure. Generally non-cohesive banks are more susceptible to fluvial erosion; therefore with higher shear stress at the bottom part, the toe of the bank starts to erode but no erosion happens in the upper cohesive part of the bank. As time passes a failure occurs due to the weight of the top cohesive layers.

1.3 *Research Objectives*

To begin a study about soil erosion, it is important to first determine whether the soil is cohesive or non-cohesive. Non-cohesive soils contain silt, sand and gravel and the main resistance force against erosion and movement is the weight of the particles. The presence of 10% clay is enough to cause the soil to become cohesive because clay particles are very fine (less than 0.002 mm) and they have electric charges that cause inter-particle bonds to become the main resisting force against erosion. Manitoba riverbanks mostly contain fine-grained soils that include high amounts of clay, and therefore normally they exhibit cohesive behaviour. The mineral content, electrochemical properties of soil and also the chemistry of the eroding fluid will become significant on the inter-particle bonds between clay particles.

Four main objectives are considered for this research to understand the behaviour of cohesive soil under different flow conditions.

1.3.1 *Critical Shear Stress and Erosion Rate*

The first and most important step in this research is to find a relationship or correlation to estimate the critical shear stress of soils relevant to this project. The critical shear stress is the minimum amount of applied shear stress exerted by the water to the riverbank that

causes the soil to begin to erode. With increasing shear stress, erosion rate increases. Both critical shear stress and erosion rate depend on soil properties and the eroding fluid. The following parameters represent the main characteristics of cohesive soils:

Physical properties:

a. Grain size distribution: Is the measure of sand, silt and clay content in a soil structure and also the size of the soil particles.
b. Plasticity index (PI): Is a measure of the plasticity of soil and is defined as the difference between the liquid limit (LL) and plastic limit (PL). These parameters are the Atterberg limits and they are basic measurements of the critical water contents of a fine-grain soil.

Mechanical properties:

c. Friction angle (∅): the primary mechanical property of a soil sample is the friction angle which is a measure of the shear strength of soils due to friction.
d. Cohesion (C): this soil property only exists for cohesive soils and is the soil shear strength in the absence of shear stress due to the electrostatic attraction between clay particles.
e. Dry or bulk density: is an extrinsic soil property which varies over depth and changing stress conditions.

Electro-chemical properties:

f. Cation exchange capacity (CEC): is defined as the degree to which a soil can adsorb and exchange cations. As discussed, cohesive soil behaviour is governed mainly by the inter-particle bonds and electrostatic attraction has a significant effect on inter-

particle bonds between clay particles (Partheniades, 2009). Therefore, CEC represents the electric activity of a soil sample. In general, higher clay and organic matters cause higher CEC (Brown & Lemon, 2014).

g. Electric conductivity (EC): Soil electrical conductivity is an indirect measurement that correlates very well with several physical and chemical soil properties such as SAR and CEC (Rashidi & Seilsepour, 2011). Electrical conductivity is the ability of a material to conduct (transmit) an electrical current.

h. Sodium Adsorption Ratio (SAR): is one of the important parameters in cohesive soils and basically represents soil salinity and also the ratio of dissolved sodium to amounts of magnesium and calcium in the soil structure which has significant effects on inter-particle bonds.

i. Organic content (OG): is the weight percentage of plant and animal matter in the soil structure.

The first objective of this research is to determine the effects of each property on soil response to fluvial erosion. Answering this question will assist with predicting the quantity and timing of fluvial erosion.

1.3.2 *Effect of Freezing and Thawing on Erosion of Cohesive Soil*

Since Manitoba is one of the coldest places in the world, investigating the effect of cold weather on soil behaviour is crucial for this research. In particular, fluvial erosion processes occur on the surface of the riverbank which is significantly impacted by seasonal freeze and thaw processes. Therefore the second objective is to quantify the effect of different freezing and thawing processes on the erodibilty of the riverbank which is necessary for providing a good estimation of the riverbank morphology in

Manitoba.

1.3.3 *Effect of Wave and Current on Cohesive Soil Erosion*

Usually the main eroding agent in open channels is the applied shear stress created by the streamwise flow; however depending on the river location and wind conditions, wave-induced erosion may become significant as well. Additionally external sources of waves such as ships or boat movements may be significant in some channels. The wave-current induced erosion is a complicated phenomenon which is necessary to study especially for those channels that connect huge lakes together. In such channels with windy conditions waves coming from lakes might significantly increase the total applied shear stresses and consequently increase the erosion rate even in low flow seasons.

1.3.4 *Numerical Modelling of Dynamic Fluvial Erosion*

After finding a good estimation of the critical shear stress, erosion rate and effects of different parameters on erosion rate, the most important aim is to develop a comprehensive model to provide a better means of estimating fluvial erosion. This model should be able to model dynamic erosion processes over time.

Note that the soil behaviour is very complicated and varies from location to location and there is no absolute answer in this field. The main goal of this research is to study erosion on Manitoba riverbanks to at least develop a good estimation of riverbank morphology thorough years and provide a good estimation for design and protection purposes. In addition this research will be helpful to better understand erosion processes based on using a wide range of soil and flow properties.

1.4 *Thesis outline*

This is a manuscript-based thesis that is based on three previously published papers in peer reviewed journals (Chapters 2-4) and one submitted paper (Chapter 5) by the author and collaborators. Chapter 2 presents an experimental study to quantify the effects of several physical, mechanical, and electrochemical properties of natural cohesive soils from different study areas within Manitoba on erodibility parameters. This is the primary step for a geomorphological study to understand the study area's material behaviour and the first objective of this thesis. Chapter 3 presents a comprehensive methodology toward the thesis objectives 2, 3, and 4 to study fluvial riverbank erosion through the Red River in Winnipeg. This chapter includes novel contributions in the field of fluvial geomorphology and river morhodynamics to answer important questions regarding the effect of seasonal freeze-thaw on the erodibility, including the effect of freeze-thaw in the analysis, and also present a comprehensive methodology for such studies. Chapter 4 introduces a novel methodology to estimate both erosion and dispersion rates using aDcp measurements and numerical modelling. The methodology is more reliable than the available methods to measure or predicate only erosion rate. Moreover, the proposed methodology applies to the Red River in Winnipeg. Chapter 5 presents a study on morphodynamics of diversion channels, focusing on two important diversion channels in northern Manitoba. This chapter highlights the role of wave action on the total shear stress within such channels. Also, the study tries to investigate the contribution of subaerial processes and different channel bank loss mechanisms on the total bed and bank loss within the study areas.

1.5 *References*

Brown, K., and Lemon, J. 2014. Soil quality. Retrieved from http://www.soilquality.org.au/factsheets/cation-exchange-capacity.

Debnath, K. and Chaudhuri, S. 2010. Cohesive sediment threshold: a review. ISH Journal of Hydraulic Engineering, **16(1)**: 36-56.

Dormer, D. (2013). City of Calgary ooficials dealing with 26 erosion sites damaged in June's floods. Calgary: Calgary Sun.

Jansen, W. (2012). Public dollars justified to halt riverbank erosion. Winnipeg: Winnipeg Free Press.

Rashidi, M., & Seilsepour, M. (2011). Prediction of soil sodium adsorption ratio based on soil electrical conductivity. Middle-East journal of scientific research, **8(2)**: 379-383.

CHAPTER 2: EXPERIMENTAL STUDY ON THE EFFECTS OF COHESIVE SOIL PROPERTIES ON THE ERODIBILITY PARAMETERS

A version of this chapter has been published in International Journal of Sediment Research: **Kimiaghalam, N.**, Clark, S. P., and Ahmari, H., 2016. *An experimental study on the effects of physical, mechanical, and electrochemical properties of natural cohesive soils on critical shear stress and erosion rate*. International Journal of Sediment Research, 31 (1): 1-15.

The field of cohesive sediment erosion is still not fully understood, in large part due to the many soil parameters that affect cohesive sediment erodibility. In this study several undisturbed natural soil samples were taken from different riverbanks in Manitoba, Canada. The samples mainly contained clay and silt with 24% to 94% clay content, thus the study covered a wide range of cohesive soil. For each sample 13 different physical, mechanical, and electrochemical properties were measured. Critical shear stress of erosion and erosion rate were quantified using an Erosion Measurement Device (EMD). Stepwise regression was used to find the variables most significantly correlated to critical shear stress and erosion rate, which led to the development of a new empirical equation to estimate the critical shear stress of cohesive soils. It was found that the critical shear stress was highly correlated with cohesion, while both cohesion and sodium adsorption ratio (SAR) had significant influence on the erosion rate.

2.1 *Introduction*

Due to the complex behavior of cohesive soil, the process of cohesive soil erosion is not currently fully understood. Cohesive soil behavior is influenced by the inter-particle bonds that are highly dependent on the interaction of physical, electrochemical, mechanical, and biological factors. Delft Hydraulics used 28 different soil and pore-water properties to characterized cohesive sediments (Huang et al., 2006). This list did not include biological factors; which some researchers such as Paterson (1994) have shown may be important. Table 2-1 shows a list of many factors that may influence the behavior of cohesive soil and sediment. Many researchers have tried to find a relationship between different physical, mechanical, and electrochemical properties of cohesive sediments and critical shear stress; however, there are only a few studies that have considered the interaction of these variables (Knapen et al. 2007, YoungHui et al. 2008, Debnath et al. 2010). Dunn (1959) found a relationship between critical shear stress and sediment shear strength (τ_s) and plasticity index (PI) :

$$\tau_c = 0.01(\tau_s + 180)\tan(30 + 1.73\ PI) \qquad \textbf{Equation 2-1}$$

Smerdon and Beasley (1961) obtained relationships between critical shear stress and plasticity index (PI) and also clay percentage (C_p):

$$\tau_c = 0.163PI^{0.84} \qquad \tau_c = 0.493 * 10^{0.0182\ C_P} \qquad \textbf{Equation 2-2}$$

Carlson and Enger (1962) reported several correlations between different physical and mechanical soil properties and critical shear stress. They used linear correlations to find a relationship for estimating cohesive soil critical shear stress. Equation 2-3 shows one of their relationships for estimating critical shear stress. However, many measurements are

required to estimate critical shear stress based on their results and also, electrochemical soil properties are not considered:

$$\tau_c = -0.03414 + 0.00001PI + 0.00031D + 0.00029k'_{\emptyset}\sigma_{\emptyset}M_{\emptyset} + 0.00325VS + 0.00004\ D\% + 0.00102\ LL \quad \textbf{Equation 2-3}$$

where D $[lb/ft^3]$ is the density of natural soil, $k'_{\emptyset}\sigma_{\emptyset}M_{\emptyset}$ is determined based on the grain size distribution, VS $[lb/ft^2]$ is the vane shear value, $D\%$ is the percent of maximum proctor density, and LL is the liquid limit.

Owen (1975) found a relation between dry density (ρ_{dry}) and critical shear stress:

$$\tau_c = 6.85 * 10^{-6}{\rho_{dry}}^{2.44} \quad \textbf{Equation 2-4}$$

Table 2-1 Potential factors that may influence cohesive soil behaviour (Winterwerp et al., 1990, Berkhovskikh et al., 1991 Huang et al., 2006, Meng et al., 2012, and Kimiaghalam et al., 2013)

	Physical Properties	Chemical Properties	Mechanical and in-situ Properties	Biological factors	Environmental factors
Soil	Grain size distribution Specific gravity Plasticity index Water content Sand, silt, clay content Porosity Atterberg limits Fissures and cracks	Mineralogy organic content Gas content Ions Cation exchange capacity Electrical conductivity pH Oxygen level Sodium adsorption ratio	Bulk density Shear strength Cohesion and friction angle Consolidation condition Upper and lower yield density Bingham viscosity Critical shear stress of erosion Critical shear stress of deposition Settling velocity Saturation condition	Different kinds of inhabitants in the soil structure or fluid such as effects of different plants, worms, crabs, fish	Climate change, freeze and thaw, weathering
Eroding fluid and pore-water	Total suspended solids Viscosity Density Temperature	Ions Salinity pH Oxygen content Redox potential Chlorinity Mineralogy	River ice forces such as border ice Pore-water pressure		

Thorn and Parsons (1980) found another relation between critical shear stress and dry density:

$$\tau_c = 5.42 * 10^{-6}{\rho_{dry}}^{2.28} \quad \textbf{Equation 2-5}$$

Otsubo and Murako (1991) presented a formulation for critical shear stress of surface erosion and mass erosion as a function of yield value (τ_{y1}). τ_{y1} was the intercept of shear stress axis after plotting measured shear stress vs shear rate curve that they were measured by a rotary viscometer. Michener and Torfs (1996) suggested a relation between sediment density and critical shear stress:

$$\tau_c = 0.15(\rho_s - 1000)^{0.73} \quad \textbf{Equation 2-6}$$

Amos et al. (1997) found relationships for critical shear stress and erosion rate for fine-grained sediment from the Fraser River Delta:

$$\tau_c = 7 * 10^{-4}\rho_b - 0.47 \quad \textbf{Equation 2-7}$$

$$E = 2.94 * 10^{-3}\emptyset^{-0.829} \quad \textbf{Equation 2-8}$$

where ρ_b is the bulk density, E is the erosion rate, and $\emptyset$ is the friction angle. Reddi and Bonala (1997) conducted an experimental study to find a relationship between cohesion and critical shear stress of sand-kaolinite mixtures. They found a linear correlation between cohesion and critical shear stress of samples with 30% kaolinite. Hanson and Simon (2001) found an experimental correlation equation 2-9 between erosion rate and critical shear stress for a cohesive bed with high erosion resistance in midwestern United States.

$$\mathrm{k_d} = 0.2{\tau_C}^{-0.5} \quad \textbf{Equation 2-9}$$

where k_d is a material dependent coefficient that can be found from erosion rate experiments using a jet device. Julian and Torres (2006) found a correlation between critical shear stress and clay-silt fraction ($SC\%$):

$$\tau_c = 0.1 + 0.1779(SC\%) + 0.0028(SC\%)^2 - 2.34 * 10^{-5}(SC\%)^3 \quad \textbf{Equation 2-10}$$

Leonard and Richard (2004) estimated critical shear stress from soil shear strength measured with a shear vane device. They found that there is a linear correlation between critical shear stress and shear strength. Mostafa et al. (2008) studied the effect of sediment specific gravity and liquid limit on the erodibilty of cohesive sediments. They found a good fitted Gamma distribution between non-dimensional Shields parameter and a function which included liquid limit and specific gravity of cohesive sediments. Meng et al. (2012) conducted an experimental study on erodibility of intertidal sediments in the Yellow River delta. They used an in-situ flume to estimate critical shear stress and also measured physical-mechanical properties such as grain size, bulk density, water content, plasticity index, and shear strength. Among these soil properties, they found a correlation between critical shear stress and shear strength.

Many researchers have investigated the effect of electrochemical parameters on the erodibility of cohesive soils. The chemistry of the fluid and the pore fluid between clay particles can play a significant role in the behaviour of such soils (Mehta and McAnally, 2007). One of the important parameters is cation exchange capacity (CEC) which is a measure of the type and amount of clay and is defined as the number of milliequivalents of exchangeable cations per 100 grams of dry soil. Ariathurai and Arulanandan (1978) showed that with increasing CEC the erosion rate decreases. Another important factor is

the total content of dissolved salts in the pore fluid (Sherard et al. 1972). Sodium Adsorption Ratio (SAR) represents salinity in soil. Arulanandan et al. (1975) showed that with decreasing SAR, erosion rate decreases. Alhammedi and Miller (2006) studied the effects of ionic strength and SAR on flocculation-dispersion behavior of eastern Arkansas soil. They found that SAR at low ionic strength has a significant effect on clay dispersibility. De Santis et al. (2010) studied effects of physical and electrochemical soil properties on clay-silt slopes of the Aliano area in Italy. They measured PH, SAR, total amount of dissolved salts (TDS), exchangeable sodium percentage (ESP), sodium percentage (PS), and CEC for their samples and found that the eroded slopes have higher PH, SAR, and PS than the non-eroded slopes. Also, they hypothesised that weathered eroded slopes can be stabilized by decreasing the SAR, PS, and ESP. Many other researchers have studied the effect of biological factors on the erodibilty of cohesive sediments (Alberts et al. 1995, Mamo and Bubenzer (2001 a,b), Gyssels et al. 2006).

This study focused on the erosion of cohesive riverbanks in Manitoba, Canada where erosion has caused considerable damage to shorelines within the Province. The main aim of this study is to find a correlation between several soil properties and the erodibilty of these natural cohesive riverbanks and to investigate the applicability of different methods of estimating cohesive soil erosion for this study area. For this purpose several samples from southern and northern Manitoba were taken and tested.

2.2 *Study Area and Soil Sampling*

Thirteen soil samples were taken from three different locations in southern and northern Manitoba. Nine samples were acquired from 8-Mile and 2-Mile Channel in northern Manitoba, Canada. Seven of these samples were taken from 8 Mile channel which had

high clay and silt contents. Two highly cohesive samples with high clay content were acquired from 2-Mile Channel. In addition four samples were taken from the banks of the Red River which flows through the city of Winnipeg in southern Manitoba. Figure 2-1 shows the sampling locations in southern and northern Manitoba where these sites are 500 km far away of each other. The sampling procedure was to remove 20 cm of top soil and take vertical samples from the surface of the banks. Standard Shelby tubes of 7.4 cm diameter and 1 m length were used to take relatively undisturbed samples from the channel banks. The reason for taking samples as close as possible to the bank surface was to investigate the natural behavior of the portion of riverbank most likely to be exposed to fluvial erosion, while neglecting the uppermost layer that would have experienced the greatest amount of weathering and freeze-thaw cycles which is very common in Manitoba. The Red River samples were taken in June 2013 and 8-Mile and 2-Mile channels samples were taken in August 2013 after winter and flood season. Soil samples were taken from the riverbank below the water surface immediately after lowering of the water level to ensure taking saturated soil samples. The wet soil samples were sealed immediately in the Shelby tubes to maintain natural water content. The sealed soil samples were kept in the refrigerator of the Geotechnical Laboratory at the University of Manitoba until testing was completed.

2.3 *Experiments*

Several sediment properties were measured and experiments for determining critical shear stress and erosion rate were conducted to understand the behavior of cohesive sediment erosion. Measurements were categorized in three main groups: physical properties, mechanical properties, and electrochemical properties. The primary soil

properties were selected based on the ASCE sedimentation engineering manual No.110. These properties are considered to be adequate to characterize cohesive soil and sediments when soil samples are not highly influenced by biochemical factors (Mehta and Mc Anally, 2007). Additionally, the authors included several other soil properties based on the results from several initial tests to ensure that a wide range of soil properties were being considered.

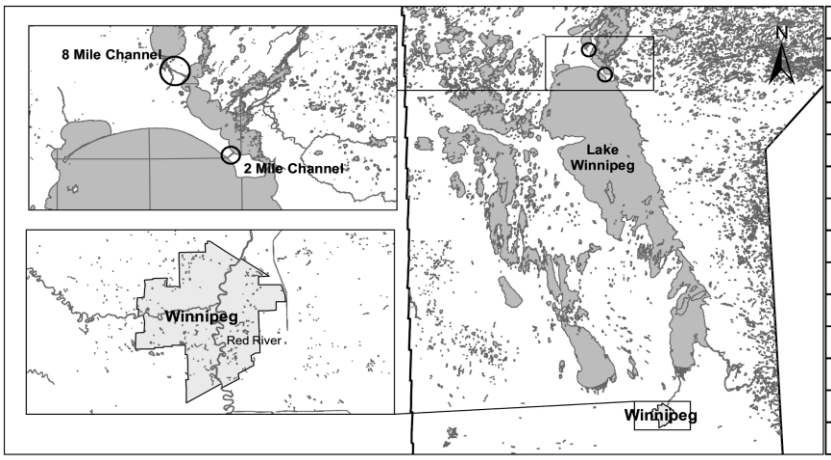

Sample ID	X	Y
RED1	635450	5519745
RED2	634659	5518568
RED3	634164	5516352
RED4	634556	5517526
2M(2-1)	562046	5957254
2M(2-2)	562205	5957138
8M(1-1)	538574	5993660
8M(2-1)	538339	5992256
8M(2-2)	538646	5992211
8M(3-1)	539216	5990250
8M(3-2)	539394	5990424
8M(6-1)	544272	5987559
8M(7-1)	545510	5986565

Figure 2-1 Sampling locations map and coordinates in UTM 14.

2.3.1 *Physical properties*

The important physical properties of cohesive sediments that were measured were grain size distribution, plasticity index, and water content. ASTM standard D6913-04 (ASTM, 2009) sieve analysis and ASTM standard D422-63 (ASTM, 2007) hydrometer analysis were used to quantify the grain size distribution of the samples. The main outputs from this test were to determine the median particle size (d_{50}), sand percentage, silt percentage and also clay percentage. Plasticity index (PI) was determined by measuring liquid limit and plastic limit according to ASTM standard D4318-10 (ASTM, 2010).

2.3.2 *Mechanical properties*

Sediment mechanical properties are highly dependent on in-situ conditions and also the stress history of the soil samples. Dry density (ρ_{dry}), cohesion (C), and friction angle ($\emptyset'_{\mathrm{cr}}$) were measured to understand the mechanical behaviour of these samples. Cohesion and friction angle are the Y-axis intercept and slope of the soil failure line which were measured by direct shear test using ASTM standard D3080-11 (ASTM, 2011) in this study (Figure 2-2).

The test had two stages; the first stage was consolidation and the second was the shear phase. Three tests with different normal stresses for each soil sample were performed to define the failure envelope. Three normal stresses of 40, 60, 80 kPa were used for the consolidation phase, which had a duration of between 24 and 48 hours. After finishing the consolidation phase, the shear phase was started with 0.0015 mm/min strain rate until a failure was observed. During the whole process of consolidation and shearing of the cohesive soil sample the shear box was filled with distilled water to ensure that the test was performed under saturated conditions. Finally cohesion and friction angle were calculated after completing three direct shear tests for each sample (Figure 2-2). Dry density was measured three times for each sample.

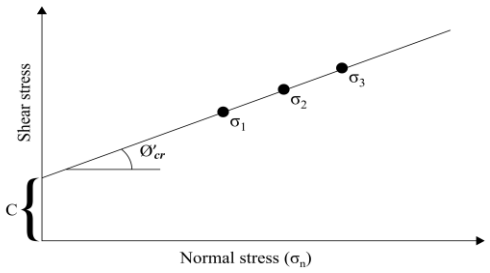

Figure 2-2 Typical direct shear test results and outputs

2.3.3 *Electrochemical properties*

To assess the soil electrochemical properties the cation exchange capacity (CEC) (Hendershot et al. 2006), sodium adsorption ratio (SAR) (Miller and Curtin, 2006), electric conductivity (EC) (Miller and Curtin, 2006), and organic content (OG) were measured at a local commercial soils laboratory. Organic content (OG) was measured by using ASTM standard D2974-13 (ASTM, 2013) and drying a soil sample under 400 ° C temperature for 8 hours. CEC was calculated by the summation of the mol equivalents of the exchangeable cations (Ca, Mg, Na and K). CEC is expressed as milliequivalents per 100g soil (meq/100g) and is calculated as follows:

$$CEC = \frac{\frac{[k]}{39.0983} + \frac{[Ca]}{20.039} + \frac{[Mg]}{12.1525} + \frac{[Na]}{22.9897}}{10} \qquad \textbf{Equation 2-11}$$

SAR and EC were measured from a saturated paste extract of the soils. Electrical conductivity of the saturated paste extract was measured potentiometrically using a combination PH/EC meter fitted with an electrical conductivity probe. SAR is calculated from measurements of the concentrations of calcium, magnesium and sodium in the saturated paste extract. The result of the following calculation yields SAR as a dimensionless ratio:

$$SAR = \frac{[Na^{+}]}{\sqrt{[Ca^{2+}] + [Mg^{2+}]}} \qquad \textbf{Equation 2-12}$$

2.3.4 *Measuring erosion rate and critical shear stress of erosion*

An erosion measurement device (EMD) was constructed by the geotechnical group of the University of Manitoba similar to the device presented by Briaud et al. (2001), and was

used to calculate the rate of erosion [mm/hour] due to different applied shear stresses. The device comprises a main flume, a water tank, a pump, and an ultrasonic flowmeter (Figure 2-3). This device has a reservoir for performing tests with water of different total suspended solids (TSS) concentrations, or a drainage system can be used to continuously circulate new water of constant TSS during an experiment. The main acrylic flume is 2.80 m long, 0.1 m wide, and 0.05 m high. A 3 HP pump controlled by a CFW-08 frequency inverter generates flow from the reservoir to a straight circular inflow pipe with 0.102 m diameter. A Dynasonic DUFX1-D1 flowmeter is installed on the straight inflow pipe. The testing section is located 2.50 m downstream of the flume to ensure that measurements were performed in or near the fully developed turbulent flow region. The flume Reynolds number, calculated as $Re = \rho VD/\mu$ varied between 6,700 and 200,000. The procedure for the EMD test was: (1) insert the sample, cut it flush with the flume bottom and fill the flume with water; (2) set the velocity to 0.1 m/s using a digital box controller; (3) push the sample 1 mm upward into the flow; (4) record how much time it takes for 1 mm soil to erode; (5) open the top lid of the flume and smooth the surface and repeat tests for higher velocities. The velocity interval increase depends on the soil behaviour, since it should be large enough to observe a measurable amount of erosion. Therefore, the velocity intervals were different for each sample but were generally between 0.10 m/s and 0.30 m/s. The shear stresses were calculated from Equation 2-13:

$$\tau_a = \frac{1}{8}\rho f V^2 \qquad \textbf{Equation 2-13}$$

where τ_a [Pa] is the shear stress, ρ [kg/m^3] is the water density, f [-] is the friction factor obtained from the Moody Chart, and V [m/s] is the mean flow velocity in the flume. The friction factor is a function of pipe Reynolds number and the pipe relative

roughness ε/D, where D is taken as the hydraulic diameter which is 0.067 m for this device. The value of ε was estimated as $0.5d_{50}$ as suggested by Briaud et al. (2001) and the sample protruded 1 mm into the flume at the start of each measurement.

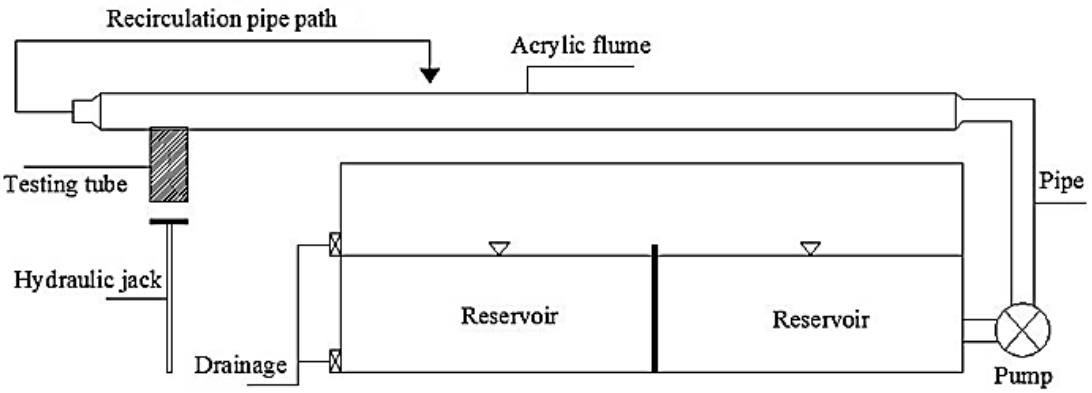

Figure 2-3 Schematic view of the EMD device at the University of Manitoba

Crowley et al. (2014) used computational modeling of piston-type erosion rate testing devices combined with previous experimental work to assess the impact of sample placement with respect to the flume bottom, as well as the impact of sample macro-roughness. Their results demonstrate that macro-roughness can cause the presence of both localized high and low shear zones across the sample, and they outline potential amplification factors that may occur. The current study did not explicitly consider these factors. The routine of cutting the sample flush with the channel bottom at the beginning of each new applied shear stress had the effect of reducing potential waviness in the sample surface. When combined with the procedure of extending the smooth surface of the sample 1 mm into the flume, these should have minimized the potential for excessive high shear zones and should also make the current results somewhat conservative. Given the complex flow characteristics that may actually occur over a rough surface that is actively eroding in a manner that was not always uniform in time or space, the estimated

applied shear stresses are somewhat of an approximation that still allows the influence of various soil parameters on erodibility to be assessed.

This test had two main results. First, the critical shear stress of each sample was obtained, and was defined as the lowest shear stress that resulted in erosion over the entire sample surface. The second important result is the slope of the erosion rate versus shear stress line which can be used for calculation of erosion rates under different conditions. The main concern for using piston-typed erosion measurement devices is the accuracy of quantifying the amount of erosion. To ensure the repeatability and accuracy of the results several measurements were undertaken. The piston was calibrated such that the amount of upward movement was known to be within ±0.1 mm. Each test was started with a smooth surface and the height of the sample was measured at the beginning of the test. Three conditions could happen after each increment in applied shear stress: 1) the entire surface of the eroded soil was below the bottom of the flume, in which case the amount of erosion was estimated using Equation 2-14:

$$E_h = h_{ps} + h_{ew} \qquad \textbf{Equation 2-14}$$

where E_h is the erosion height, h_{ps} is the total movement of the piston, h_{ew} is the equivalent water height between the surface of the sample and the bottom of the flume; 2) the surface of the eroded soil was above the bottom of the flume, in which case the amount of erosion was estimated using Equation 2-15:

$$E_h = h_{ps} - h_{rs} \qquad \textbf{Equation 2-15}$$

where in this equation h_{rs} is the equivalent height of the remaining sample after each step. Since in our procedure we cut the sample at each step to flush the sample surface

with the bottom of the flume, it was straight forward to measure the weight of the portion of the sample above the bottom. The weight of the remaining soil was converted to an equivalent height; 3) a portion of the sample was below the flume bottom and a portion remained above the bottom, in which case Equation 2-16 was used to calculate the equivalent erosion height:

$$E_h = h_{ps} + h_{ew} - h_{rs} \quad \textbf{Equation 2-16}$$

Generally, most measurements fell into case 3; however, the eroded surface elevations were relatively flush with the bottom of the flume. Since it was very important to measure an accurate critical shear stress, the first data point of the experiment was vital. Several tests were performed at velocities lower than the velocity where erosion was observed, to find the first data point. Additionally, several long term tests were conducted for durations of 24 hours to 48 hours at these lower velocities to examine the validity and consistency of the first point.

As an additional check of the validity of the results based on the erosion height measurements, water samples were acquired from the well-mixed reservoir after each velocity increment. Total suspended solids (TSS) was quantified according to the ASTM standard D5907 (ASTM, 2011). After calculating the weight of the eroded soil particles, the amount of total volume of the eroded material was calculated using equation 2-17:

$$V_{er} = (1 + e)V_s \quad \textbf{Equation 2-17}$$

Where V_{er} is the total eroded volume, e is the soil void ratio, and V_s is the volume of the soil particles. The equivalent erosion rate could then be calculated by Equation 2-18:

$$E_h = \frac{V_{er}}{A_{ts}}$$ **Equation 2-18**

where A_{ts} is the testing tube surface area. For higher velocities that experienced chunks of soil detaching from the surface, the deposited chunks were weighted and the equivalent soil height was added to Equation 2-18. Results from the above two methods were consistent.

Figure 2-4 shows results of the EMD test for three different samples from the Red River, 2-Mile Channel and 8-Mile Channel. The erosion rate of cohesive soil is generally proportional to the excess shear stress and can be expressed by Equation 2-19 (Partheniades, 1965; Maa et al, 1998):

$$E = k_d\,(\tau_a - \tau_c\,)^a$$ **Equation 2-19**

where E [mm/hr] is the erosion rate of cohesive sediment, k_d is a material dependent coefficient which is the slope of the erosion rate versus shear stress line, τ_a [Pa] is the applied shear stress which can be calculated from Equation 2-13 for different velocities, τ_c is the critical shear stress, and a is the exponent generally considered to be 1 for surface erosion. Using the results from the EMD testing, both τ_c and k_d were calculated. After plotting erosion rate vs shear stress, a linear trend line was fitted to the results of the EMD. The reported value of τ_c was the x-intercept of the trend line and k_d was the slope of the trend line.

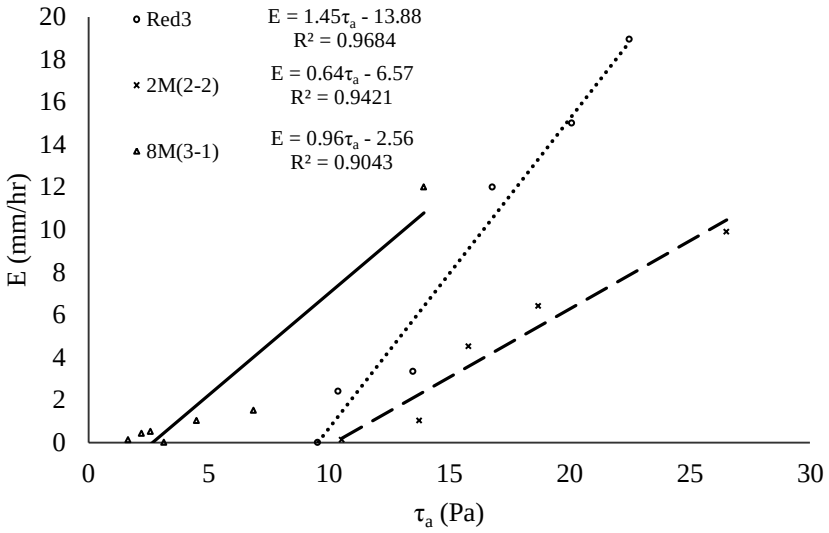

Figure 2-4 EMD results for samples Red3 from the Red River, 2M(2-2) from 2-Mile Channel, and 8M(3-1) from 8-Mile Channel

2.4 *Results and Discussion*

In this section a summary of the measurements and experimental results is provided. Stepwise regression was used to assess the effect of each variable on erodibility and also to select the most important variables on critical shear stress and erosion rate. We were interested in fluvial surface erosion and tests were performed to assess erodibility over a range of applied shear stresses that were plausible for low gradient Manitoba rivers. Measurements were stopped at the beginning of the mass erosion process where a large portion of the sample starts to erode and the erosion rate increased rapidly. Different erosion patterns were observed among the samples. The erosion process started with small particles detaching from the surface of the sample and ended with the erosion of relatively larger chunks. Samples with lower cohesion such as 8M (7-1) with low clay content had relatively uniform behavior where particle erosion was observed over a large range of applied shear stresses. Erosion rate estimation for such samples was easier and

less time consuming. On the other hand, medium and highly cohesive samples erosion pattern started with erosion of very small chunks (< 2 mm^3) and with higher shear stresses, soil large chunks (> 100 mm^3) detachment was also observed. At the end of the each step different eroded surfaces were observed. For such samples, erosion rate measurement was time consuming and needed to use engineering judgment as well as using measurements methods. Table 2-2 shows the measured properties and characteristics for the soil samples. ASTM standard D2487-11 (ASTM, 2011) was used to classify the soil samples. The stepwise regression was designed to find the most effective input variables on output variable when the numbers of input variables are large. The regression works based on maximizing the coefficient of determination (R^2) with using each input variable and also a combination of these variables. Basically in this method at each step, a variable is selected or removed based on a t-test and it will stop when no more variables can be justified for selection or removal from the regression. The regression starts with each variable separately and then tries to improve the output by adding and removing other variables. Results of stepwise regression for critical shear stress showed that cohesion had the highest t-value and lowest p-value which indicates that cohesion had the highest impact on critical shear stress. All other variables had low t-value and failed in the test. The results of stepwise regression for k_d, suggest that SAR had a significant effect on k_d while the other variables were not significant.

Table 2-2 Soil sample characteristics and properties

Sample ID	CEC (meq/100g)	EC (dS/cm)	OM (%)	SAR	d_{50} (mm)	ρ_{dry} (kg/m^3)	C (KN/m^2)	tan (Ø')	Sand %	Silt %	Clay %	w %	PI %	Soil type	τ_c (Pa)	K_d
Red 1	30.7	0.72	2.2	0.992	0.015	1312	9.5	0.597	39	28	33	39	29	CH	9.38	1.327
Red 2	17.2	0.352	1.0	0.89	0.045	1415	2.37	0.731	48	25	27	29	12	CL	0.98	1.53
Red 3	31.29	0.855	9.0	0.92	0.0056	1209	10.4	0.624	18	41	41	44	34	CH	9.55	1.454
Red 4	30.28	0.888	6.6	1.16	0.0081	1133	1.16	0.743	17	43	40	54	40	CH	1.72	0.797
2M(2-1)	23.6	0.446	1.1	1.071	0.002	1567	8.3	0.551	14	44	42	28	21	CL	7.81	0.673
2M(2-2)	23.1	0.462	1.0	1.075	0.002	1542	11	0.435	5	45	50	34	24	CL	10.25	0.641
8M(1-1)	29.2	0.406	1.4	1.621	0.0004	1419	8.5	0.551	2	4	94	35	27	CH	4.85	0.325
8M(2-1)	28.2	0.284	1.4	1.373	0.0011	1512	10	0.572	6	34	60	27	17	CL	8.57	0.898
8M(2-2)	27.1	0.288	1.9	0.28	0.0013	1445	1.7	0.74	2	33	65	23	14	CL	1.62	8.674
8M(3-1)	28.1	0.314	2.8	0.639	0.0015	1378	2	0.738	17	27	56	40	24	CL	2.68	0.98
8M(3-2)	24.7	0.386	2.1	1.035	0.0017	1605	2.9	0.75	1	45	54	38	18	CL	2.74	0.42
8M(6-1)	21.6	0.204	1.2	0.239	0.02	1843	2.4	0.897	39	37	24	17	13	CL	1.6	6.95
8M (7-1)	26.3	0.206	1.0	0.358	0.0074	1747	1	0.869	25	50	25	22	5	CL-ML	0.31	3.683

2.4.1 *Effect of median grain size*

One advantage of these samples was the wide range of grain size distribution that helped to elucidate the effect of different types of soil on critical shear stress and erosion rate of cohesive sediments. Samples from 8-Mile Channel had both lowest and highest median grain sizes (d_{50}) that varied between 0.0004 mm for high clay content soil to 0.02 mm for high sand content samples. Figure 2-5a shows that there was a weak correlation between critical shear stress and d_{50}, but the general trend shows that with increasing grain size critical shear stress decreased. Figure 2-5b shows the variation of k_d with d_{50} demonstrating that there was no correlation between these two variables.

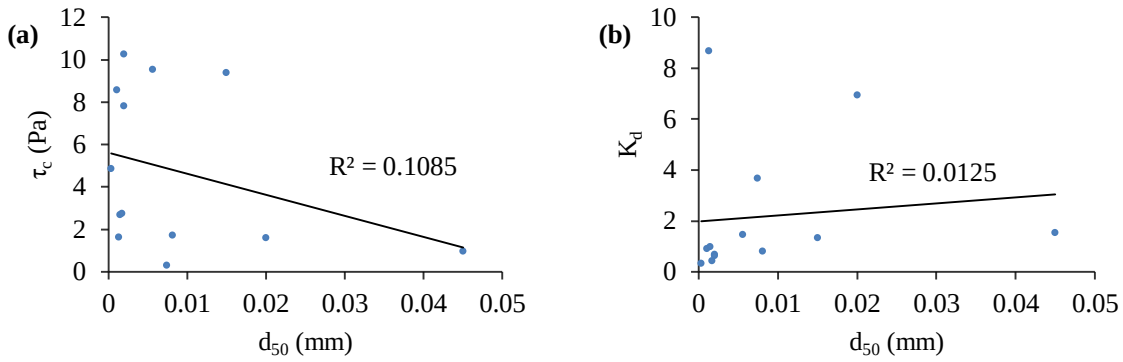

Figure 2-5 (a) Critical shear stress versus median grain size (b) k_d versus median grain size.

2.4.2 *Effect of clay content*

The main difference between cohesive and non-cohesive sediment is the nature of resistance force against motion of the sediment particles. In cohesive soils electrochemical forces acting on the particle surface cause a resistance to motion, and the magnitude of these forces depends on the particle specific surface area. Specific surface area is the ratio of particle surface area to particle weight. Clay particles have the highest specific surface area compared to coarser particles, thus they impose higher electrochemical forces (Garcia, 2007). Presence of 10% clay in the sediment matrix is sufficient to govern the sediment behavior (Debnath and Chaudhuri, 2010). Clay content of the samples used in this study varied from 24 % to 94%. Figure 6a shows the variation of critical shear stress with clay content and demonstrates that there was no correlation between critical shear stress and clay content, which is not in agreement with several past studies such as Smerdon and Beasley (1961) and Middleton (1930). However, Briaud (2005) found a similar result using a similar device for a wide range of soil samples. This result indicates that natural cohesive soil erodibility is more highly influenced by in-situ conditions such as soil stress history and freeze-thaw processes than its inherent properties. Figure 2-6b shows the variation of k_d with clay content. A weak correlation

between clay content and k_d was observed which indicated that with increasing clay content k_d decreased.

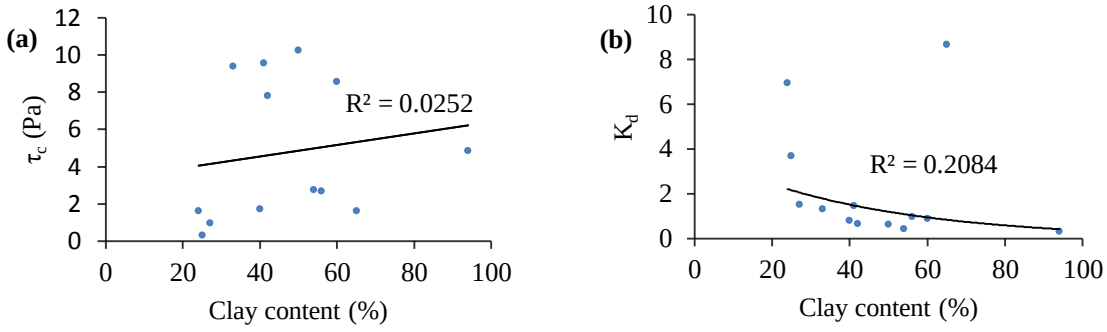

Figure 2-6 (a) Critical shear stress versus clay content (b) k_d versus clay content

2.4.3 *Effect of silt content*

Silt content in the soil samples varied from 4 % to 50%. Figures 2-7a and 2-7b show that there was no correlation between silt content and critical shear stress, and between silt content and k_d, respectively. Results from this section and section 2.4.2 suggest that Equation 2-10 is not a good predictor in this study area and there was no relation between critical shear stress and fraction of silt-clay for these samples.

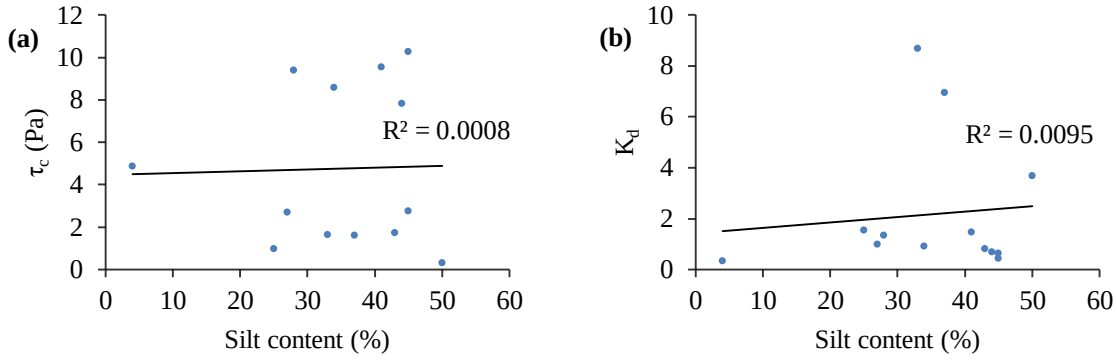

Figure 2-7 (a) Critical shear stress versus silt fraction (b) $k_d$versus silt fraction

2.4.4 *Effect of sand content*

Sand content in the soil samples varied from 1% to 48%. Figure 2-8a shows the variation of critical shear stress with sand content in different samples and as shown in the figure there was no correlation between critical shear stress and sand content. Figure 2-8b shows variation of k_d with sand content with no correlation between these two variables.

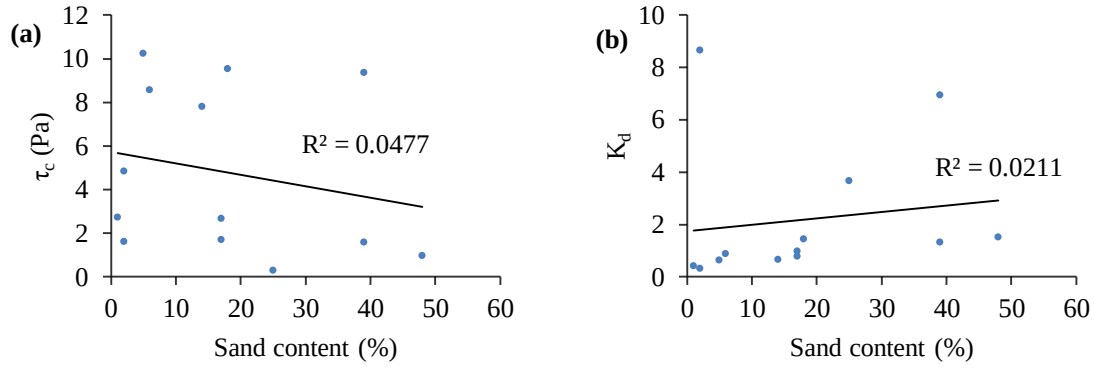

Figure 2-8 (a) Critical shear stress versus sand fraction (b) k_d versus sand fraction

2.4.5 *Effect of natural water content*

Another important variable is natural water content which varied between 17% and 54% for the current samples. Figure 2-9a shows that there was no relation between natural water content and critical shear stress. Figure 2-9b shows the variation of k_d with water content, and as shown there was a weak correlation between these variables. However, this graph shows that with increasing water content k_d decreased.

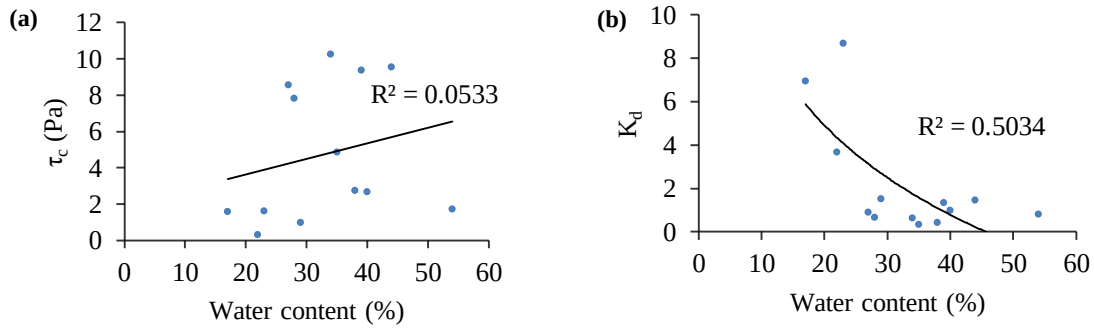

Figure 2-9 (a) Critical shear stress versus natural water content (b) k_d versus natural water content

2.4.6 *Effect of plasticity index*

Another important property of cohesive sediments is plasticity index which basically indicates the ability of a soil to deform without cracking. Generally, high plastic soils are highly cohesive, thus plasticity index is one of the important factors that may affect the erodibilty. Figure 2-10a shows the variation of plasticity index with critical shear stress, and as shown there was a weak correlation between plasticity index and critical shear stress of erosion. This result does not support Equation 2-2 but generally critical shear stress tends to increase with increasing plasticity index. Figure 10b shows the relationship between k_d and plasticity index, where again the correlation between these two variables was weak. However, the data indicates a general trend of decreasing k_d with increasing plasticity index.

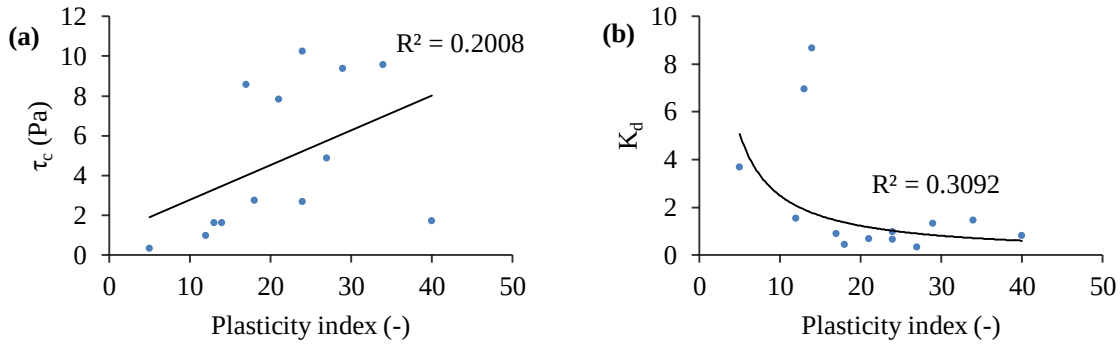

Figure 2-10 (a) Critical shear stress versus plasticity index (b) k_d versus plasticity index

2.4.7 *Effect of cohesion*

One of the important mechanical properties of the cohesive soils is cohesion, which is the shear strength of the soil when the applied normal stress is zero. Cohesion has value of zero for non-cohesive soils, and generally depends on the physical, mechanical, and electrochemical properties of clay particles in the soil matrix (Budhu, 2000). In this study

several direct shear tests were used to determine shear strength of the samples and the failure line. The direct shear test was used rather than the triaxial test for clay since the direct shear test is inexpensive and quicker than the triaxial test and also because the shearing procedure is similar to the shear stress applied by a fluid. Figure 2-11a shows that there was a strong linear correlation with critical shear stress and cohesion where increasing cohesion causes an increase in critical shear stress. Of all soil properties measured in this study, cohesion was the most important parameter on threshold of movement based on the statistical analysis. Crowley et al. (2012) and Slagle (2006) found similar results for erosion of rock and stiff clay. Figure 2-11b shows the variation of k_d versus cohesion. The data shows only a weak correlation between k_d and cohesion, suggesting that cohesion is most significant at the onset of motion. Figure 2-11b shows that with increasing cohesion k_d decreased. Figure 2-12 shows behavior of some samples from the study area under the direct shear test. The samples behaved normally consolidated and lightly over consolidated, indicating that the ratio of pre-consolidation stresses and in-situ stresses were close to each other. Another considerable behavior was the high ratio of the shear strengths to the normal stresses. Figure 2-12 also shows the difference between shear strengths with increasing the normal stress from 40 to 80 kPa.

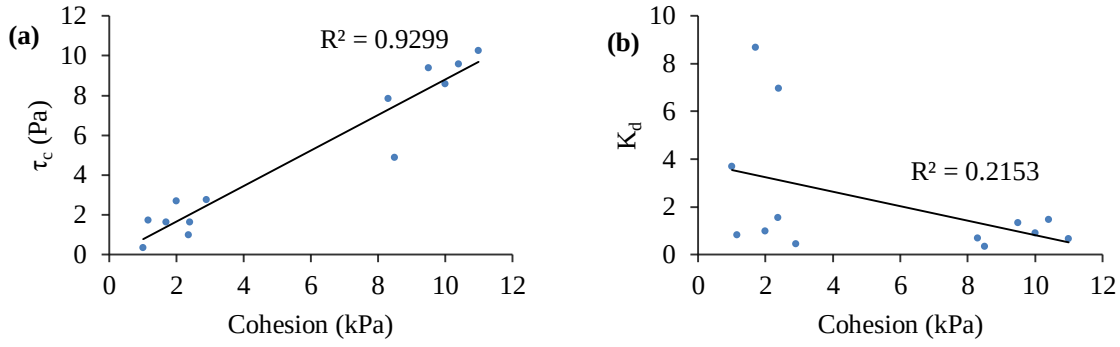

Figure 2-11 (a) Critical shear stress versus cohesion (b) k_d versus cohesion

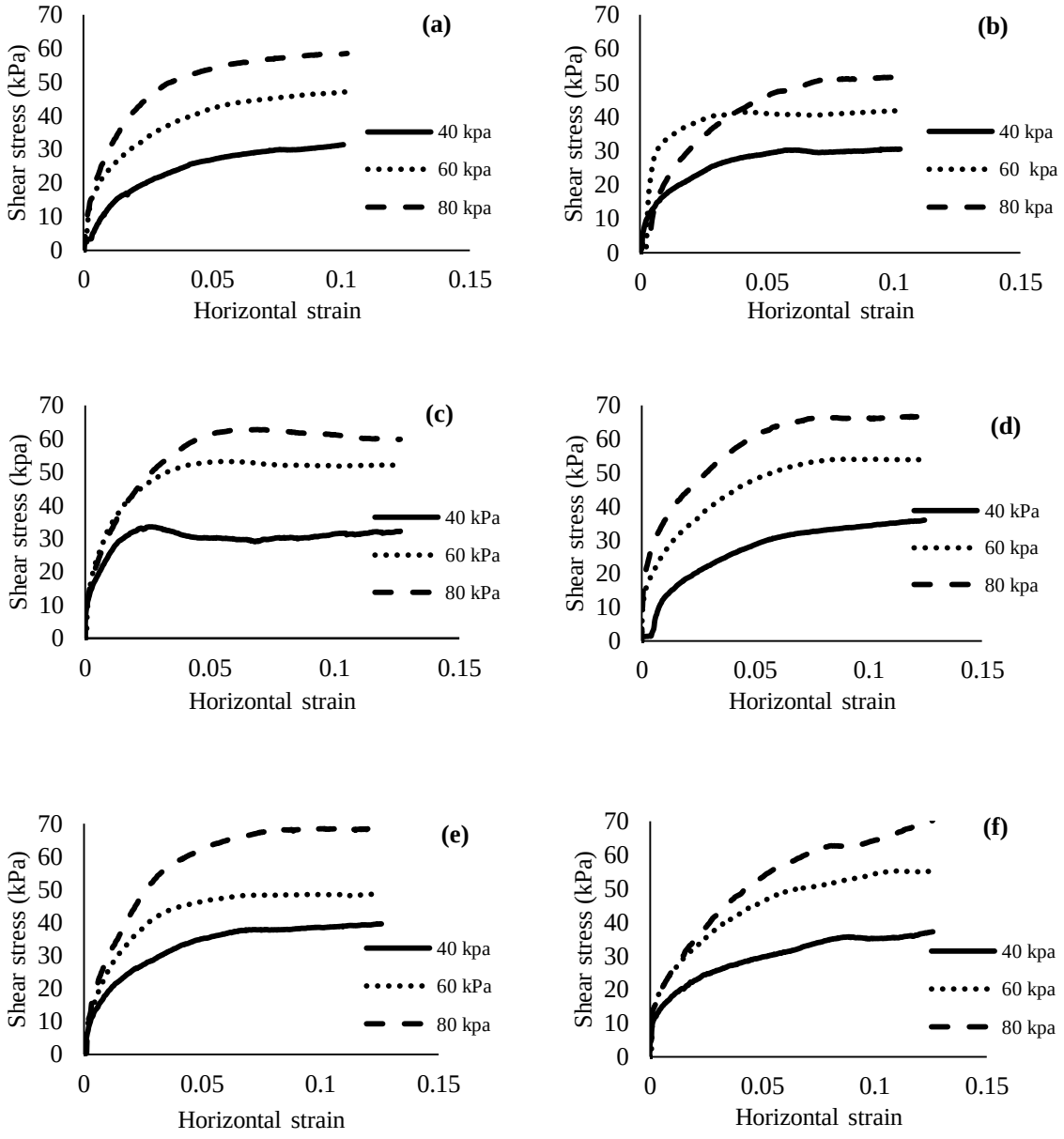

Figure 2-12 Shear stress versus horizontal strain from the direct shear test; (a)-(b) samples from 2-Mile Channel; (c)-(d) samples from 8-Mile Channel; (e)-(f) samples from the Red River

2.4.8 *Effect of friction angle*

Another output from the direct shear test is the friction angle. Generally coarser material have higher friction angle because of higher internal friction between particles. Figure 2-13a shows the correlation between friction angle and critical shear stress. The R^2 was

0.73 but analysis of the stepwise regression indicated that this variable failed the t-test. However, as this figure shows with increasing friction angle critical shear stress decreased. Figure 2-13b shows that with increasing friction angle k_d increased exponentially but the correlation was not strong. Results from this section and section 2.4.7 do not support Equation 2-1 which indicates that with increasing shear strength, critical shear stress increases. Usually non-cohesive soils with coarser particle size have higher friction angle and lower cohesion (Budhu, 2000) whereas with lower cohesion, lower critical shear stress is expected.

2.4.9 *Effect of dry density*

Several researchers presented relations between dry density and critical shear stress of erosion such as Equations 2-4 and 2-5. Figure 2-14a shows that dry density showed no correlation with critical shear stress in this study which does not support using Equations 2-4 and 2-5 for this study area. Figure 2-14b shows the variation of dry density with k_d. Correlation between these variables was weak but the general trend showed that with increasing dry density, $k_d$increased.

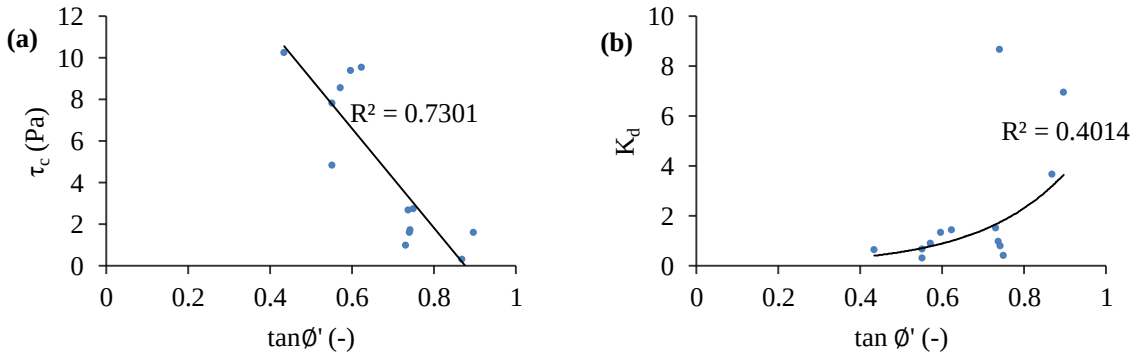

Figure 2-13 (a) Critical shear stress versus tan $\emptyset'$ (b) k_d rate versus tan $\emptyset'$

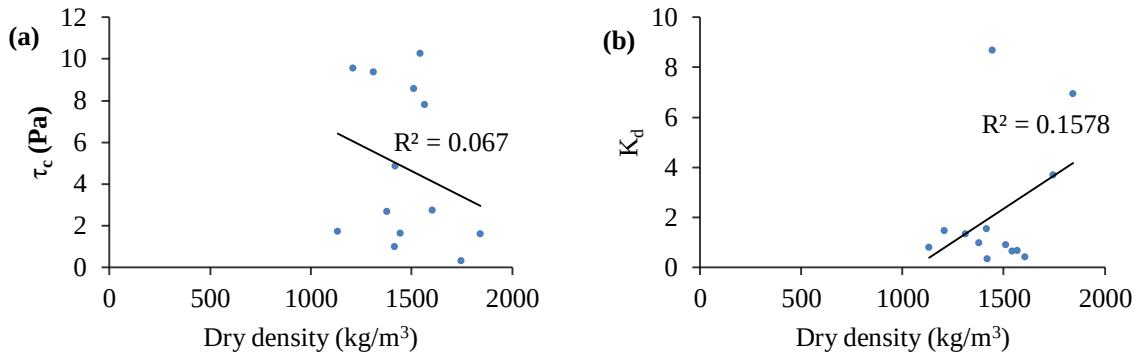

Figure 2-14 (a) Critical shear stress versus dry density (b) k_d versus dry density

2.4.10 *Effect of cation exchange capacity*

Clay and organic soil have negative charges that can release positively-charged nutrients, thus higher clay content and organic matter content causes higher CEC values. In cohesive material CEC depends on the type of mineral in clay particles, thus different types of clay have different CEC values. Montmorillonite has the highest value of CEC in the clay soils between 70 to 100 meq/100 gr (Carroll, 1959). Measurements showed variation of CEC from 17.2 to 31.3 in this study. Figure 2-15a shows the variation of critical shear stress versus CEC where there was a weak correlation between these two variables but the general trend shows ascending behavior of critical shear stress with increasing CEC. Figure 2-15b shows the variation of k_d with CEC and results indicate that there was no correlation between these two variables. These results do not confirm the results by Arithurai and Arulanandan (1978) where they found with increasing CEC, erosion rate decreased.

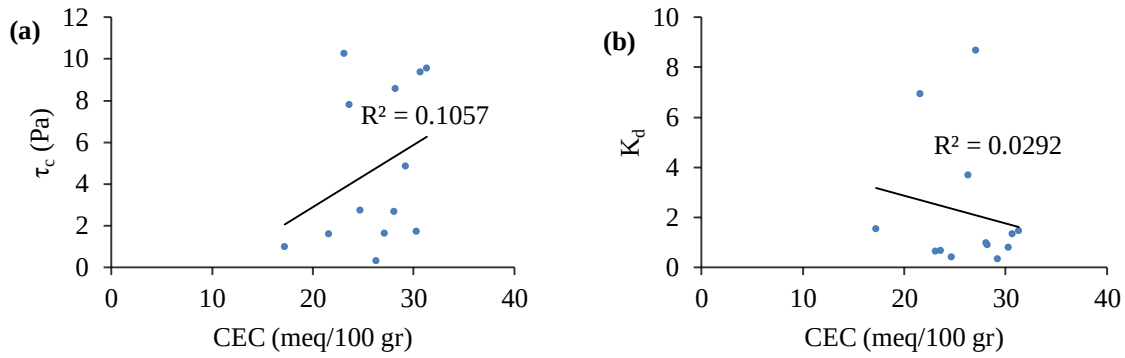

Figure 2-15 (a) Critical shear stress versus CEC (b) $k_d$versus CEC

2.4.11 *Effect of electric conductivity*

Since sand has low and clay has high electric conductivity, this variable correlates with grain size and soil texture. Also higher salinity causes higher electric conductivity (Barbosa and Overstreet, 2011). Electric conductivity varied between 0.204 ds/cm for high sand content samples from 8-Mile Channel to 0.888 ds/cm for the Red River samples with moderate clay and silt content. Figures 2-16a and 2-16b show weak correlation between electric conductivity and critical shear stress and k_d. However, these figures show that with increasing electric conductivity critical shear stress increased but k_d decreased.

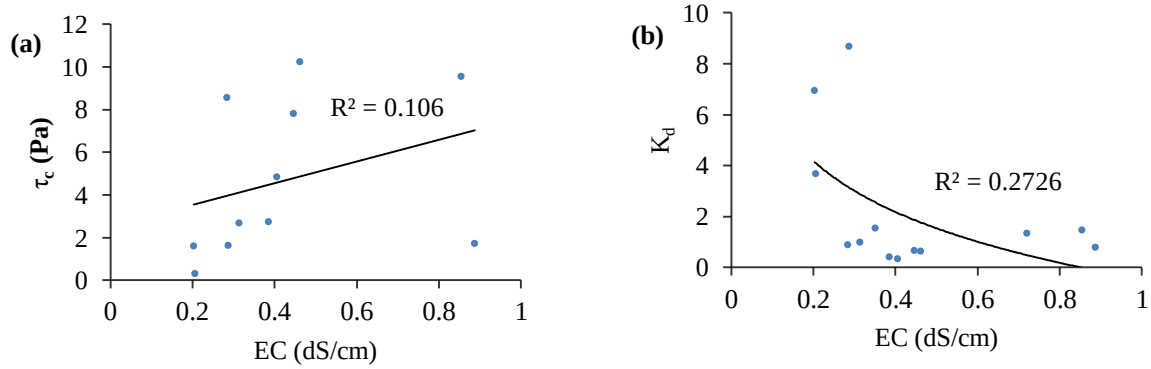

Figure 2-16 (a) Critical shear stress versus EC (b) k_d versus EC

2.4.12 *Effect of sodium adsorption ratio (SAR)*

Sodium adsorption ratio is a ratio of dissolved sodium to calcium and magnesium measures and estimates the amount of salinity in soils. When SAR is greater than 13, the soil is called a sodic soil and causes weaker bonds between soil particles that avoid the formation of soil aggregates (Sonan et al., 2012). SAR varied between 0.24 and 1.62 in this study which is not a wide range of variation for SAR. Figure 2-17a shows a weak correlation between SAR and critical shear stress and the general trend is that critical shear stress increased with increasing SAR. Figure 2-17b shows k_d versus SAR which shows a good logarithmic correlation between these two variables and shows that with increasing SAR, k_d decreases. Rashidi and Seilsepour (2011) indicated that with increasing salinity the EC and SAR increased and they presented a linear relationship between SAR and EC. The present results are at the low range of SAR (SAR<2), and are in contrast with past studies such as Arulanandan (1975), where they indicated that with increasing SAR erosion rate increases. Therefore, it can be concluded that an increase in SAR can decrease erosion rate in a soil sample with low sodium content.

2.4.13 *Effect of organic content*

Organic content may have an effect on soil properties especially on cohesive riverbanks due to the surface vegetation and close distance to the surface. Figures 2-18a and 2-18b show no correlations between this variable and critical shear stress and also k_d. Organic content varied between 1% and 9% in the samples.

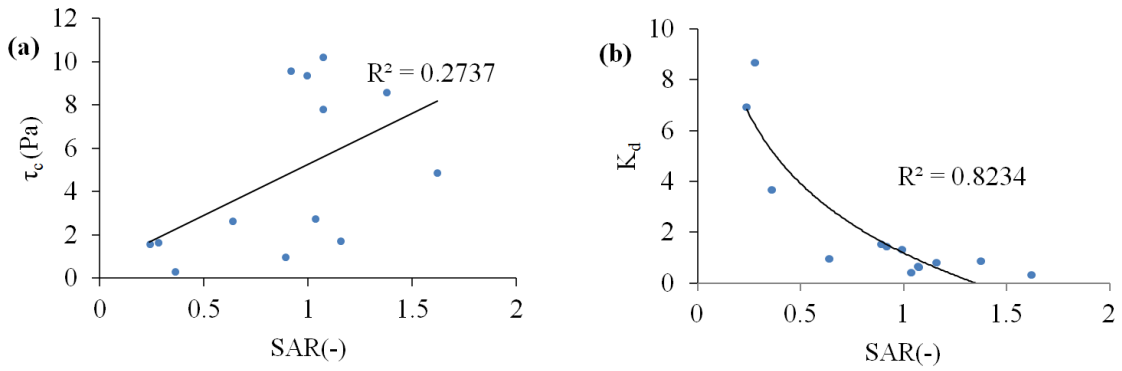

Figure 2-17 (a) Critical shear stress versus SAR (b) k_d versus SAR

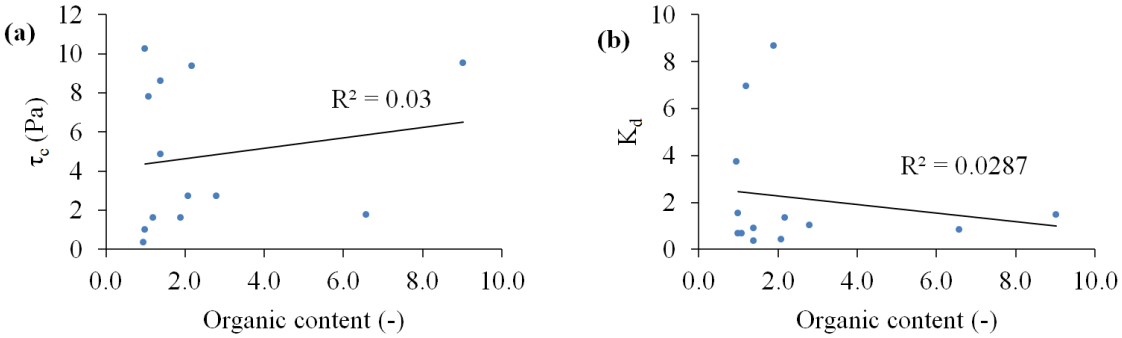

Figure 2-18 (a) Critical shear stress versus organic content (b) k_d versus organic content

2.4.14 *Effect of critical shear stress*

Figure 2-19 shows critical shear stresses versus $k_d$where critical shear stresses varied between 0.31 Pa to 10.25 Pa and k_d varied between 0.325 and 8.674. The highest critical shear stress was observed in 2-Mile Channel where the sample had high cohesion among the other samples (C=11 kPa) and the lowest critical shear stress was observed in the 8-Mile Channel where in that location silt content was very high and clay content was low. A significant correlation between τ_c and k_d was not observed in this study. Using Equation 2-9 to estimate erosion rate would not be appropriate for the soils tested in this

study as the weak power correlation function found here had a constant coefficient that was an order of magnitude greater than that found by Hanson and Simon, 2001. Figure 2-20 shows typical samples from these sites.

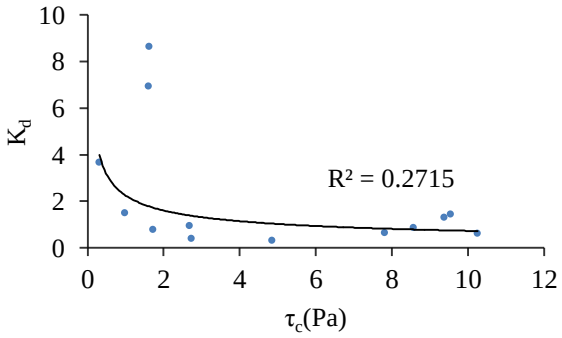

Figure 2-19 Critical shear stress versus

2.4.15 *Summary of the results and analysis*

These experiments showed that the only parameter that had high correlation with critical shear stress of erosion is cohesion which was calculated from the direct shear test. Also, results of the stepwise regression indicated that the only variable that mainly impacted on the samples was cohesion. The best regression fit was linear and critical shear stress can be estimated by Equation 2-20:

$$\tau_c = \alpha\, C + \beta \qquad \textbf{Equation 2-20}$$

where τ_c is the critical shear stress [Pa], C is the cohesion [kPa], α and β are empirical constants where for this study $\alpha = 0.89$ and $\beta = -0.1$. These empirical constants will change with changing clay minerals. Thus to estimate the critical shear stress of erosion in these study reaches performing a direct shear test on a sample is a good option. Cohesion is one of the important cohesive soil mechanical properties and highly depends

on inter-particle bonds between clay particles and in-situ condition of the soil. Freezing and thawing which is very significant in Manitoba may also affect the mechanical properties of riverbank soils as well as the cohesion.

Results from the statistical analysis on the samples showed that the only soil property that affects k_d is SAR, which in this research varied between 0.24 and 1.62. However, k_d varied between 0.8 and 1.50 for the Red River samples, between 0.325 and 8.674 for the 8-Mile Channel samples, and was relatively constant around 0.65 for the 2-Mile Channel samples. The largest k_d and erosion rate were observed in 8-Mile Channel for two locations. The first location had low clay content with high amount of silt. The second location had high clay content with several fissures within the soil structure probably due to the effect of freezing and thawing. Both samples from these two locations had the lowest SAR values. Figure 2-21 shows typical soil samples taken from these locations in 8-Mile Channel. The lowest erosion rate was observed in 8-Mile Channel where the soil sample had the highest amount of clay (94%) and also the highest value of SAR.

Linear form of Equation 2-19 was used for predicting surface erosion rate.

$$E = f(\tau_a, \tau_c, SAR) \qquad \textbf{Equation 2-21}$$

By substituting Equations 2-20 and 2-21 into the linear form of Equation 2-19, the following equation can be used for estimating erosion rate of cohesive river banks in the study regions:

$$E = f(\mathrm{SAR})(\tau_a - [\alpha C + \beta]) \qquad \textbf{Equation 2-22}$$

where τ_a [Pa] is the applied shear stress and C [kPa] is the cohesion. Equation 2-22 is a new equation that had reasonable results for the samples taken from the Red River, 8-Mile Channel, and 2-Mile Channel where soil samples from these sites have low value of SAR. However, results may change with changing sites and soil properties. A logarithmic trend was fitted to the data for this study and k_d was estimated by the following equation:

$$k_d = -3.9 \ln(SAR) + 1.1 \qquad \textbf{Equation 2-23}$$

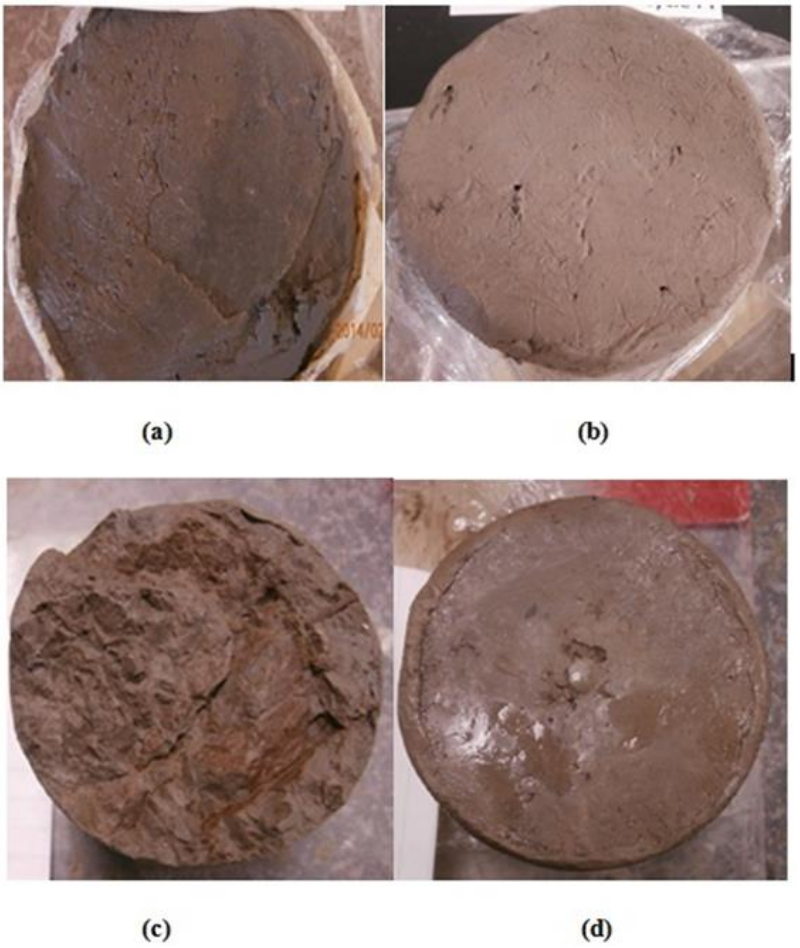

Figure 2-20 Typical soil samples from the sampling locations (a) sample from the Red River (b) sample from the 2-Mile Channel (c) and (d) sample from the 8-Mile Channel

By substituting Equation 2-23 into the Equation 2-22, the following equation can be used for estimating erosion rate of cohesive river banks in the study regions:

$$E = [-3.9\ln(SAR) + 1.1](\tau_a - 0.89\ C + 0.10) \qquad \textbf{Equation 2-24}$$

Figure 2-22 shows the results of measured data using EMD test versus estimated erosion rate by Equation 2-24.

Figure 2-21 (a) Sample from 8-Mile Channel with high amount of silt, low cohesion with k_d=3.683 (b) Sample from 8-Mile Channel with high amount of clay, low cohesion with k_d=8.67

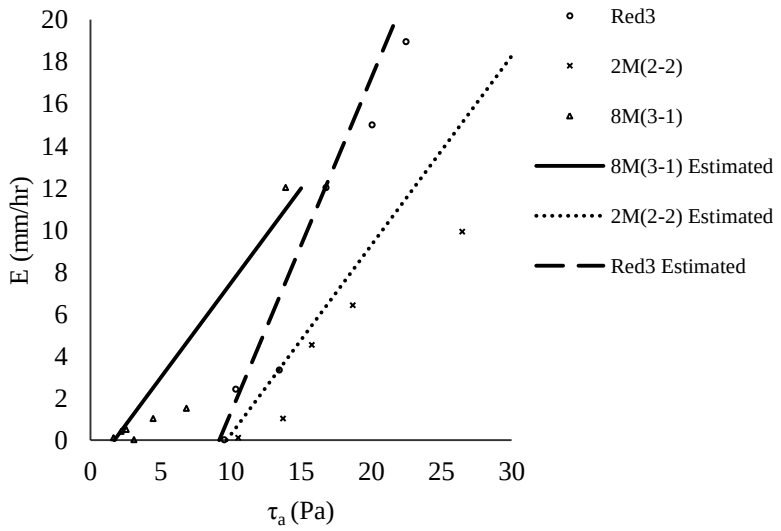

Figure 2-22 Measured erosion rate using the EMD test versus estimated erosion rate line by Equation 2-24.

2.5 *Conclusion*

In this study relatively undisturbed river banks soil samples from different locations in Manitoba, Canada were taken, and for each sample 13 important physical, mechanical, and electrochemical properties were measured. The main advantage of this study was that experiments were performed on natural samples taken from close to the soil surface which represented the behavior of natural riverbank due to fluvial surface erosion. Samples varied in a wide range of properties, in particular, clay content varied from 24% to 94% which indicated different range of cohesive sediments. Samples taken from northern Manitoba were different from those taken from southern Manitoba in texture and type of clay. Samples from northern Manitoba contained brown clay with high amount of clay, silt and also organic content but samples from the Red River in southern Manitoba contained grey clay with high plasticity. Therefore, this study can represent behavior of cohesive river banks erodibility in Manitoba over a wide range of soil and sediment properties.

Cohesion measured by the direct shear test was the most significant soil property that affected critical shear stress, and a linear correlation was observed between cohesion and critical shear stress. Clay fraction, silt fraction, sand fraction, water content, dry density, and organic content showed no correlation with the critical shear stress. Other measured properties had a weak correlation with the critical shear stress or failed in the t-test but generally trends from statistical analysis for these variables showed that the critical shear stress of cohesive soil may increases with increasing CEC, EC, SAR, and plasticity index. Also, critical shear stress decreases by increasing d_{50} and $\tan \emptyset'$.

SAR was the most significant variable that affects k_d in this study. CEC, organic content,

sand fraction, silt fraction, and d_{50} showed no correlation with k_d. Other measured properties had a weak correlation with k_d or failed in the t-test, but generally trends from the statistical analysis showed that the k_d of cohesive soil decreases with increasing EC, cohesion, clay fraction, natural water content, plasticity index, and also critical shear stress of erosion. Also erosion rate may increase by increasing dry density, and $\tan \emptyset'$.

Generally, results are in good agreement with several recent studies such as Briaud (2005) and Crowley et al. (2012). It can be concluded that in-situ soil condition and properties have the most significant effect on erodibility of cohesive soil. It is therefore essential to include the effect of in-situ conditions like soil stress history, as well as additional factors such as freeze-thaw history and weathering to understand the erodibility of cohesive soils.

2.6 *References*

Alberts E.E., Nearing M.A., Weltz M.A., Risse L.M., Pierson F.B., Zhang X.C., Laflen J.M., and Simanton J.R. 1995, Soil component.USDA-Water Erosion Prediction Project. Hillslope profile and Watershed Model documentation. NSERL Report 10.

Alhammadi M.S. and Miller M. 2006, Effect of ionic strength and sodium adsorption ratio on the flocculation/dispersion of two surface soils from eastern Arkansas. Soil science, **171**: 960-967.

Amos C.L., Feeney T., Sutherland T.F., and Luternauer J.L. 1997, The stability of fine-grained sediment from the Frase River Delta. Estuarine, coastal and shelf science, **45**: 507-524.

Ariathurai R., and Arulanandan K. 1978, Erosion rates of cohesive soils. Journal of Hydraulics Engineering, ASCE, **104(2)**: 279-283.

Arulanandan K. 1975, Fundamental aspects of erosion of cohesive soils. Journal of Hydraulics Engineering, ASCE, **101(5)**: 635-639.

ASTM standard D422-63. 2007, Standard Test Method for Particle-Size Analysis of Soils. ASTM International, West Conshohocken, PA.

ASTM standard D2487-11. 2011, Standard practice for classification of soils for engineering purposes (unified soil classification system). ASTM International, West Conshohocken, PA.

ASTM standard D2974-13. 2013, Standard Test Methods for Moisture, Ash, and Organic Matter of Peat and Other Organic Soils. ASTM International, West Conshohocken, PA.

ASTM standard D3080-11. 2011, Standard test method for direct shear test of soils under consolidated drained conditions. ASTM International, West Conshohocken, PA.

ASTM standard D4318-10. 2010, Standard Test Methods for Liquid Limit, Plastic Limit, and Plasticity Index of Soils. ASTM International, West Conshohocken, PA.

ASTM standard D5907-09. 2009, Standard test method for filterable and nonfilterable matter in water. ASTM International, West Conshohocken, PA.

ASTM standard D6913-04. 2009, Standard Test Methods for Particle-Size Distribution (Gradation) of Soils Using Sieve Analysis. ASTM International, West Conshohocken, PA.

Barbosa R.N., and Overstreet C. 2011, What is soil electrical conductivity. LSU Ag Center publication, pub.3185.

Berkhovskikh V.F., Debolsky V.K., Vishnevskaya G.N., and Zolotareva N.S. 1991, Erosion of cohesive bottom sediments: the influence of the Benthos. Journal of Hydraulic Research, **29(2)**: 149-160.

Briaud J.L., Ting F.C.K., Chen H.C., Cao Y., Han S.W., and Kwak K.W. 2001, Erosion function apparatus for scour rate predictions. Journal of Geotechnical and Geoenvironmental Engineering, **127(2)**: pp.105-113.

Briaud J.L. 2005, Erodibility of fine grained soils and new soil test. Erosion of Soils and Scour of Foundations, ASCE, GSP 135.

Budu M. 2000, Soil mechanics and foundations. John Wiley and Sons Inc.

Carroll D. 1959, Ion exchange in clays and other minerals. Geological Society of America Bulletin, **70(6)**: 749-780.

Carlson E.J. and Enger P.F. 1962, Studies of tractive forces of cohesive soils in earth canals. US Department of the Interior Bureau of Reclamation, Denver, USA, Report N0. Hyd-504.

Crowley R.W., Bloomquist D., and Robeck C. 2012, Description of erosion rate testing devices and correlations between rock erosion rate and cohesion. ICSE6, Paris, pp. 205-213.

Crowley R.W., Robeck C., and Thieke R.J. 2014, Computational modeling of bed material shear stresses in piston-type erosion rate testing devices. Journal of

Hydraulic Engineering, ASCE, **140(1)**: 24-34.

Debnath K. and Chaudhuri S. 2010, Cohesive sediment threshold: A review. ISH Journal of Hydraulic Engineering, **16(1)**: pp. 36-56.

De Santis F., Giannossi M.L. Medici L., Summa V., and Tateo F. 2010, Impact of physico-chemical soil properties on erosion features in the Aliano area (southern Italy), Catena, **81**: 172-181.

Dunn I. S. 1959, Tractive resistance of cohesive channels. Journal of Soil Mechanics and Foundations, **85**: 1-24.

Dynasonics. 2001, Model UFX ultrasonic flow meter operation manual. Dynasonics, USA.

Gyssels G., Poesen J., Van Dessel W., Knapen A., and Debaets S., 2006, Effects of cereal roots on detachment rates of single and double-drilled topsoils during concentrated flow. European Journal of Soil Science, **57**: 381-391.

Hanson G.J. and Simon A. 2001, Erodibility of cohesive streambed in the loess area of the midwestern USA. Hydrological Processes, **15**: 23-38.

Hendershot W.H., Lalande H., and Duquette M. 2006, Ion exchange and exchangeable cations. Soil sampling methods and analysis, Canadian society of soil science. Tylor & Francis group for CRC press chapter 18.

Huang J., Hilldale R.C., and Greimann B.P. 2006, Cohesive sediment transport. Erosion and sedimentation manual, Chapter 4, US Department of the Interior Bureau Reclamation.

Julian J.P, and Torres R. 2006, Hydraulic erosion of cohesive riverbanks. Geomorphology, **76**: 193-206.

Kimiaghalam N., Goharrokhi M., Clark S.P. and Ahmari H. 2013. Riverbank erosion on the Red River in Winnipeg. 21st Canadian Hydrotechnical Conference (CSCE), Alberta, Canada, paper: CSCE-64.

Leonard L. and Richard G. 2004, Estimation of runoff critical shear stress for soil erosion from soil shear strength, Catena, **57**: 233-249.

Maa J.P.Y., Sanford L. and Halka J.P. 1998, Sediment resuspension characteristics in Baltimore Harbor, Maryland. Marine Geology, **146:** 137-145.

Mamo M., Bubenzer G.D. 2001a, Detachment rate, soil erodibility and soil strength as influenced by living plant roots part I: laboratory study. Transactions of the ASAE, **44(5)**: 1167-1174.

Mamo M. and Bubenzer G.D. 2001b, Detachment rate, soil erodibility and soil strength as influenced by living plant roots part II: field study. Transactions of the ASAE, **44(5)**: 1175-1181.

Mehta A.J. and McAnally W.H. 2007, Fine-grained sediment transport. In Sedimentation engineering, H. Garcia (eds), ASCE manuals and reports No. 110, ASCE, Chapter 4, pp. 253-307.

Meng X.M., Jia Y.G., Shan H.X., Yang Z.N. and Zheng J.W. 2012, An experimental study on erodibility of intertidal sediments in the Yellow River delta, International Journal of Sediment Research, **27**: 240-249.

Middleton H.E. 1930, Properties of soils which influence soil erosion. USA Department of Agriculture, Washington D.C., Technical Bulletin No.178.

Miller J.J. and Curtin D. 2006, Electrical conductivity and soluble ions. Soil sampling methods and analysis, Canadian society of soil science. Tylor & Francis group for CRC press chapter 15.

Mitchener H, and Torfs H. 1996, Erosion of mud/sand mixtures. Coastal Engineering, **29**: 1-25.

Mostafa T.S., Imran J., Chaudhry M.H. and Khan I.B. 2008, Erosion resistance of cohesive soils. Journal of Hydraulics Research, 46(6): 777-787.

Otsubo K,and Muraoka K. 1988, Critical shear stress of cohesive bottom sediments. Journal of Hydraulics Engineering, ASCE, **114(10)**: 1241-1256.

Partheniades E. 1965, Erosion and deposition of cohesive soils. Journal of Hydraulics Engineering, ASCE, **91(1)**: 105-138.

Paterson D.M. 1997, Biological mediation of sediment erodibility: ecology and physical dynamics. In Cohesive sediments, N. Burt, R. Parker, and J. Watts (eds), John Wiley and Sons, pp.215-229.

Rashidi M. and Seilsepour M. 2011, Prediction of soil sodium adsorption ratio based on soil electrical conductivity. Middle-East journal of scientific research, **8(2)**: 379-383.

Reddi L.N. and Bonala M.V.S. 1997, Critical shear stress and its relationship with cohesion for sand-kaolinite mixtures. Canadian Geotechnical Journal, **34**: 26-33.

Sanson L.S., Saha U. and Kissel D.E. 2010, Soil salinity testing, data interpretation and recommendations. University of Georgia.

Sherard J.L., Decker R.S. and Ryka N.L. 1972, Piping in earth dams of dispersive clay. ASCE soil mechanics and foundation conference, Perdue University, Lafayette.

Slagle P.M., 2006. Correlations of erosion rate-shear stress relationships with geotechnical properties of rock and cohesive sediments. M.S. thesis, University of Florida, Gainesville, FL.

Smerdon E.T., and Beasley R.P. 1961, Critical tractive forces in cohesive soils. Agricultural Engineering, **42(1)**: 26-29.

Thorn M.F.C, and Parsons J.G. 1980, Erosion of cohesive sediments in estuaries: an engineering guide. Proc 3rd International Symposium on Dredging Technology. Bedford: BHRA, 349-358.

Winterwerp J.C., Cornelisse J.M., and Kuijper C. 1990, Parameters to characterize natural muds. In Abstract Volume, Int. Workshop on Cohesive Sediments, Brussels, KBIN Brussels, 103-105.

YoungHui Z., JinYou L., Hongzhi L., JiaSheng W., BeiLin F. and ShiMing Y. 2008, Research on cohesive sediment erosion by flow: An overview. Science in China, **51(11)**: 2001-2012.

CHAPTER 3: COMPREHENSIVE FLUVIAL GEOMORPHOLOGY STUDY OF RIVERBANK EROSION ON THE RED RIVER IN WINNIPEG, MB, CANADA

A version of this chapter has been published in Journal of Hydrology:

Kimiaghalam, N., Goharrokhi, M., Clark, S. P., and Ahmari, H., 2015. *A comprehensive fluvial geomorphology study of riverbank erosion on the Red River in Winnipeg, Manitoba, Canada*. Journal of Hydrology, 529: 1488-1498.

Riverbank erosion on the Red River in Winnipeg, Manitoba has raised concerns over the last 20 years and more. Although several recent studies have shown that fluvial erosion can reduce riverbank stability and promote geotechnical slope failure, there are too few that have focused on this phenomenon. The present study includes field measurements, experimental testing, and numerical modelling to quantify fluvial erosion through an 8.5 km reach of the Red River. Results have shown that seasonal freeze-thaw processes can dramatically reduce the critical shear stress and increase erodibilty of the riverbanks. Moreover, a simple method has been employed using hydrodynamic numerical models to define the applied shear stresses on the river banks based on the river water level, which will be useful for further research and design purposes. The TEMP/W numerical model was used to define seasonal frost depth to estimate freeze-thaw effects. Finally all field measurements, experimental and numerical models results were used to predict annual

fluvial erosion through this reach of the river.

3.1 *Introduction*

Riverbank erosion has physical, ecological and socio-economic effects on fluvial environments (Rinaldi and Darby, 2007). Riverbank erosion has two important consequences: 1) land loss during fluvial or slope failures that can cause economic losses or safety issues; and 2) impact on downstream water quality, such as increased turbidity and sediment concentration which may be harmful for aquatic environments. One of the main differences between riverbanks and riverbeds is the direct contact of riverbanks with the surrounding environment; therefore changes in weather and climate have a more direct influence on riverbank behaviour. Riverbank erosion is a function of its soil properties, and any change in the soil structure may change the soil behavior. These effects are significant in cohesive soils since clay particle behavior is highly impacted by any natural or engineering process that changes the physical relationship between these particles (Torrance 1975). In Canada, subaerial processes like seasonal freeze-thaw are the most common physical processes that can affect riverbank soil properties (Graham and Au, 1985). In particular, Manitoba in Western Canada is famous for its severe cold weather during the winters. Thus, it is essential to understand the effects of freeze-thaw processes on riverbank erodibility, in addition to the effect of various hydraulic factors.

The main riverbank failure mechanisms are: 1) fluvial or hydraulic erosion due to the applied shear stress induced by flow or waves; 2) geotechnical slope failure due to the variation of effective stress and pore water pressure through the soil structure; 3) a combination of fluvial and geotechnical failures, which is especially common in composite banks. Quantifying the effect of each scenario is very difficult due to the

complex nature of fluvial erosion and geotechnical instabilities. Moreover, the situation becomes more complicated when riverbanks contain cohesive soil. Studies suggested that 10% clay content in a soil structure is sufficient to cause the soil to behave like a cohesive soil (Debnath and Chaudhuri (2010)). Erosion problems on the Red River banks in Winnipeg, Manitoba are therefore complicated due to high clay content in the riverbank material matrix. Riverbank erosion in Winnipeg has accelerated since the 1990s, particularly on the Red River due to a number of spring and summer floods and this has caused an increase in property taxes (Jansen 2012). Several researchers have conducted slope stability studies on the Red River where the main focus was mass slope failure. Baracos and Graham (1981) conducted a study to investigate parameters that affect slope stability on the Red River. Baracos and Lew (2003) suggested that fluvial erosion may impact the slope stability safety factor, and Fernando (2009) conducted a study to quantify the effect of fluvial erosion on the slope stability safety factor. All these studies were focused on slope failures due to geotechnical factors, however there are few studies on fluvial surface erosion due to hydraulic forces in this area. Kimiaghalam et al. (2015) conducted an experimental study to find effective variables on critical shear stress and erosion rate of cohesive riverbanks in Manitoba (including the Red River) due to fluvial surface erosion. Of the 15 different physical, mechanical, and electrochemical soil properties tested, soil cohesion was the best predictor of critical shear stress and erosion rate. Results also indicated that sodium adsorption ratio (SAR) had an effect on erosion rate. The following equations were suggested to estimate the critical shear stress and erosion rate of cohesive Manitoban riverbanks:

$$\tau_c = \alpha\, C + \beta \qquad \textbf{Equation 3-1}$$

$$E = f(SAR)(\tau_a - [\alpha C + \beta]) \quad \textbf{Equation 3-2}$$

where τ_c is the critical shear stress [Pa], C is the cohesion [kPa], α and β are empirical constants ($\alpha = 0.89$ and $\beta = -0.1$), τ_a [Pa] is the applied shear stress and E [mm/hr] is the erosion rate.

Subaerial processes like wetting and drying (change in natural water content) of the soil and seasonal freeze-thaw can affect both fluvial erosion and mass slope failure processes (Thorne, 1982, Lawler et al. 1997, 1999). Lawler (1993) estimated that 32-43% of total bank erosion within the River Ilston in UK was caused by needle ice formation. Yumoto et al. (2006) found 20-60% contribution of subaerial processes on total bank erosion along a small stream in central Japan. Couper and Maddock (2001) suggested that subaerial processes were underestimated on the River Arrow in UK and can have significant impact on erosion. Couper (2003) studied remoulded samples from the River Arrow and found that freeze-thaw cycles had a more significant effect on the riverbank erosion than wetting-drying cycles. Wynn et al. (2008) used a submerged-jet type erosion measurement device to show that critical shear stress and slope of erosion rate varied seasonally, and that erodibility increased with increasing number of freeze-thaw processes in their study area within the Stroubles Creek watershed in Virginia, USA. Seasonal freeze-thaw (FT) can alter cohesive soil behaviour; however, due to the different clay minerals in different locations, these changes may not have a similar pattern and quantity. Therefore it is vital to understand the effect of FT processes on local soil in a study area. There is currently no specific study on the effect of FT on riverbank erodibility in Manitoba. Graham and Au (1985) conducted an experimental study to investigate the effect of 5 FT cycles on the stress-strain behavior of Winnipeg clay at low

normal stresses. They found a reduction in shear strength after 5 FT cycles. Mixtures of silt and clay are more susceptible than non-cohesive soils to significant negative FT effects (Couper 2003). In particular, the silt content can control the intensity of these effects because voids between silt particles are small enough to form high capillary forces to move water toward the soil surface where cold air can freeze the pore water between the voids. On the other hand, voids between silt particles are big enough to allow ice lenses to form inside the soil structure. As ice lenses form in the soil structure the frozen water expands and inter-particle bonds become weaker, therefore lower shear strength and critical shear stress are expected after thaw. Still, there is no numerical formulation to predict the behaviour of different soils under different FT conditions. The intensity of the effect of freezing and thawing varies with soil texture, moisture, and extent of freezing. Several investigators hypothesised that freezing and thawing increase soil erodibility. Formanek et al. (1984) found that the shear strength of a silt loam was reduced to less than half its original strength after one FT cycle but the second and third cycles resulted in little reduction. Van Klaveren (1987) suggested that the critical shear stress of soil might be half of its initial value after the first cycle. Edwards et al. (1995) found that a mean sediment yield for frozen soil was 25% greater than a similar soil with no freezing history. Van Klaveren & McCool (1998) found that erodibility of thawed soils increased slightly after a single FT cycle. Ferrick and Gatto (2005) performed three experiments with low (16%-18%), mid (27%-30%), and high (37%-40%) water content over different freezing periods and a 24 hour thawing period. They found significant increase in erosion rate during runoff with increasing water content. Van Klaveren and McCool (2010) found that when silt loam soil freezes, resistance against erosion increased, but when the

thawing process started, the soil surface began to reduce its erosion resistance.

This study focused on flow-induced surface erosion on the Red River bank in Winnipeg, Manitoba, Canada and the effect of seasonal freeze-thaw on this process. The study included field measurements, experimental testing, and numerical simulations to summarize fluvial erosion on the riverbanks for both practical and research purposes. Moreover, this study includes new findings on the effect of several freeze-thaw (FT) processes on the behavior of natural cohesive riverbanks in Winnipeg that would be useful for the design of erosion protection projects.

3.2 *Study Area, Sampling, and Field Measurement*

The study area was an 8.5 km reach of the Red River passing through the City of Winnipeg in Western Canada; flowing from the South Perimeter Bridge (49°47'04" N and 97°08'07" W) to the Fort Gary Bridge (49°49'17" N and 97°08'35" W) (Figure 3.1). Winnipeg is famous for its harsh winters with an average low temperature of -20.2°C in winters (The Forks station, Environment Canada). The riverbank consists of a combination of lacustrine clay soils and alluvial deposits. Water elevation can be influenced by the St. Andrews Lock and Dam (50°05'02" N and 96°56'28" W), located 36 km downstream. Water level variation is typically on the order of 6 m annually. Mean annual discharge is 176 m^3/s, with peak discharges on the order of 1300 m^3/s. At mean flow conditions the average channel top width and water depth are 130 and 3.5 m, respectively. The river is highly sinuous within the city of Winnipeg, and has an average channel bottom drop of 3.8 m per 100 km, with side slopes varying from gradual to steep. Typical midsummer total suspended sediment concentrations are on the order of 121

mg/L, with peak values on the order of 1500 mg/L during high flow conditions. Total suspended solids drop to a concentration of approximately 10 mgL^{-1} under a solid ice cover during the winter months (Weiss, 2012).

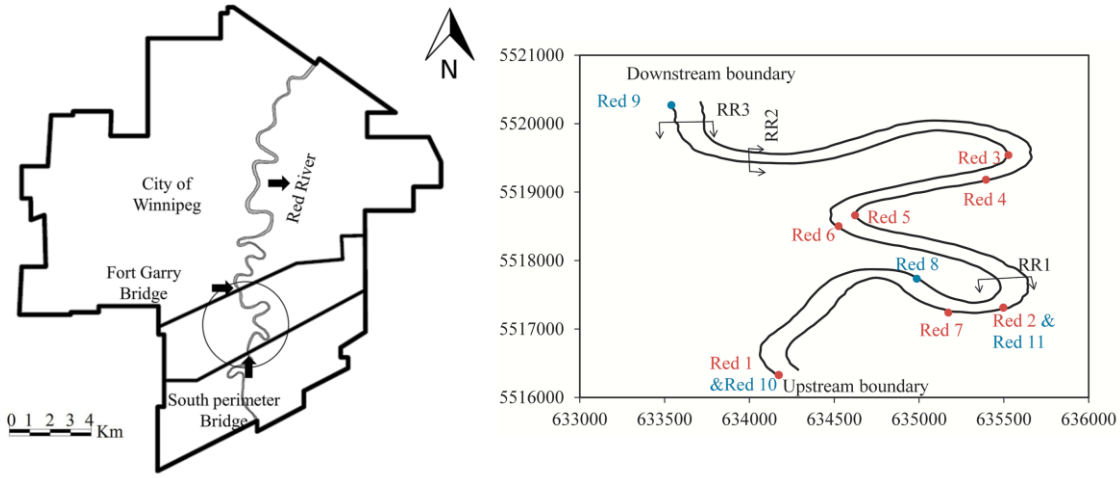

Figure 3.1 Study area and sampling map in UTM 14 coordinate (Red 1-Red 7 samples were used to perform erodibility test under normal condition without FT processes, Red 8- Red 11 were used to perform erodibility test under normal and FT process, and RR1-RR3 show locations of velocity profile measurement using an ADCP for hydrodynamic model validation

Eleven soil samples were taken from different locations along the riverbanks. The sampling procedure was to remove the disturbed top soil layer and take vertical samples from the surface of the bank. Samples were collected at least 0.5 m below the bank surface at locations near the water surface that had just recently been exposed to the atmosphere. For this purpose standard ASTM Shelby tubes were used to take relatively undisturbed samples which were essential for this study. To maintain the natural water content, the soil samples were sealed and kept in a refrigerator. Seven soil samples, Red 1 to Red 7, were used to measure the erodibility of natural cohesive riverbanks and the four remaining samples, Red 8 to Red 11, were used to investigate the effects of seasonal freeze-thaw on riverbank erodibility. Samples Red 10 and Red 11 were taken from the same location as Red 1 and Red 2, respectively. Sample Red 7 was taken from freshly

deposited, post-flood material with high plastic clay to understand the resistance of this material to fluvial erosion.

Measuring high-resolution bathymetry and flow data was another important component of this study that was essential for developing an accurate numerical model and understanding the river behaviour over time. A SonTek River Surveyor M9 acoustic Doppler current profiler (ADCP) was used to collect bathymetric data and flow characteristics in 2012. This device was equipped with a RTK-GPS system with ± 3 cm resolution. The ADCP was mounted to a hydroboard and pulled with a boat at a speed of less than 1 m/s. The procedure was to combine streamwise profiles with lateral transects at approximately 12 m spacing. Moreover, in June 2013, August 2014, and September 2014 after high flow events, 8 km of the study area was resurveyed to quantify morphological changes between 2012 and 2014.

3.3 *Experimental Setup*

3.3.1 *Fluvial erosion properties*

A piston-type erosion measurement device (EMD) similar to that described in Briaud et al. (2001) was used to estimate critical shear stress and erosion rate of each soil sample for different flow conditions. Constructed by the geotechnical group of the University of Manitoba, the device includes an acrylic rectangular conduit, a reservoir, and a pump (Figure 3.2). An ultrasonic flow meter was installed on the straight circular inflow pipe to measure discharge through the conduit. The main acrylic conduit is 2.80 m long, 0.1 m wide and 0.05 m high. A piston and sampling tube is located 2.50 m downstream of the conduit entrance to ensure that all flow measurements were taken in relatively fully

developed turbulent flow. The test procedure was to flush the soil sample with the bottom of the conduit, wait until the flow became steady and push the sample up 1 mm into the flow for an hour and record the amount of erosion (Figure 3.2). The procedure was repeated several times with different flow rates to obtain enough points for estimating critical shear stress and erosion rate. The following equation was used to calculate applied shear stresses:

$$\tau_a = \frac{1}{8} f \rho V^2 \qquad \textbf{Equation 3-3}$$

where V [ms^{-1}] is the measured conduit mean velocity, f [-] is the friction factor that is calculated from Colebrook's equation (Munson et al., 2012):

$$\frac{1}{\sqrt{f}} = -2\log\left(\frac{\varepsilon/D}{3.7} + \frac{2.51}{Re\sqrt{f}}\right) \qquad \textbf{Equation 3-4}$$

where ε [m] is the sample surface roughness which was estimated as $0.5d_{50}$ according to Briaud et al. (2001), D [m] is the hydraulic diameter, and Re [-] is the conduit Reynolds number that varied between 6,000 and 220,000 and was calculated by the following equation:

$$Re = \frac{\rho V D}{\mu} \qquad \textbf{Equation 3-5}$$

where μ [Ns/m^2] is the dynamic viscosity. ASTM standards D422-63 (ASTM, 2007) and D2487-11 (ASTM, 2011a) were used to measure the grain size distribution of the soil samples, as well as sand, silt, and clay fractions.

Equivalent height of erosion was estimated based on measurements and engineering judgment. Long-term tests (24-48 hours) were performed to ensure consistency and repeatability of the erosion rates, in addition to the regular one hour duration tests. The

piston was calibrated to ensure that its movement was within ± 0.1 mm for each step. While smoothening the surface of the sample at each step using a wire, the weight of the protruded portion was measured and based on the location of this piece with respect to the conduit bottom this weight was converted to the equivalent height of the sample and added to or reduced from the total protrusion of the sample at each step.

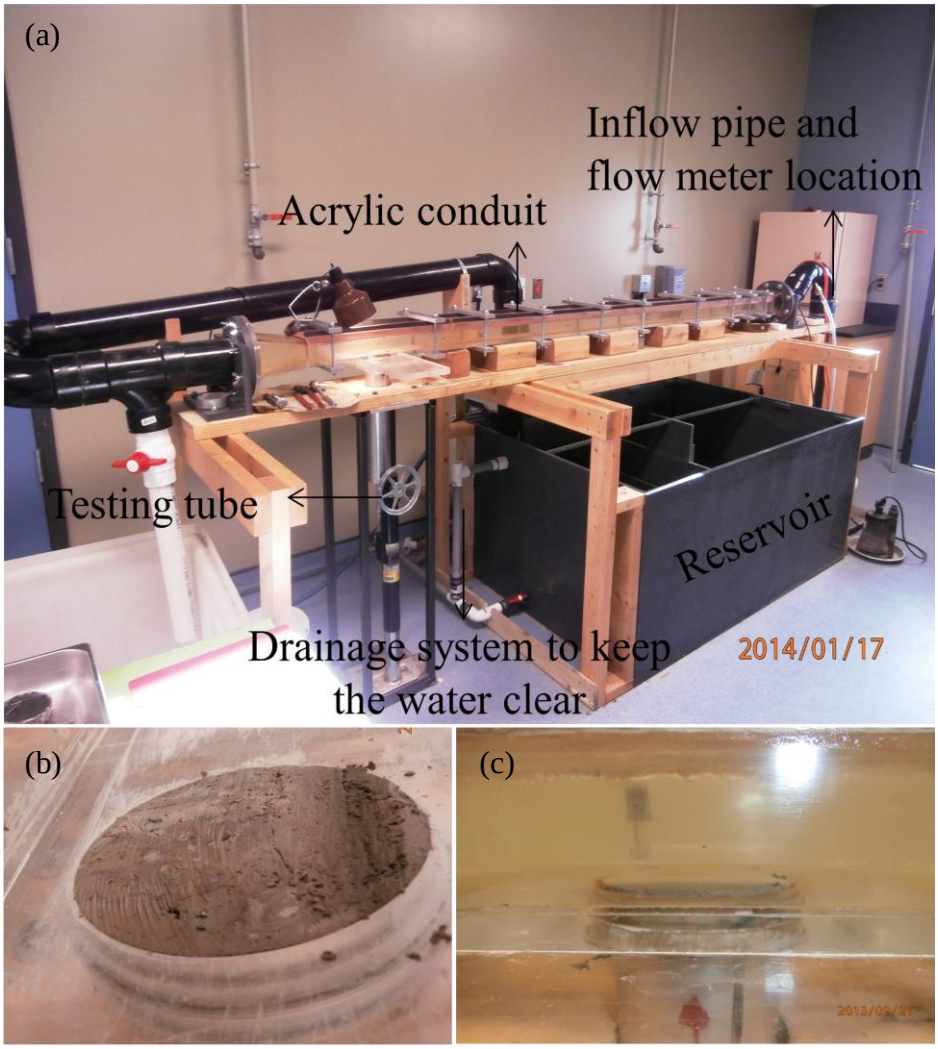

Figure 3.2 (a) Erosion Measurement Device, (b) flushing the sample surface before starting the test , and (c) 1 mm sample protrusion after starting the test

Finally, Partheniades (1965) erosion model was used to calculate the critical shear stress and material dependent coefficient of the soil samples:

$$E = k_d(\tau_a - \tau_c) \qquad \textbf{Equation 3-6}$$

where E [mm/hr] is the erosion rate, k_d is a material dependent coefficient, and τ_c [Pa] is the critical shear stress. For each soil sample a linear trend was found for measured erosion rates versus calculated applied shear stresses, and τ_c was estimated as the shear stress axis intercept while k_d was taken as the line slope (Figure 3.3).

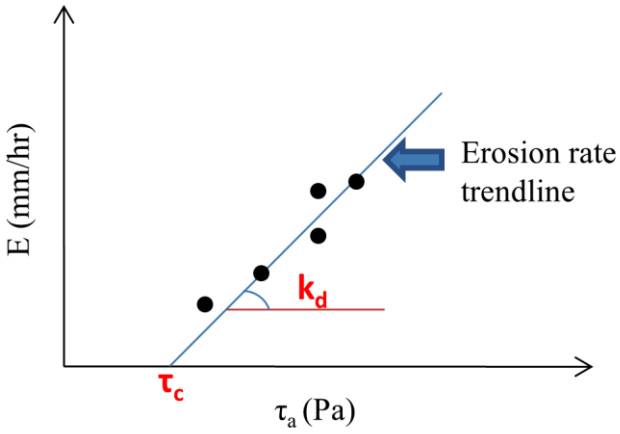

Figure 3.3 Typical EMD test result

3.3.2 *Freeze-thaw effects on erodibility*

Previously, Kimiaghalam et al. (2015) found a linear correlation between critical shear stress and cohesion of the Red River banks soil samples. Samples Red 8 to Red 11 were taken close to the downstream and upstream boundaries to conduct an experimental study to understand erodibilty properties of the riverbank after seasonal FT process. These soil samples were taken from the same depth using a core sampler of 7.4 cm diameter and 15.24 cm length. Soil samples were taken after a high flow event in August 2013 and from the depth that material had not experienced any FT cycle.

Freezing processes were undertaken using an ice room in the hydraulics laboratory at the University of Manitoba; where each soil sample experienced one, five, and ten FT cycles. The freezing and thawing durations were 24 hours each, and the freezing temperatures used were -2^{o}C and -15^{o}C. During the whole FT process, the soil samples were kept inside the original sealed plastic sleeves used for sampling to maintain natural water content without any access to extra water and also to avoid lateral displacement. Critical shear stress and erosion rate were obtained for each FT condition and also for normal condition without any FT history using both Equations 3.1 and 3.2 for Red 8 and Red 9 samples and also direct measurement using the EMD method for Red 10 and Red 11 samples.

To calculate erodibility properties of the soil sample according to Equation 3.1_and also to understand changes in mechanical properties of the riverbank, direct shear tests were conducted according to the ASTM standard D3080-11 (ASTM, 2011b) under completely saturated conditions to ensure that only FT effects were assessed. Each direct shear test had two phases and at least three direct shear tests were needed to calculate cohesion of these samples from the failure envelope. Each sample was first consolidated for 24 hours. Consolidation pressures were 40, 60, and 80 kPa based on the sampling depth and also to understand the behavior of the soil sample over the entire active layer thickness. The active layer in this study was defined as the soil thickness that experienced both seasonal freeze and thaw. A 0.0015 mm/min shearing rate was used according to standard procedures. Figure 3.4 shows typical results of the direct shear test for each sample. After finding the failure line based on the strain versus shear stress graphs, cohesion was found as the intercept of the failure line on the shear strength versus consolidation stress graph.

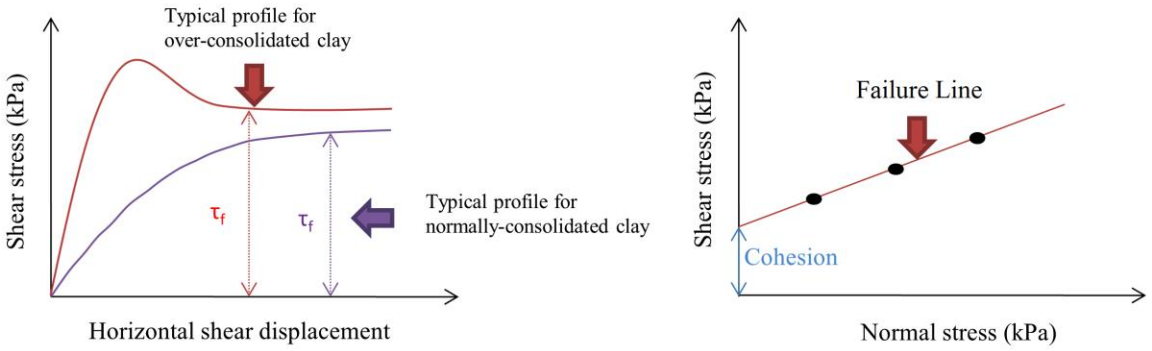

Figure 3.4 Typical direct shear test results

3.4 *Thermal Modelling*

3.4.1 *Main governing equations and key input variables*

The TEMP/W model by Geo-Studio is a 2D finite element model that was used to estimate the active soil layer thickness and the number of freeze-thaw cycles through the study area over 2010-2014. One of the main reasons for using TEMP/W was its ability to use climate data as a boundary condition for transient analysis since in-situ soil temperature measurements were not made. The main governing heat flow equation in the model is as follows:

$$\frac{\partial}{\partial x}\left(k_x \frac{\partial T}{\partial x}\right) + \frac{\partial}{\partial y}\left(k_y \frac{\partial T}{\partial y}\right) + Q_T = \lambda \frac{\partial T}{\partial t} \qquad \textbf{Equation 3-7}$$

where k_x [W/(mK)] is the thermal conductivity in the x-direction, k_y [W/(mK)] is the thermal conductivity in the y-direction, Q_T [W/m^2] is the applied thermal boundary flux, T [$^\circ$C] is the soil temperature, λ [J/(kgK)] is the heat capacity, and t [s] is time.

A full thermal material model was used to input essential soil thermal properties to the model. Thermal conductivity, unfrozen volumetric water content, volumetric heat

capacity, and in-situ volumetric water content were the essential properties for the thermal modelling. Thermal conductivity was entered as a function of temperature in the model. Unfrozen and frozen thermal conductivity were calculated using Farouki's (1985) equations that were developed for fine-grained soils:

$$k_{uf} = 0.1442(0.9\log w - 0.2)(10)^{0.6243\rho_d} \quad \textbf{Equation 3-8}$$

$$k_f = 0.001442\ (10)^{1.373\rho_d} + 0.01226(10)^{0.4994\rho_d} w \quad \textbf{Equation 3-9}$$

where w [%] is the in-situ water content, ρ_d [kg/m^3] is the soil bulk density, k_{uf} [W/(mK)] is the unfrozen thermal conductivity, and k_f [W/(mK)] is the frozen thermal conductivity. Unfrozen water content was estimated by TEMP/W functions for different soil types. In-situ volumetric water content (θ) [m^3/m^3] was calculated using measured gravimetric water content and bulk density as follows:

$$\theta = \frac{w}{1+w}\left(\frac{\rho_b}{\rho_w}\right) \quad \textbf{Equation 3-10}$$

where ρ_b [kg/m^3] is the soil bulk density and ρ_w [kg/m^3] is the water density.

Frozen and unfrozen volumetric heat capacity for the saturated soil samples were calculated using measured bulk density and in-situ water content using the following equations Farouki (1985):

$$c_{vf} = \left(\frac{\rho_d}{\rho_w}\right)(0.18 + 0.5\frac{w}{100})c_{vw} \quad \textbf{Equation 3-11}$$

$$c_{vu} = \left(\frac{\rho_d}{\rho_w}\right)\left(0.18 + \frac{w}{100}\right)c_{vw} \qquad \textbf{Equation 3-12}$$

where c_{vf} [MJ/m^{3o}C] is the frozen volumetric heat capacity, c_{vu} [MJ/m^{3o}C] is the unfrozen volumetric heat capacity, and $c_{vw} = 4.187$ MJ/m^{3o}C is the water volumetric heat capacity. Table 3-1 shows the thermal properties of the material used in the modelling.

Numerical models were developed to simulate the riverbank temperature profiles between June 2010 and June 2014. To solve this transient analysis an initial condition and the soil surface boundary condition were necessary.

Table 3-1 Thermal modelling key input material properties

Sample ID	K_{uf} (Wm^{-1}K^{-1})	K_f (Wm^{-1}K^{-1})	C_{vf} (MJm^{-3o}C^{-1})	C_{vu} (MJm^{-3o}C^{-1})	θ (m^3/m^3)
Red1	1.17	2.25	3.13	2.06	0.37
Red2	1.23	1.94	2.78	1.93	0.32
Red3	1.05	2.23	3.14	2.02	0.37
Red4	1.00	2.49	3.42	2.13	0.40
Water & ice	0.58	4.18	2.31	1.84	1.00

3.4.2 *Initial and boundary conditions*

Steady state analysis was run to find the initial isotherm of the riverbank to use as an initial condition for the transient analysis. Thermal boundary conditions at the top and bottom of the riverbank were needed to develop the steady state analysis. The start date of the simulation was June 1, 2010. The top boundary condition was calculated as a function of air temperature with the assumption that the n-factor was equal 1 for this

initial condition. The bottom boundary condition was assumed to be constant temperature of 2°C based on the initial run of the model. Maximum and minimum daily temperature, maximum and minimum relative humidity, daily precipitation, wind speed, and latitude were the essential parameters for the top boundary condition. The Environment Canada weather station at the Forks in Winnipeg (49°53'18" N and 97°07'46" W) was used for the Red River. Geo-Studio used these climate parameters to find the temperature at the soil surface that is necessary for predicting the temperature profile through the soil. Generally the following equation was used to calculate soil surface temperature when there was no snow cover:

$$T_s = T_a + \frac{1}{\gamma f(u)}(Q^* - E) \qquad \textbf{Equation 3-13}$$

where T_s [°C] is the temperature at the soil surface, T_a [°C] is the air temperature, γ [-] is the psychrometric constant, Q^* [mm/day] is the net radiant energy available at the surface, E [mm/day] is the actual vertical evaporation flux, and $f(u)$ is a wind function. If there was snow cover, surface temperature was determined based on the energy balance equations. If there was precipitation and the air temperature was cold enough, a fresh snow albedo of 0.85 was used.

3.4.3 *Analysis and results*

The general geometry of the sites was obtained from bathymetry measurements for the Red River. Also, the elevation of the average winter ice cover was around 224 m. The soil was assumed to be homogenous and seepage and water flow through the riverbanks were neglected since the cohesive riverbanks had low hydraulic conductivity, in

particular during the frost process. Water elevation was assumed to be constant during the frost seasons. Square meshes with dimension of 0.30 m were assigned to the model.

For estimating the freeze-thaw pattern of the riverbank, a transient analysis was run for a duration of 1492 days for 4 soil samples with different properties. Steady-state analysis was run to find the necessary initial isotherm of the model with available data on June 1st, 2010. Figure 3.5 shows the numerical model results for the study area and variation in thickness of the active layer for each year. Most of the riverbank experienced just one FT cycle annually but the top 0.4 m of the soils experienced an average of 3 FT cycles annually. The maximum depth of the active layer varied between 1.2-2.3 m.

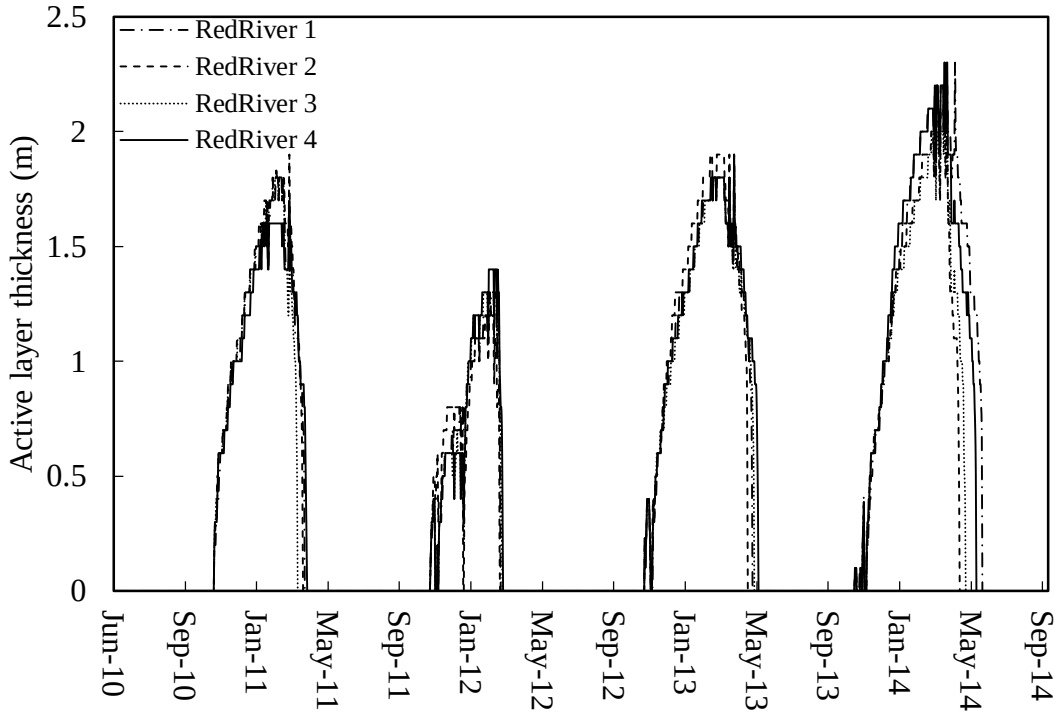

Figure 3.5 Variation of the active layer thickness between 2010 and 2014

3.5 *Hydrodynamic Numerical Modelling*

To estimate the applied shear stresses over the riverbanks a MIKE 21 flow model with flexible mesh was developed. The hydrodynamic module (HD) was used to simulate the study area to find essential hydrodynamic flow properties, while the Mud Transport module (MT) was used to calculate applied shear stresses over the river boundaries.

3.5.1 *Hydrodynamic simulation using MIKE 21 FM-HD*

The HD module is based on a finite volume solution of the two-dimensional Navier-Stokes equations for shallow water (DHI, 2012a). An accurate study domain, water levels at the boundaries, and upstream discharge are the key input parameters to develop a good hydrodynamic model. Bathymetry was acquired from ADCP measurements and the flexible mesh method were used to create the study domain. Mesh elements with a maximum allowable area of 150 m^2 and smallest allowable angle of 26^o were used.

Upstream discharge (used as upstream boundary condition) and water level were obtained from the Environment Canada hydrometric station 05OC008 at South Perimeter Bridge and the downstream water level (downstream boundary condition) was obtained from the City of Winnipeg gauge at Fort Garry Bridge. A Manning coefficient of 0.025 was used based on calibration to obtain the best fit between the measured and simulated upstream water level. Figure 3.6 shows the results of the model validation for the open water seasons of 2010 to 2014. As an additional model performance measure, Figure 3.7 shows the good agreement between measured and simulated velocity distributions over 6 different cross sections of the river along the study area on July 23, 2013 when the discharge was 231 m^3/s. Table 3-2 shows measured and simulated mean velocities for the

river for different discharges. All results demonstrate that the model was well calibrated and could be used to estimate applied shear stresses over the study area.

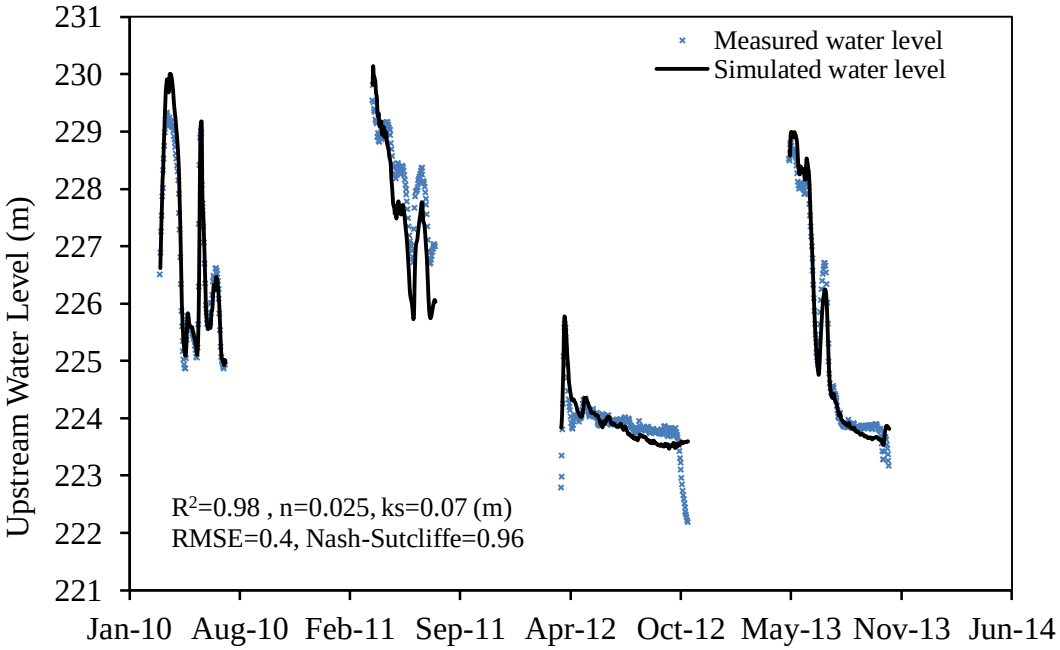

Figure 3.6 MIKE 21 FM model validation for 4 years between 2010 and 2014

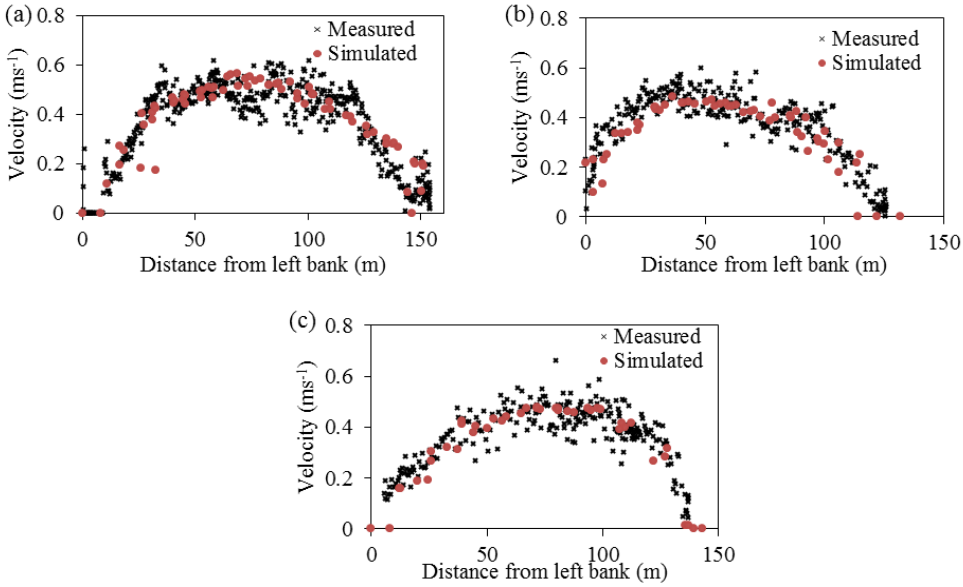

Figure 3.7 Measured velocity profile using ADCP versus simulated velocity profile using MIKE 21 on July 23th, 2013 (a) cross section RR1 (b) cross section RR2 (c) cross section RR3

Table 3-2 Measured and simulated Red River mean velocity

Discharge (m^3/s)	Mean observed velocity (m/s)	Mean simulated velocity (m/s)	Number of observed samples	Difference (%)
780	0.78	0.74	12956	5
660	0.67	0.65	13336	3
591	0.66	0.6	19621	9
458	0.51	0.54	18337	6
417	0.58	0.52	14340	10
367	0.55	0.49	9584	11

3.5.2 *Calculating applied shear stress using MIKE 21 FM-MT*

The MT module was paired with the HD module to calculate the applied shear stress distribution over the entire wetted perimeter of the river. Since wave action was neglected; the following equation was used to calculate the purely current-induced shear stress:

$$\tau_{a,c} = \frac{1}{2}\rho f_c V^2 \qquad \textbf{Equation 3-14}$$

where $\tau_{a,c}$ is the current applied shear stress, V is the mean current velocity, and f_c is the current friction factor that was calculated using (DHI, 2012b):

$$f_c = 2(2.5(\ln\left(\frac{30h}{k_s}\right) - 1)^{-2} \qquad \textbf{Equation 3-15}$$

where h [m] is the water depth and k_s [m] is the bed roughness. Water depth was directly calculated from the HD module and the average bed roughness (k_{s-ave}) over the boundaries was calculated based on the calibrated Manning's number using (DHI, 2012c):

$$\frac{1}{n} = \frac{25.4}{{k_s}^{1/6}}$$ **Equation 3-16**

Therefore, the average Red River bed roughness was found to be approximately 0.07 m. Figure 3.8 shows how the average simulated shear stress varied with discharge for the whole river as well as over the riverbanks alone. Based on the measured bathymetry and field observations, mesh elevations above 220 m were considered as riverbank and below 220 m were considered as the bed.

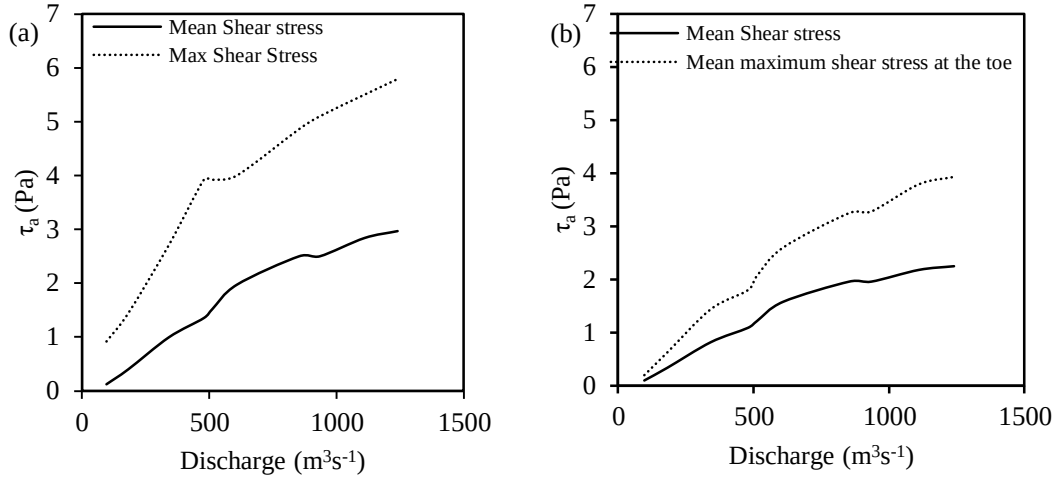

Figure 3.8 Variation of average and maximum applied shear stresses with river discharge for (a) the entire river, and (b) over the river banks only

3.6 *Results and Discussion*

3.6.1 *Red River flow and applied shear stress*

Results from the model indicated that a linear trendline with R^2=0.99 can be used to estimate river discharge from the measured water level at the upstream boundary:

$$ELE_{upstream} = 0.0046Q + 223.38$$ **Equation 3-17**

where $ELE_{upstream}$ [m] is the measured water level at the South Perimeter Bridge, and Q [m^3s^{-1}] is the river discharge. The average and maximum applied shear stresses on the riverbanks, at the toe, and the whole entire river can be estimated using Figure 3.8. Therefore, from the results of the hydrodynamic model, average shear stress over the riverbank and bed were calculated for different flow rates. Since the total amount of erosion is a function of time, a statistical analysis was done on the measured Red River discharges over four recent years to understand the duration of applied shear stresses over the riverbanks. Figure 3.9 shows the results of a frequency analysis on the Red River open water discharge for 2010 to 2014. On average, the open water season lasted 167 days per year and ice covered conditions were not considered since the discharge becomes very low during the winter. Figure 3.8 and 3.9 can be used together to provide a relatively straight forward tool that can be used to estimate both the magnitude and duration of specific applied shear stresses along this reach of river. These results are combined in Table 3-3, which could be used by a practicing engineer to assess the flow power for erosion. The down side of this tool, however, is that it does not take into account the timing of the events. For instance, a high applied shear stress on a completely frozen riverbank would potentially cause less erosion than the same shear stress on a bank that had recently experienced freeze-thaw processes.

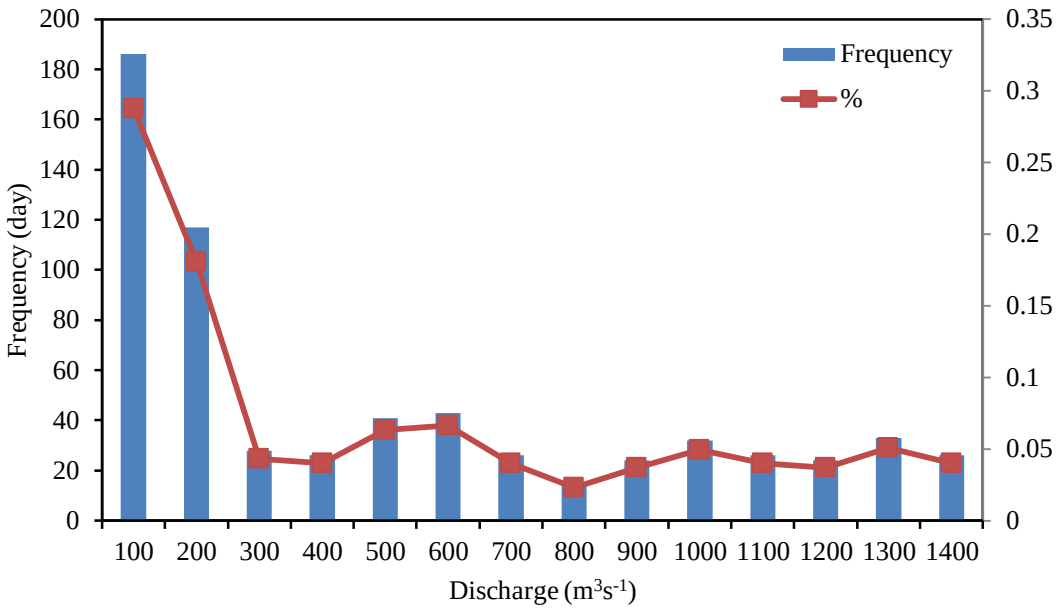

Figure 3.9 Frequency analysis on the river flow rates between 2010 and 2014

Table 3-3 Annual Red River discharge and applied shear stress distribution

Number of days	Discharge range (m^3/s)	Average applied shear stress on the riverbanks (Pa)	Maximum applied shear stress at the toe (Pa)
47	100	0.1	0.2
29	200	0.4	0.6
7	300	0.7	1.25
7	400	0.95	1.6
10	500	1.15	1.9
11	600	1.55	2.6
7	700	1.75	2.9
4	800	1.9	3.15
6	900	1.95	3.25
8	1000	2.05	3.5
7	1100	2.15	3.75
6	1200	2.25	3.9
8	1300	2.35	3.95
7	1400	2.4	4.1

3.6.2 *Erodibility properties of the Red River bank material*

Table 4-4 shows a summary of the EMD test results under normal conditions without any effect of FT processes and d_{50} of the soil samples. Red 4, Red 6, and Red 7 samples had median grain size of less than 2 μm which indicates that these soil samples had high clay content. Red 1, Red 2, and Red 3, and Red 5 had median grain size of less than 75 μm which indicates that that soil samples had very fine particles in the silt range. Overall, all the soil samples contained very fine grain material with considerable amounts of clay in their structure. These results indicate that there was no relationship between clay content and critical shear stress and erosion rate in this study area since soil samples with similar clay content had very different critical shear stresses and erosion rates. Red 5 sample with the lowest clay content and relatively high sand content had the lowest critical shear stress among the samples; while the other samples with similar grain size distribution had very different resistance to fluvial erosion. Except samples Red 1, Red 3, and Red 7, the other soil samples had a low critical shear stress and they were susceptible to erosion based on the calculated applied shear stresses over the riverbank (see Figure 3.8). It can be concluded that the banks of the Red River are impacted by fluvial erosion when flow rates exceed approximately 600 m^3/s. According to the frequency analysis (Figure 3.9) just less than 20% of the 4 year period during open water seasons would have had applied shear stresses that were high enough to cause riverbank erosion. The other interesting result from the EMD test was the relatively high erosion resistance of the freshly deposited sample, Red 7. This suggests that while a high shear stress will promote fluvial erosion during the peak of the annual hydrograph, the material deposited during the receding limb of the hydrograph may form a protective layer above the newly exposed

bank material.

Table 3-4 Riverbank soil properties without FT processes

Sample ID	d_{50} (mm)	Clay %	Silt %	Sand%	k_d	τ_c (Pa)
Red 1	0.0056	45	40	15	1.45	9.5
Red 2	0.0081	40	35	25	0.80	1.7
Red 3	0.015	33	28	39	1.32	9.4
Red 4	0.0017	40	55	5	1.19	1.9
Red 5	0.052	22	33	45	1.58	1
Red 6	0.0013	45	50	5	9.35	1.8
Red 7	0.0013	45	47	8	1.74	5.9

3.6.3 *Effect of freeze-thaw on the riverbank behavior*

Measurements and experiments showed that seasonal freeze-thaw processes can significantly affect the behavior of the cohesive riverbanks on the Red River. This is aided by the high variation of water level and severe cold weather during the winters in Winnipeg. The average winter water level in Winnipeg is 223 m, which is 4 meters above the toe of the riverbanks. Figure 3.10 shows a typical temperature profile from the TEMP/W model for a cross section close to the Red 1 sampling location on March 26th, 2010 which indicates that the depth of the active layer below the water surface elevation is quite similar to the rest of the bank that was exposed to the air. The zone between the blue lines is the location where temperatures were below freezing. The winter of 2014 was the coldest on record for Winnipeg in the recent years. Since the water depth during the winter is typically around 4 m, and the thermal model estimated an active layer thickness of 2.3 m in 2014, it can be concluded that the soil near the toe of the riverbank

will not experience any FT processes. Figure 3.11 shows the variation of cohesion and friction angle under different frost temperatures and different number of FT cycles. These results indicate that the first FT cycle can significantly affect cohesion of the riverbanks while friction angle was relatively constant. Moreover, the frost temperature did not significantly affect the mechanical behavior of these samples. After the first FT cycle the cohesion of the samples decreased by approximately 80% and after the fifth cycle the soil samples became relatively cohesionless. The TEMP/W model results showed that except for the 40 cm of the top layer that experienced an average of 3 FT cycles, the remainder of the riverbank experienced one FT cycle annually.

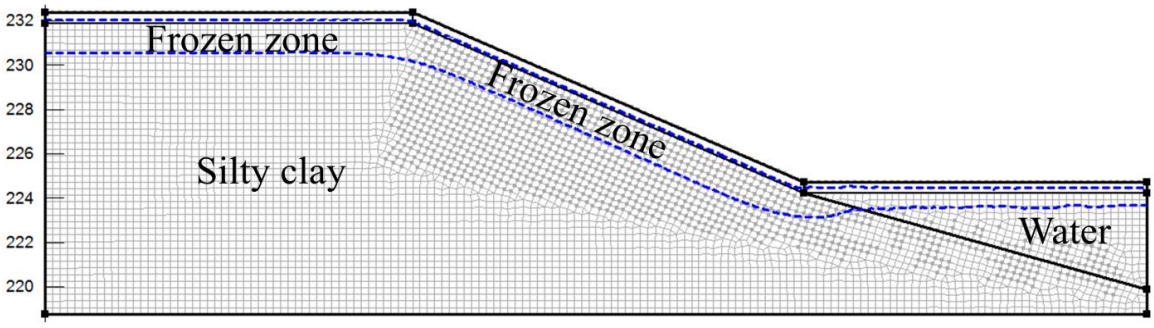

Figure 3.10 TEMP/W simulation for a Red River cross section close to the Red 1 sampling location on March 26th, 2011

Table 3-5 Results of the EMD test for samples Red 10 and Red 11 before and after 5 Ft cycles

Sample ID	Before FT		After 5 cycles FT	
	τ_c (Pa)	k_d	τ_c (Pa)	k_d
RED 10	9.5	1.45	0.5	1.5
RED 11	1.7	0.8	0	1.0

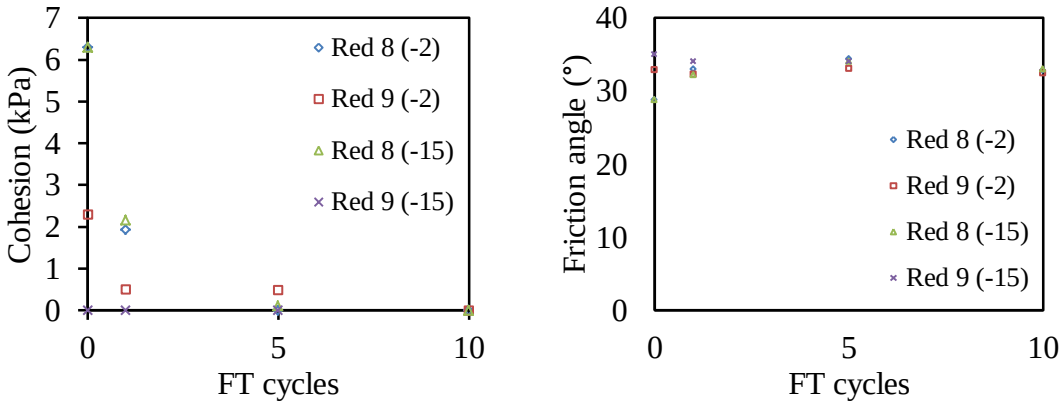

Figure 3.11 Variation of cohesion and friction angle of soil samples Red 8 and Red 9 with number of FT cycles and frost temperature

Visual investigation of the soil samples confirmed the effect of FT processes on the soil samples. Figure 3.12 shows a typical soil sample (Red 11) after one and five FT cycles at -2°C. Fissures and cracks became visible after the first cycle, and after the fourth and fifth cycle the soil structure became brittle and there was no evidence of any physical cohesion within the soil matrix and without any surrounding confining pressure the soil samples fell apart. Change in the cohesion of the failure line due to the FT process suggests two important considerations in design procedures. The first one is the significant effect of FT process on the riverbank erodibility. According to the Kimiaghalam et al. (2015), critical shear stress in the study area had a linear relationship with cohesion; therefore, it can be estimated that reducing the cohesion by 80% will result in an 80% reduction in critical shear stress of the soil samples. However, their results indicated that k_d is a function of SAR that could be considered constant. Table 3-5 shows a comparison between the erodibility of the soil samples before and after 5 FT cycles using the EMD to validate the effect of cohesion on the critical shear stress of the soil samples after FT processes. Samples Red 10 and Red 11 were taken from similar locations to sample 1 and 2; however, after 5 FT cycles samples became very weak and

brittle. These samples had shown resistance to fluvial erosion before any FT processes, especially sample Red 1; however, after 5 FT cycles the samples fell apart and there was no evidence of resistance to fluvial erosion.

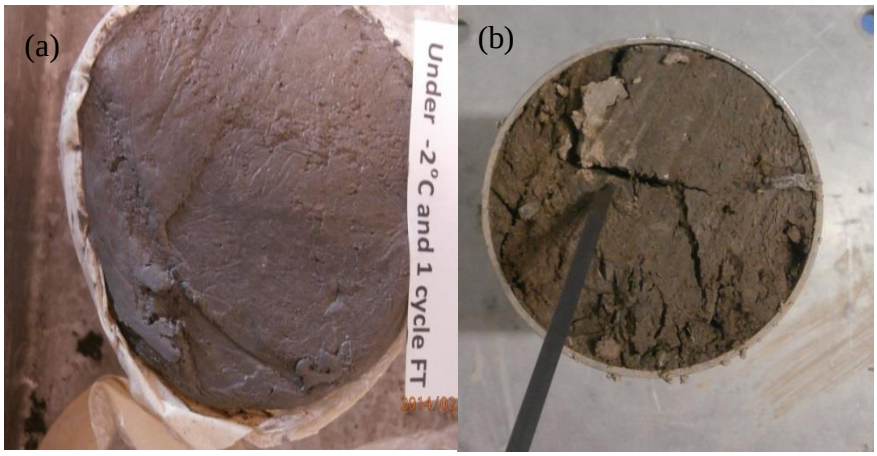

Figure 3.12 Typical Red River soil sample (a) after one and (b) five freeze-thaw cycles

Further evidence of significant change in erodibility of the riverbank due to FT processes was obtained using ADCP measurements between 2013 and 2014. Figure 3.13 shows a graph of measured mean erosion and deposition using ADCP bathymetry data versus elevation and average maximum shear stresses. Results from this figure support the experimental study results on the effect of FT processes, since higher bank elevations experienced greater amounts of erosion despite experiencing a smaller applied shear stress. It is hypothesized that the FT processes decreased the critical shear stress in these areas sufficiently to promote this erosion.

The second consideration suggests that in low stress slope stability analysis using the failure line soil cohesion should be ignored if FT processes have occurred. Since cohesion is an important part of the shear strength in soil close to the surface due to the low normal stresses, and since soils close to the surface are more susceptible to seasonal

FT and therefore a reduction in the amount of cohesion, ignoring this soil strength will lead to a more conservative calculation.

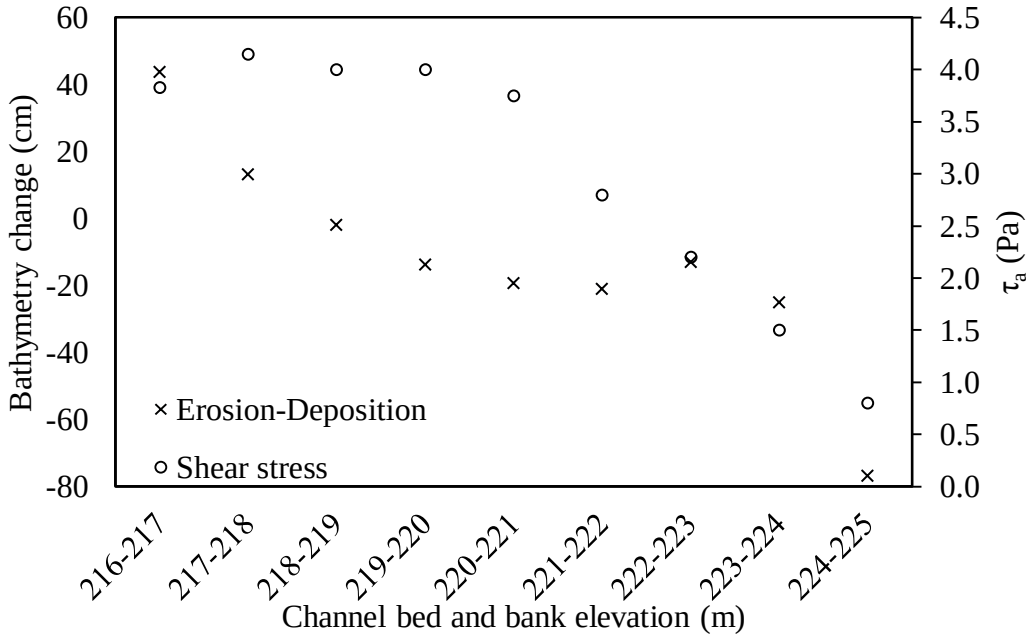

Figure 3.13 Average elevation change between 2013 and 2014 based on bathymetric measurements using an ADCP (positive values show deposition and negative values show erosion)

3.6.4 *An application of the results summary on local riverbank materials*

Figure 3.14 summarizes an application of the present study to predict the total amount of erosion in 2013 at two locations on the Red River bank. These samples were taken in October 2012 from Red 1 and Red 2 sampling locations. According to the results of the thermal model (Figure 3.5) riverbank soil started to freeze in November 2012 and become completely unfrozen on May 12th, 2013; therefore, the analysis began from May 12th, 2013 since frozen soils have high resistance to fluvial erosion (Czudra and Hohmann (1997), Arenson et al. (2004)) and also, applied shear stresses are not high

during ice cover condition. According to the thermal model results, the maximum thickness of the active layer was 1.9 m in 2013 which means that critical shear stress of the top 1.9 m of the riverbank soil layer can be reduced to 20% of its original measured critical shear stress in 2012 and the soil below this top layer maintained its original critical shear stress. The toe of the bank was not exposed to FT processes and maintained its original critical shear stresses in 2012, however according to the results of the thermal model, the riverbank above elevation 221 m was affected by FT. Average applied shear stresses at the toe and bank were obtained using Figure 3.8 and the statistical discharge analysis over this period. Accumulated erosion was calculated based on the water level elevation and assumption of linear applied shear stress distribution over the riverbank using Equation 3.6. The maximum total expected erosion for Red 1 sample was around 0.3 m for the riverbank above elevation 221 m and was zero for the toe. The maximum expected erosion for Red 2 sample that had low critical shear stress was 3.4 m at the toe and the maximum expected erosion at the bank was around 1.8 m. This result did not include the amount of deposition which maybe high due to the high suspended load of the river and very low flow rates during the previous ice covered season. It can be concluded from the statistical analysis (Figure 3.9) that during open water most of the time the river had low discharge without enough erodibility power and this can cause a high amount of deposition over time that will reduce the effect of shoreline loss due to fluvial erosion.

3.7 *Conclusion*

The strength of the cohesive riverbank material of the Red River was shown to be very susceptible to FT processes. Erosion experiments and laboratory observations demonstrated that the first FT cycle had the most significant effect on the Red River bank

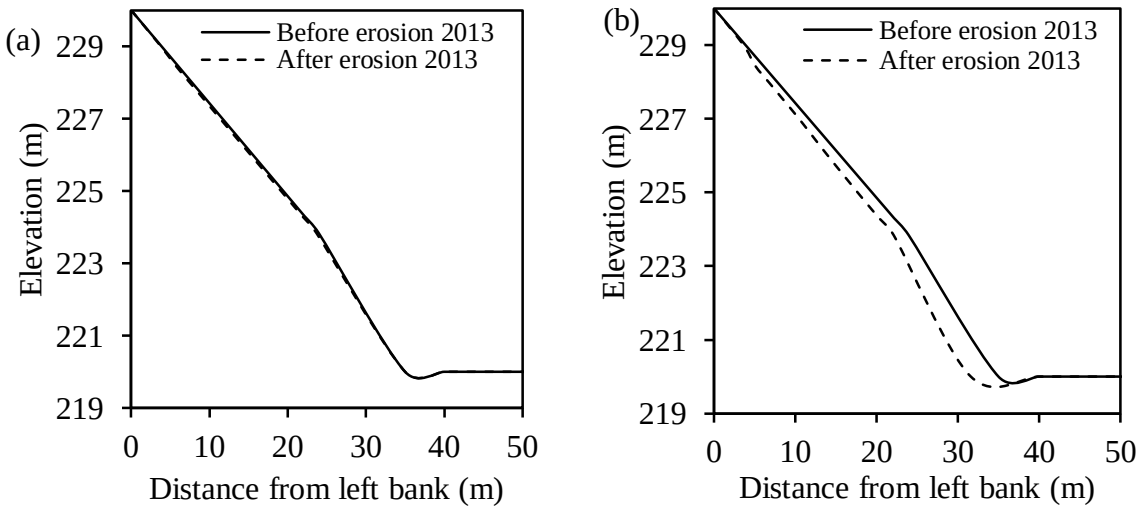

Figure 3.14 Erosion pattern in 2013 for two soil samples (a) Red 1 (b) Red 2

material and caused a decrease in critical shear stress of up to 80% of its original strength. After the fifth FT cycle, macro cracks became visible and caused the material to become cohesionless. The frost temperature itself was shown to be of much less importance than the number of FT cycles. It is therefore suggested that the erodibility properties of cohesive sediment should considered to be dynamic parameters that will change over time in northern climates. The use of a thermal model has been suggested to estimate variation of the active layer depth that experiences FT processes as well as the number of FT cycles over time. While experimental results regarding the effect of FT processes have been presented by other researchers in the past, this paper has demonstrated how one might incorporate these types of results into practice.

For the current study, bathymetric measurements, a thermal model, and a hydrodynamic model were combined together to show that despite higher applied shear stress over the river bed than riverbank, the amount of measured erosion rate was greater on the riverbank, confirming the significant effect of subaerial processes. Therefore, it can be concluded that river banks become more susceptible to fluvial erosion than the bed in low

gradient natural channels located in cold regions such the Red River.

The present study suggests a methodology to investigate cohesive riverbank erosion to obtain an improved understanding of the fluvial erosion process using a combination of field bathymetric measurements, experimental analysis, and numerical models. The deposition process can play an important role in geomorphological changes along low gradient rivers. Future work is needed to more accurately quantify the effect of deposition on the river geomorphology, however, the current experimental results on freshly deposited unconfined material showed that a high resistance to fluvial erosion may be present which can reduce the amount of predicted land losses over time.

Moreover, this study includes new contributions to this specific study region that are very useful for the future design and protection within Winnipeg. The regional investigation of cohesive soil that contains clay is essential due to the variation of clay soil behavior due to the variation of physical, mechanical, and electrochemical properties of such soil in different locations. A very simple methodology has been suggested to quantify the Red River erosion rate in 3 steps: a) estimating applied shear stress distribution using water level and statistical analysis over 4 year of study; b) modifying critical shear stress over time using results of a thermal model and water level; c) using Equation 3.6 to estimate annual erosion rate within the study area. In addition, mechanical property test results indicate that cohesion can be negligible in geotechnical slope failure models and friction factor does not change with FT processes.

3.8 *References*

Arenson, L.U., Johansen, M. M., Sprignman, S. M. 2004. Effect of volumetric ice content and strain rate on shear strength under triaxial conditions for frozen soil samples. Permafrost and Periglacial Processes, **15**: 261-271.

ASTM standard D422-63. 2007, Standard Test Method for Particle-Size Analysis of Soils. ASTM International, West Conshohocken, PA.

ASTM standard D2487-11. 2011a, Standard practice for classification of soils for engineering purposes (unified soil classification system). ASTM International, West Conshohocken, PA.

ASTM standard D3080-11. 2011b, Standard test method for direct shear test of soils under consolidated drained conditions. ASTM International, West Conshohocken, PA.

Baracos, A. & Grham, J., 1981. Landslide problems in Winnipeg. Canadian Geotechnical Journal, 18: 390-401.

Baracos, A. & Lew, K., 2003. Riverbank Slides, Erosion and Deposition at 758 Crescent Drive, Winnipeg, Manitoba-Volume 1 Report, Winnipeg: s.n.

Briaud, J. et al., 2001. Erosion function apparatus for scour rate predictions. Journal of Geotechnical and Geoenvironmental Engineering, **127(2)**: 105-113.

Couper, P. R. & Maddock A. P. 2001. Subaerial river bank erosion processes and their interaction with other bank erosion mechanisms on the river arrow, warwickshire, uk. Earth Surface Processes and Landforms, **26**: 631-646.

Couper, P., 2003. Effects of silt-clay content on the susceptibility of river banks to subaerial erosion. Geomorphology, **56**: 95-108.

Czudra, K. A., & Hohmann, M. 1997. Freezing effect on shear strenght of clayey soils . Applied Clay Science, **12**: 165-187.

Debnath, K. & Chaudhuri, S., 2010. Cohesive sediment threshold: a review. ISH Journal of Hydraulic Engineering, **16(1)**: 36-56.

DHI, 2012a. MIKE 21 & 3 FLOW model FM hydrodynamic and transport module scientific documentation. P.3: DHI Group.

DHI, 2012b. MIKE 21 & 3 FLOW model FM mud transport module scientific documentation. P.27: DHI Group.

DHI, 2012c. MIKE 21 & 3 FLOW model FM hydrodynamic and transport module scientific documentation. P. 17: DHI Group.

Edwards, L., Burney, J. R. & Frame, P. A., 1995. Rill sediment transport on a prince Edward Island (Canada) fine sandy loam. Soil Technology, **8**: 127-138.

Farouki, O. T., 1981. Thermal properties of soils, s.l.: U.S. Army Cold Regions Research and Engineering Laboratory.

Farouki, O. T., 1985. Ground Thermal Properties. New York: ASCE.

Fernando, L., 2009. The effect of flow induced erosion on riverbank stability along the Red River in Winnipeg. M.Sc. theses, Department of Civil Engineering, University of Manitoba, Winnipeg, MB.

Ferrick, M. G. & Gatto, L. W., 2005. Quantifying the effect of a freeze–thaw cycle on soil erosion: laboratory experiments. Earth Surface Processes and Landforms, **30**: 305-326.

Formanek, G., McCool, D. & Papendick, R., 1984. Freeze-thaw and consolidation effects on strength. Transactions of the ASAE, **27(6)**: 1749-1752.

Gatto, L., 2000. Soil freeze-thaw-induced changes to a simulated rill: potential impacts on soil erosion. Geomorphology, **32**: 147-160.

Graham, J. & Au, V. C. S., 1985. Effect of freeze-thaw and softening on a natrual clay at low stress. Canadian Geotechnical Journal, **22**: 69-78.

Jansen, W., 2012. Public dollars justified to halt riverbank erosion, Winnipeg: Winnipeg Free Press.

Kimiaghalam, N., Clark, S. & Ahmari, H., 2015. An experimental study on the effects of physical, mechanical, and electrochemical properties of natural cohesive soils on critical shear stress and erosion rate. International Journal of Sediment Research, http://dx.doi.org/10.1016/j.ijsrc.2015.01.001.

Lawler, D.M., 1993. Needle ice processes and sediment mobilization on river banks — the River Ilston, West-Glamorgan, UK. Journal of Hydrology, **150**: 81–114.

Lawler, D.M., Thorne, C.R., Hooke, J.M., 1997. Bank erosion and instability. In: Thorne, C.R., Hey, R.D., Newson, M.D. (Eds.), Applied Fluvial Geomorphology for River Engineering and Management. John Wiley & Sons, New York, pp. 137–172.

Lawler D. M., Grove J.R., Couperthwaite J.S., & Leeks G. J. L. 1999. Downstream

change in river bank erosion rates in the Swale–Ouse system, northern England. Hydrological Processes, **13**: 977–992.

Munson, B. R., Okiishi, T. H., Wade, W. H. & Rothmayer, A. P., 2012. Fundamentals of Fluid Mechanics. USA: John Wiley & Sons, Inc.

Partheniades, E., 1965. Erosion and deposition of cohesive soils. Journal of Hydraulics Engineering, ASCE, **91(1)**: 105-138.

Rinaldi, M. & Darby, S., 2007. Modelling river-bank erosion processes and mass failure mechanisms: progress towards fully coupled simulations. In: H. Habersack, H. Piegay & M. Rinaldi, eds. Gravel-Bed Rivers VI: from Process Understanding to River Restoration. Amsterdam: Elsevier, pp. 213-239.

Smagorinsky, J., 1963. General circulation experiments with the primitive equations. Monthly Weather Review, **91**: 91-164.

Torrance, J. K., 1975. On the role of chemistry in the development and behavior of the sensitive marine clays of Canada and Scandinavia. Canadian Geotechnical Journal, **12**: 326-335.

Thorne, C.R., 1982. Processes and mechanisms for river bank erosion.In: Hey, R.D., Bathurst, J.C., Thorne, C.R. (Eds.), Gravel-Bed Rivers: Fluvial Processes, Engineering, and Management. John Wiley & Sons, New York, pp. 227–259.

Van Klaveren, R. W. & McCool, D., 2010. Freeze–Thaw and water tension effects on soil detachment. Soil & Water Mangement, **74(4)**: 1327-1338.

Van Klaveren, R. W., 1987. Hydraulic erosion resistance of thawing soil. PhD

dissertation. Washington State University.

Van Klaveren, R. & McCool, D., 1998. Erodibility and critical shear of a previously frozen soil. Transactions of the ASAE, **41(5)**: 1315-1321.

Weiss, A. The use of acoustic Doppler current profiler technology to quantify total suspended solids under ice. M.Sc. thesis, Department of Civil Engineering, University of Manitoba, Winnipeg, MB.

Wynn, T. M., Henderson, M. B., & Vaughan, D. H. 2008. Change in streambank erodibility and critical shear stress due to subaerial processes along a headwater stream, southwestern Virginia, USA. Geomorphology, **97**: 260-273.

Yumoto, M., Ogata, Matsuoka, T., , & N., Matsumoto , E. 2006. Riverbank freeze–thaw erosion along a small mountain stream, Nikko Volcanic Area, Central Japan. Permafrost and Periglacial Processes, **17**: 325–339.

CHAPTER 4: ESTIMATING COHESIVE SEDIMENT EROSION AND DEPOSITION RATES IN WIDE RIVERS

A version of this chapter has been published in Canadian Journal of Civil Engineering:
Kimiaghalam, N., Goharrokhi, M., and Clark, S. P., 2016. *Estimating cohesive sediment erosion and deposition rates in wide rivers*. Canadian Journal of Civil Engineering, 43 (2): 164-172.

Sediment erosion and deposition rates are two of the most important factors that influence fluvial geomorphology. Several experimental devices have been constructed to estimate cohesive sediment erosion rate. However, estimated erosion rates may not be reliable for large rivers due to limited soil sampling and a high dependency of cohesive sediment behaviour on several physical, mechanical, and electrochemical properties of the sediment and eroding fluid. A new methodology has been developed to estimate the erosion and deposition rate of wide rivers using in-situ measurements. To test this methodology, an acoustic Doppler current profiler (ADCP) was used to collect bathymetry and velocity profiles over a study area along the Red River in Winnipeg, Canada. Sediment concentration profiles along an 8.5 km reach of the river were measured several times under different flow conditions. Finally, an advection-dispersion equation was numerically solved using measured and calculated streamwise dispersion coefficients, flow and channel characteristics to calculate net erosion and deposition over

the study area. Moreover, an exponential relationship was obtained between the river discharge and longitudinal dispersion coefficient for the Red River.

4.1 *Introduction*

The field of cohesive sediment transport has not yet been fully understood, in large part due to the complex behavior of cohesive sediment. The presence of at least 10% clay in a soil structure is enough to control the behavior of the soil (Debnath & Chaudhuri, 2010). Several researchers have conducted experimental studies to find a relationship between critical shear stress, erosion rate, and deposition rate with different mechanical, physical, electro-chemical, and biological soil properties (Winterwerp et al. 1990, Berkhovskikh et al. 1991, Huang et al. 2006, Meng et al. 2012, Kimiaghalam et al. 2015a). Many in-situ and laboratory devices have been constructed for measuring critical shear stress and erosion rate of cohesive soil. However, it still remains to be seen how reliable these devices are for natural rivers.

Most erosion measurement devices are only able to measure the erosion rate, but in low gradient rivers, deposition can play an important role in the geomorphological changes along the river. Therefore, it is essential to develop a new methodology for estimating both the erosion and deposition rate. Generally, three types of erosion measurement devices have been constructed by researchers: piston-type, rotating-type, and submerged jet-type.

SEDFlume (McNeil et al. 1996), ASSET (Roberts et al. 1998), EFA (Briuad et al. 2001), SERF (Crowley et al. 2012), EMD (Jianfar, 2014) are examples of the piston-type erosion measurement devices. Usually, these devices are used in laboratories for

estimating erosion rate under different flow rates. There are also several similar portable devices that can be used in situ like ISEF (Houwing and Van Rijn, 1997). Generally, piston-type devices contain a circular or rectangular flume; a sampling tube to push a soil sample into the flow; and a pump to regulate flow in the flume. The general testing procedure for these kinds of erosion measurement devices is to push the soil sample a small distance into the flow or keep it flush with the flume bottom and measure how much erosion happens over time, under a particular applied shear stress. After obtaining several measurements, with the assumption of an exponential or power function relating erosion rate and applied shear stress, critical shear stress and erosion rate can be estimated (Partheniades 1965, Parchure and Mehta 1985, and Maa et al. 1998). Figure 4.1a shows a typical piston-type erosion measurement device and experimental setup. Soil samples are taken using ASTM standard Shelby tubes or boxes to obtain relatively undisturbed samples for experiments. Undisturbed samples are essential for such studies since cohesive soil behavior is highly impacted by changes in natural conditions. Soil conditions may also be altered due to natural subaerial processes like seasonal freezing-thawing and wetting-drying. Several criticisms exist for the application of these devices. The first criticism is related to the soil sampling procedure and the number of soil samples that are used for predicting riverbank or riverbed geomorphologic changes. Using standard tubes to take samples does not entirely avoid the disturbance of soil, but it does help to reduce the soil disturbance. In addition, many precautions need to be taken for transferring soil samples into laboratories such as properly sealing samples to maintain the natural water content. Moreover, transferring a soil sample from a Shelby tube to a testing tube has the potential to create another source of soil sample disturbance.

Therefore, the sampling procedure can cause uncertainty in the final results. In addition, acquiring minimally-disturbed soil samples from a riverbed requires more effort and has higher costs than sampling from riverbanks. The presence of vegetation can greatly influence the performance of the test, since it is difficult to quantify the amount of vegetation in the soil structure and in the study area. The assumption of a homogeneous soil distribution throughout the study area may not be reasonable, and has the potential to introduce significant uncertainty if an insufficient number of sampling locations is used. Uncertainty in measuring erosion rate using experimental results from small soil samples may also be an issue. Common irregular erosion patterns at the surface of the sample may result in considerable uncertainty in estimating the applied shear stress over a soil sample due to the roughness variation over the sample surface (Crowley et al. 2014). Moreover, using natural river water with the same chemical and physical properties can result in different erosion rates than using regular tap water in a laboratory.

Rotating-type erosion measurement devices were developed for measuring erosion rates on stiff cohesive sediment and rocks (Henderson 1999, Kerr 2001, Sheppared et al. 2005, Bloomquist et al. 2012). These kinds of devices are comprised of a soil sample that is placed inside f a rotating cylinder with water filling the space between the inner cylinder wall and the soil sample (Figure 4.1b). The cylinder rotates and causes an applied shear stress on the surface of the soil sample. The applied torque is measured with and converted to applied shear stress with a simple calculation. However, these devices have limitations that restrict their applicability in some cases. They can be used only for self-supporting samples like stiff clay and rocks; however, surface fluvial erosion may often occur with very soft sediment and unconfined soil. Moreover, like the piston-type

devices, soil sampling procedures can cause uncertainty in the estimation of erosion rate. A distinct disadvantage of using rotating devices is the curved shape of the devices which results in a different shear stress distribution over the sample than the natural process observed in channels. Also, secondary flow is generated in these devices that can accelerate the erosion rate in an unrealistic fashion (Graham et al. 1992).

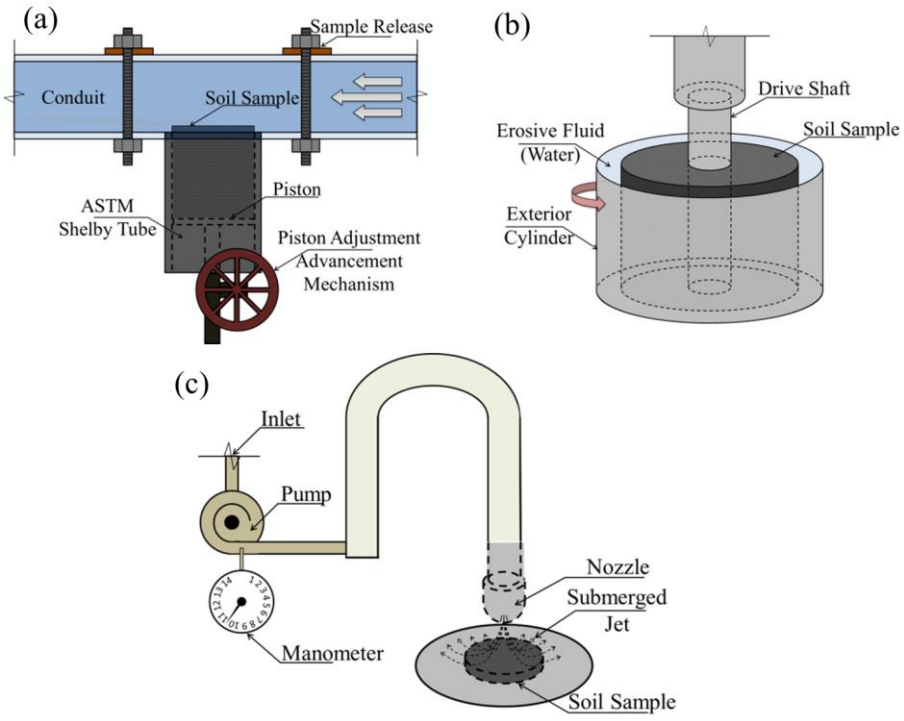

Figure 4.1 Different types of erosion measurement devices: (a) piston-type erosion measurement device, (b) rotating-type erosion measurement device, and (c) submerged jet-type erosion measurement device

The submerged jet-type device was developed and used by several researchers (Rouse (1940), Moore and Masch (1962), Hanson (1991), Mazurek et al. (2001), and Hanson and Cook (2004)). This device can be used to perform an in-situ erosion rate test on an exposed riverbank and several researchers suggested that these kinds of erosion measurement devices are more reliable for measuring in-situ local scour properties than the other devices such as in-situ flume erosion measurement devices (Charonko (2010)

and Weidner (2012)). However, it cannot be used in-situ for an unexposed surface like a riverbed, thereby requiring an undisturbed soil sample to be taken for testing (ASTM D5852, 2011). Figure 4.1c shows a typical jet device. A submerged jet erodes the soil sample surface constantly for a certain duration, after which the amount of erosion underneath of the jet is measured and the process is repeated for different applied shear stresses. These methods have the limitation of location and sampling scale while studying long reaches and wide channels.

Recent development in the field of acoustic Doppler in-situ measurement techniques has led to the use of acoustic Doppler velocimeters (ADVs) for estimating cohesive sediment transport characteristics. Andersen et al. (2007) suggested a method for in-situ estimation of erosion and deposition thresholds and local erosion rate in coastal areas using two ADVs. Using long and short term ADV data, applied shear stress and local bed elevation changes were calculated under different flow conditions. Fugate and Friedrichs (2002) used an ADV to calculate cohesive sediment settling velocity based on the expression of turbulent diffusion that leads to the following equation for estimating particle fall velocity (Maa and Kwon (2007)):

$$w_s C = \langle w' C' \rangle \qquad \textbf{Equation 4-1}$$

where w_s is the fall velocity, $\langle \quad \rangle$ represents time-average, w' is the vertical velocity fluctuation, and $C = \langle C' \rangle$ is the time average suspended sediment concentration. The ADV was used to calculate w' from its velocity measurements and C' from the acoustic scatter signal strength. Moreover, several studies have been conducted to calibrate available numerical models such as MIKE 21C using ADCP measurements and measured

sediment flux to assess morphodynamic changes in rivers (Guerrero et al. (2013a&b) and Guerrero et al. (2015)).

This paper outlines a methodology to estimate the average erosion and deposition rate in a wide river based on in-situ ADCP and sediment concentration measurements combined with the numerical solution of the cohesive sediment transport governing equation. The methodology attempts to minimize the uncertainties found in the other erosion measurement devices since it does not require the acquisition of undisturbed soil samples, and implicitly incorporates the effects of natural conditions such as seasonal freeze-thaw, sediment desiccation and vegetation, and sediment property heterogeneity. The methodology gives a realistic estimation of both erosion and deposition over the entire wetted perimeter of a natural channel which is helpful for research and practical purposes.

4.2 *Methodology*

4.2.1 *Governing equation*

The main governing cohesive sediment transport equation is the key component to this study and can be written as a 2-D advection-dispersion equation (Huang et al., 2006):

$$\frac{\partial(hc_i)}{\partial t}+\frac{\partial(huc_i)}{\partial x}+\frac{\partial(hvc_i)}{\partial y}=\frac{\partial}{\partial x}\left(D_x h\frac{\partial c_i}{\partial x}\right)+\frac{\partial}{\partial y}\left(D_y h\frac{\partial c_i}{\partial y}\right)+S \qquad \textbf{Equation 4-2}$$

where h [m] is the water depth, c_i [m^3/m^3] is the depth-averaged volumetric sediment concentration, t [s] is time, u and v [m/s] are the depth-averaged velocity component in the streamwise and spanwise directions, respectively, D_x and D_y [m^2/s] are the dispersion coefficients in the streamwise and spanwise directions, respectively, and S [m/s] is the

source (erosion) or sink (deposition) terms. Erosion increases sediment concentration in a river and detached material from the bed or bank will be transported downstream and simultaneously undergo a mixing process. Longitudinal dispersion is the main mechanism of transport (Shen, et al., 2010) and the transverse dispersion coefficient becomes negligible. The sink and source terms can be calculated from the numerical solution of Equation 4-2 if a calibrated hydrodynamic model is available and if D_x is also calculated.

4.2.2 *Estimation of hydrodynamic parameters*

Flow depth, stream wise and spanwise velocities, and dispersion coefficients are essential for the numerical solution of Equation 4-2. To facilitate the calculation of these parameters over a range of hydraulic conditions it is convenient to use a calibrated hydrodynamic model. Many options are available for this task; however, for this study the MIKE 21 Flow Model HD was used since it had already been created for the case study location. For developing a good hydrodynamic model, three measurements are required: 1) study area bathymetry; 2) upstream and downstream boundary water surface elevations; 3) flow rate. Utilizing these measurements over time, the model can be calibrated by adjusting the Manning number. The complete methodology for modeling and field measurements will be discussed in the case study section.

Longitudinal dispersion coefficient is another important hydrodynamic parameter that is essential for the solution of the advection-dispersion equation. Several experimental equations to estimate this coefficient have been suggested by numerous researchers (Fischer et al. (1979), Seo and Cheong (1998), Deng et al. (2001), and Kashefipour and Falconer (2002)). Most of these studies are only valid for their specific study area and

flow conditions, therefore, application of these experimental equations can result in high uncertainty for different locations. The dispersion coefficient is often estimated from tracer studies on small rivers. However, tracer studies can be costly and time consuming for large rivers (Shen, et al., 2010). Since hydrodynamic modeling and measurements are an essential part of fluvial geomorphology studies, the dispersion coefficient can be estimated based on the theory of turbulent shear flow (Fischer et al. 1979):

$$D_x = -\frac{1}{A}\int_0^w u'(y)h(y)\int_0^y \frac{1}{D_y h(y)}\int_0^y u'(y)h(y)dydydy \qquad \textbf{Equation 4-3}$$

where A [m^2] is the cross sectional area, W [m] is the cross section top width, and $u'(y) = u(y) - U$; where $u(y)$ [m/s] is the depth-averaged streamwise velocity and U [m/s] is the cross sectional streamwise average velocity. The spanwise mixing coefficient can be estimated by (Rutherford (1994)):

$$D_y = \theta u_* H \qquad \textbf{Equation 4-4}$$

where H [m] is the cross section average depth and u_* [m/s] is the average frictional velocity which can be calculated as follows:

$$u_* = \sqrt{gRS_f} \qquad \textbf{Equation 4-5}$$

Where g [m^2/s] is the gravitational acceleration, R [m] is the hydraulic radius, and S_f [-] is the slope of the energy grade line. The coefficient θ is calculated using following equation (Deng et al. 2001):

$$\theta = 0.145 + \frac{1}{3520}\left(\frac{U}{u_*}\right)\left(\frac{W}{H}\right)^{1.38} \qquad \textbf{Equation 4-6}$$

The turbulent shear flow method is based on the assumption of a well-mixed flow and that the river width to the water depth ratio exceeds 10 (Fischer et al. 1975). Therefore, this method can be used only for wide rivers. Acoustic Doppler current profilers (ADCP) can be used for collecting channel bathymetry and water velocity data which are useful for developing hydrodynamic models and for determining D_x based on Equation 4-3. Since the ADCP can obtain measurements at a high spanwise resolution, the integrals in Equation 4-3 can accurately be replaced by summing the relevant measured variables. Carr and Rehmann (2007) and Shen et al. (2010) showed that using turbulent shear flow theory and ADCP data can improve D_x calculation accuracy and reduces the cost of the tracer studies, in particular for wide rivers.

4.2.3 *Estimation of erosion and deposition rate*

The advection-dispersion equation can be solved using calculated hydrodynamic characteristics and dispersion coefficients if water sediment concentration profile measurements available within the study area. In this study, the MIKE 21 FM AD model was paired with the MIKE 21 FM HD model, and therefore, hydrodynamic characteristics of the calibrated model were used to solve Equation 4-2 with the estimation of D_x and D_y from the previous section.

For a specific discharge, the average cross section sediment concentration can be measured between the upstream and downstream boundaries by sampling the water at particular intervals and depths. To estimate the erosion and deposition rate, the study reach can divided into small subareas. For each subarea average cross sectional sediment concentration can be measured. The measurements must be done in a stepwise fashion from upstream to downstream with respect to the flow velocity and sediment travel time.

The advection-dispersion model should be calibrated stepwise by adding sinks and sources in each subarea from upstream to downstream in order to obtain similar simulated concentrations to those that were measured. The terms sink and source are the erosion or deposition rate from each subarea, respectively, which are a function of flow rate, applied shear stresses, river bed and bank soil critical shear stresses and properties, and natural water properties through the river. This method gives a realistic estimation of the erosion and deposition over an entire study area with consideration to all of the natural conditions such as vegetation and subaerial processes.

4.3 *Case Study: Red River in Winnipeg, Canada*

The proposed methodology was applied to an 8.5 km reach of the Red River in Winnipeg, Manitoba, Canada extending from the South Perimeter Bridge (49°47'04" N and 97°08'7" W) to the Fort Garry Bridge (49°49'17" N and 97°08'35" W) (Figure 4.2). The mean annual river discharge is 176 m^3/s, with peak discharge on the order of 1300 m^3/s with an average gradient of 4 m per 100 km. Water surface elevation typically varies between 223 m and 229 m annually. At mean flow conditions the average channel top width and depth are 130 m and 4 m, respectively, resulting in a width to depth ratio far greater than 10. Therefore, application of Equation 4-3 was reasonable for this river. Total suspended sediment concentration varies between 10 mg/L and 1500 mg/L, during low flow (ice-covered conditions) and high flow conditions, respectively. The suspended sediment contains silt and clay with grain sizes ranging between 0.0011-0.0062 mm (Goharrokhi and Clark, 2015). The riverbank mostly contains silt and clay (Kimiaghalam et al. 2013, 2015a,b).

Figure 4.2 Study reach through the Red River in Winnipeg, MB (Map data: Google). Cross sections L0-L9 show the location of where water sampling occurred, sinks and sources in the models were added downstream of each cross section (coordinates are in UTM 14).

Several researchers have tried to experimentally quantify the fluvial erosion rate on the Red River. Jianfar (2014) and Fernando (2009) focused on evaluating the effect of fluvial erosion on riverbank stability. Kimiaghalam et al. (2015b) conducted a comprehensive numerical and experimental study on fluvial geomorphology through the Red River and they used a piston-type erosion measurement device to test the erodibility of riverbank material under natural conditions and after several freeze-thaw cycles at different freezing temperatures. They concluded that the common process through the river is deposition and it is important to quantify the deposition rate as well as erosion rate to predict future fluvial geomorphological changes along the river. Goharrokhi and Clark (2015) found that sediment distribution over the depth and cross section of the Red River in Winnipeg was relatively uniform. Blanchard et al. (2011) found that 99% of the total

sediment load through the Red River approximately 300 km upstream of the present study reach was suspended load, and that the bed load contribution in total sediment in the Red River was negligible. Goharrokhi and Clark (2015) confirmed that these results were true for the Red River within the city of Winnipeg as well.

4.3.1 *Field measurements*

Field measurements were a critical part of the methodology, and included ADCP measurements to collect bathymetric data, velocity profiles over the study reach, and discharge, as well as water sampling to measure sediment concentration. Measuring high-resolution bathymetry and flow data were essential to develop an accurate numerical model since bathymetry was a primary input parameter in the hydrodynamic numerical model and velocity profiles were necessary to calculate the longitudinal dispersion coefficients.

A Sontek River Surveyor M9 ADCP was used to collect bathymetric data and flow characteristics in 2013 and 2015. This device was equipped with a RTK-GPS system with $\pm$ 3 cm horizontal resolution. To collect bathymetry data, the ADCP was mounted to a hydroboard and pulled from the boat at a speed of less than 1 m/s over the entire study area. The procedure was to combine stream wise profiles with spanwise transects spaced at approximately 12 m in the streamwise direction. For discharge and velocity profile measurements, the ADCP was pulled at a speed less than the mean current velocity. This procedure was repeated over these two years for different flow rates and cross sections to find a relation between flow rate and the longitudinal dispersion coefficient.

Water samples were taken at 10 cross sections (L0-L9) between the upstream and

downstream boundary spaced at approximately 1 km intervals on June 12, August 15, and October 10 in 2013, and May 27 and June 18 in 2015 (Figure 4-2). These dates were selected based on the flow rates in the river to cover common discharges during low, average, and relatively high flow events. Figure 4.3 shows the sampling date conditions on 2013 and 2015 Red River hydrographs. The sampling procedure started from the upstream boundary and finished at the downstream boundary. Six water samples were taken from each cross section, close to the left and right bank and center of the river near from the surface and at depth. The sampling volume was 500 ml and ASTM standard D3977-97 (ASTM, 2013) was used to measure the water sample sediment concentrations. Since the sediment concentration distribution was relatively uniform, the average of all water samples at each cross section was used in the numerical model.

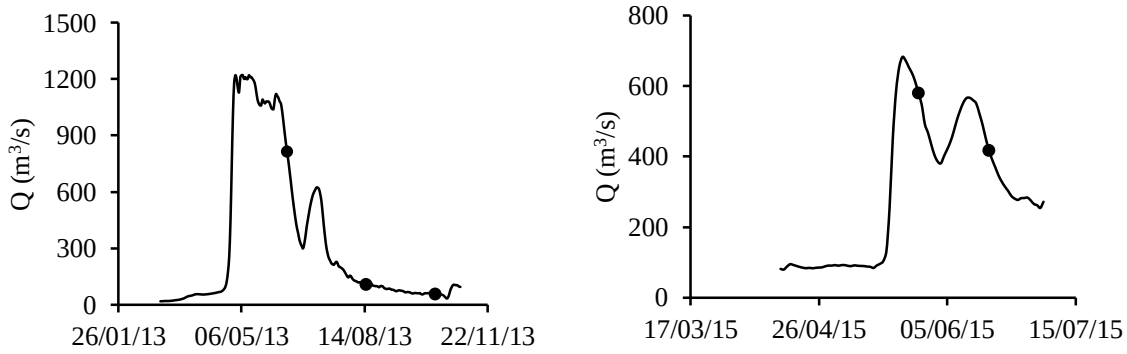

Figure 4.3 Water sampling dates on 2013 and 2015 Red River hydrographs

4.3.2 *Numerical modelling*

The measured bathymetry was used to develop a hydrodynamic model using the MIKE 21 Flow Model. MIKE 21 FM HD is a 2-D numerical hydrodynamic model that solves the depth-averaged Navier Stokes equations. Using this model, essential flow parameters like flow depth, stream wise and spanwise velocities are calculated. the model domain

was created using measured bathymetric data and a grid spacing of 20 m. Upstream discharge and downstream water surface elevation were used as the upstream and downstream boundary conditions. These data were obtained from a continuous Environment Canada gauge at the South Perimeter Bridge and a City of Winnipeg water surface elevation gauge at the Fort Garry Bridge. The initial water elevation was set as the average water surface elevation between these two boundaries, and a sufficient model spin-up time was used. A Manning number of 0.025 was found through calibration to obtain the best fit between measured and simulated upstream water surface elevations. The model was validated for 4 years between 2010 and 2014 and produced R^2 = 0.98 (Kimiaghalam et al. 2015b).

An advection-dispersion (AD) model was paired with the HD model to simulate sediment concentration along the Red River. The model solves the general 2-D advection-dispersion equation (Eq. 2) that $S = Q_s(c_S - c)$; where Q_s [$m^3/s/m^2$] is the sink and source discharge, c_S [m^3/m^3] is the concentration of compound in the source and sink discharge, and c [m^3/m^3] is the compound concentration (DHI, 2012). The computational grid was fixed at 20 m*20 m. Five separate models were developed based on the calibrated model to simulate sediment concentration on June 12, August 15, and October 10 in 2013, and May 27 and June 18 in 2015. The measured upstream and downstream concentrations (South Perimeter Bridge and Fort Garry Bridge) were the primary boundary conditions of the AD model and initial upstream concentration was considered as the initial condition. The dispersion coefficient for each was obtained based on the ADCP measurements and Equation 4-3. Therefore, this parameter was considered as a known input and the AD module was calibrated based on adding sink and source

parameters. Distributed sinks and sources were added starting from the upstream and ending at the downstream boundary to obtain the best fit between simulated and measured sediment concentration. Sinks or sources in the models were added at the downstream of each subarea (L0-L9 cross sections) that sediment concentrations were measured (Figure 4.2). The sink and source discharge was assumed equal to 1 and the model was calibrated for c_S to obtain the best fit between measured and simulated concentration. Finally, the sink and source term (S) was calculated using the final c_S and c values.

4.4 *Results*

4.4.1 *Red River flow rate and longitudinal dispersion coefficient relationship*

Table 4-1 shows a summary of measured and calculated hydraulic characteristics of the Red River using the ADCP measurements. The values of *U*, *W*, and *H* were found directly from the ADCP measurements; U* was calculated using Equation 4-5; the average applied shear stress (τ_a) was calculated as ρU^{*2} where ρ [kg/m^3] is the density of the water; and D_x was calculated using Equation 4-3. These results covered a wide range of typical Red River flow rates over the 2 year study duration, and should therefore be representative of much of the hydraulic conditions that typically occur on the River. The first important finding from the study was that D_x generally increased with increasing river discharge, and this relationship (Equation 4-7) can be well represented by an exponential function with $R^2 = 0.70$ (Figure 4.4).

$$D_x = 16.6\, e^{0.0018Q} \qquad \textbf{Equation 4-7}$$

This is the first study on the Red River near this study reach to estimate D_x, and results will be useful for future environmental research. Moreover, these results are based on measurements at different locations on the river, therefore, it can be concluded that the fitted curve can be used to estimate D_x along the entire study reach.

Table 4-1 Red River flow characteristics and calculated longitudinal coefficient of dispersion

No.	Discharge (m^3/s)	U (m/s)	W (m)	H (m)	U* (m/s)	τ_a (Pa)	D_x (m^2/s)
1	1231	1.09	180	6.75	0.063	3.97	173
2	1152	1.05	176	6.74	0.06	3.60	176
3	1143	1.07	178	5.7	0.062	3.84	141
4	1026	1.02	169	6.27	0.06	3.60	92
5	1021	1.05	179	5.9	0.061	3.72	93
6	1019	1.04	172	6.1	0.061	3.72	76
7	756	0.84	142	6.74	0.048	2.30	95
8	746	0.84	139	6.71	0.048	2.30	85
9	641	0.84	152	5.33	0.051	2.60	41
10	603	0.82	151	5.21	0.05	2.50	30
11	600	0.83	148	5.23	0.05	2.50	35
12	560	0.71	133	6.1	0.041	1.681	36
13	556	0.66	131	5.7	0.038	1.44	16
14	512	0.74	145	4.94	0.045	2.03	54
15	404	0.57	141	5.24	0.034	1.16	55
16	402	0.6	131	5.01	0.035	1.225	53
17	293	0.56	142	3.9	0.035	1.23	54
18	259	0.5	130	3.83	0.032	1.02	35
19	207	0.44	128	3.4	0.029	0.84	31
20	166	0.39	125	3.28	0.025	0.63	20
21	73	0.14	120	3.2	0.009	0.081	10

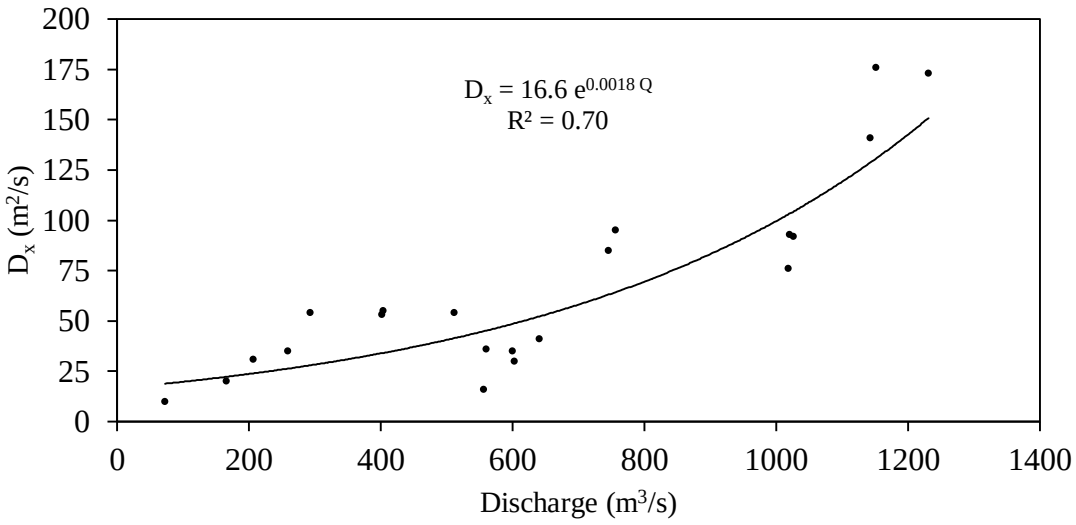

Figure 4.4 Variation of longitudinal dispersion coefficient with Red River discharge

4.4.2 *Red River erosion and deposition pattern*

Figures 4.5a-4.5e show the final simulated and measured sediment concentration profiles along the study reach for each field test based on the adding all sinks and sources to produce the best fit to the measured data. There is a general decrease in sediment concentration in the downstream direction indicating that deposition is the dominant mode of sediment transport when looking at the entire reach. The variability within these profiles indicates that subareas within the reach have varying sediment transport rates, including some areas that experience erosion rather than deposition. Figure 4.6 summarizes the sink and source quantities for each of the nine subareas. Positive values represent sources of sediment to the flow (ie. erosion) and negative values represent sinks from the flow (i.e. deposition). Riverbank erodibility varied within the study reach for each flow rate which indicates that riverbank material had different erodibility properties such as critical shear stress and erosion rate. This conclusion confirms the previous measurements by several researchers such as Kimiaghalam et al. 2015b, Jianfar (2014),

and Fernando (2009). On average, most subareas besides subareas 4 and 6 experienced deposition at the different flow rates, therefore, it can be concluded that subareas 4 and 6 contained material with lower critical shear stress or erosion rate than the other subareas. Moreover, the average net erosion and deposition rate was negative along the entire study reach; therefore, it can be concluded that deposition is the most common fluvial process in the Red River since the average river flow rate is 176 m^3/s and these current measurements varied between 73 and 739 m^3/s. As previously mentioned, peak flows on the Red River in this area can be on the order of 1300 m^3/s; however, it was unfortunately not possible to access the river using a boat during these high flows due to safety concerns from floating debris. It is anticipated that erosion does in fact become the dominant mode of sediment transport during high flow events; however, these events are relatively short in duration. The proposed methodology would be equally applicable to quantify erosion rates on wide rivers during a time of active erosion throughout the entire reach, and would have been used in this case study if it had been possible.

According to Table 4-1 the average applied shear stress increased with increasing flow rate; however, according to the Figure 4.7a the average deposition rate did not have a clearly defined relationship with flow rate, hence it can be concluded that the deposition rate was not a function of applied shear stresses alone. Figure 4.7b shows the variation of the average deposition rate with the reach-averaged sediment concentration. It was initially hypothesized that the deposition rate would increase with decreasing applied shear stress, and this found to be true for 4 of the 5 simulations. The exception was October 10, which experienced the lowest applied shear stress but also the lowest deposition rate. It is hypothesized that the deposition rate was not only a function of

applied shear stress, but also a function of available sediment concentration in the river. In other words, although the very low applied shear stress on October 10 had a high potential to promote sediment deposition, the very low suspended sediment concentration in the river limited the deposition rate. This intuitively suggests that at times when very low sediment concentrations and flow rates occur simultaneously, such as during the late fall and winter, the amount of sediment deposition and erosion would be essentially zero.

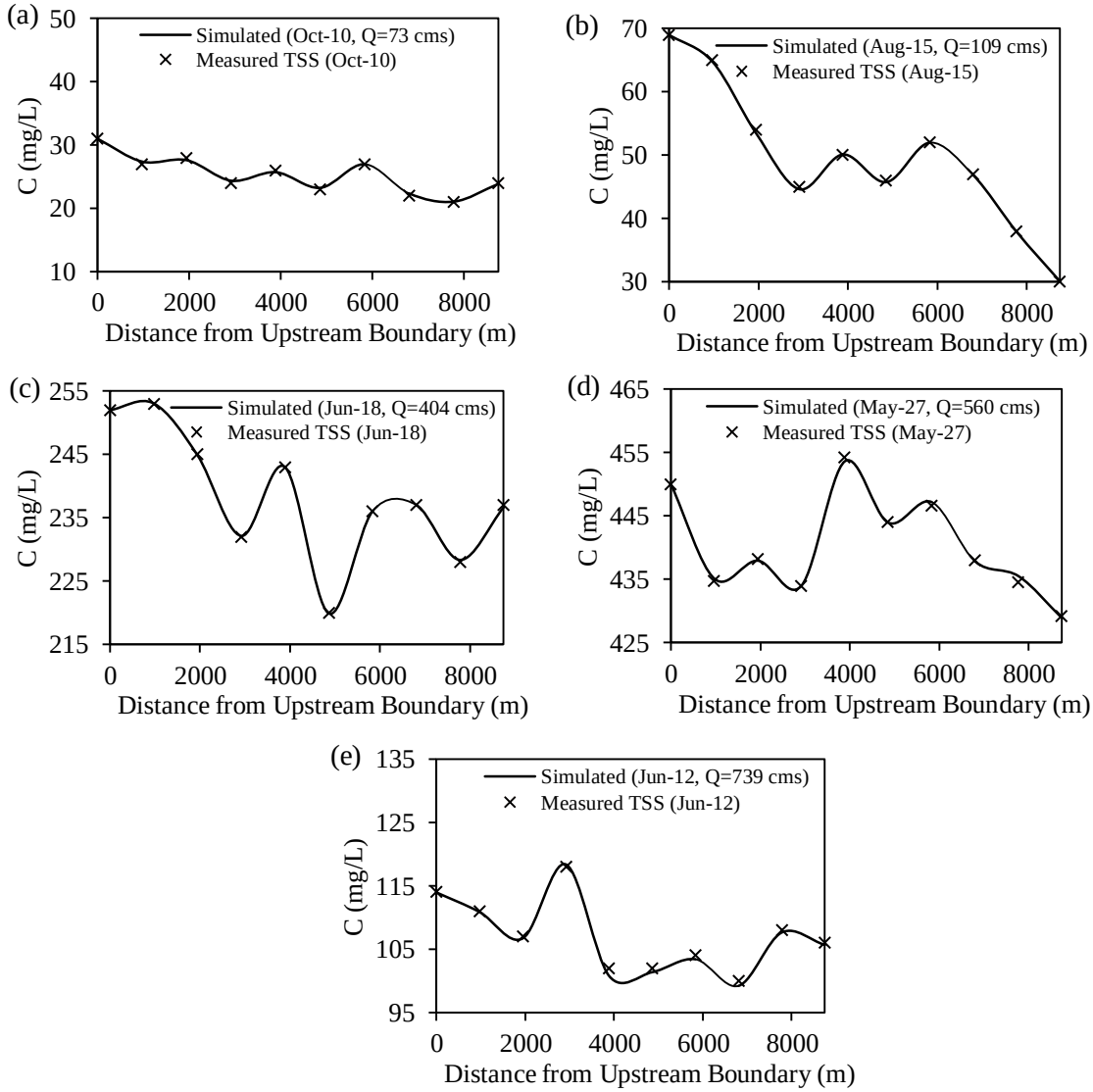

Figure 4.5 Variation of the measured and simulated average sediment concentration along the study reach and in different flow rates

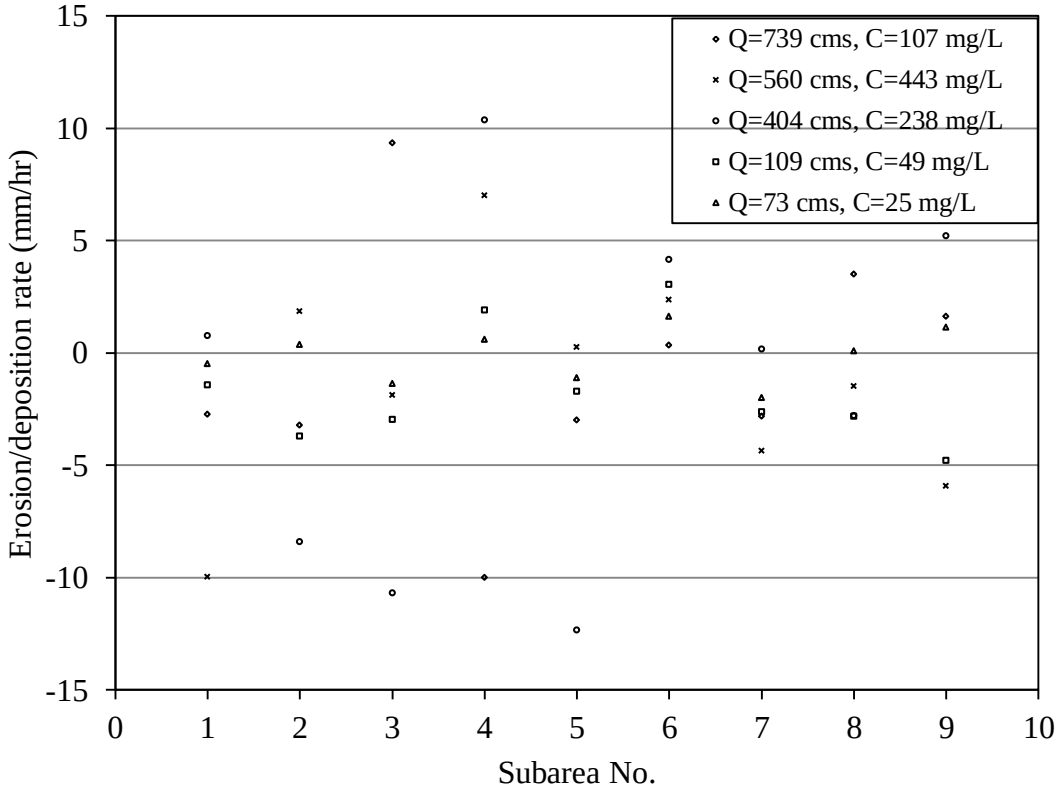

Figure 4.6 Erosion and deposition rate on the Red River under different flow rates based on the results of the MIKE 21-FM AD model (+ is source (erosion) and – is sink (deposition)).

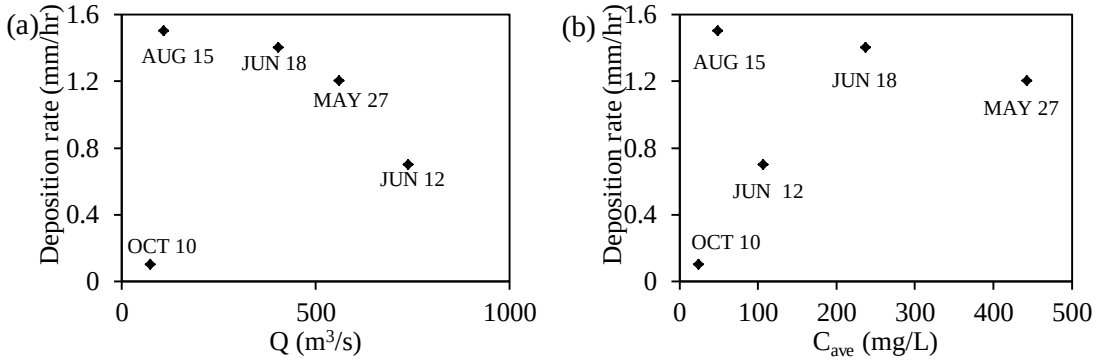

Figure 4.7 (a) Effect of river discharge on the reach-averaged deposition rate, and (b) effect of reach-averaged sediment concentration on reach-averaged deposition rate

4.5 *Conclusion*

A methodology has been suggested using field measurements and numerical solution of cohesive sediment transport governing equation to have a reliable calculation of both erosion and deposition rate in wide rivers. The distinct advantage of this method is the direct in-situ measurement of the erosion and deposition rates over an entire study area and under natural conditions to minimize sampling and testing uncertainties. Reducing the distance between the sampling cross sections may improve the final resolution of the results; however, it may still not be a suitable replacement for direct measurement of a heterogeneous soil's susceptibility to local scour.

An equation has been suggested to estimate the longitudinal dispersion coefficient within the Red River which will be very useful for future sediment transport and environmental studies on the Red River in Winnipeg. Also, estimation of the longitudinal dispersion coefficient is a very important parameter for estimating and managing the spread of contaminations through the river.

The present study gives a better understanding on the morphodynamics of the Red River in Winnipeg which is useful to combine with the current erosion studies to quantify geomorphological changes along the river. As results showed the deposition process was not only a function of the applied shear stress and many factors such as available sediment budget in the river can affect this process; However, study showed that there was not a strong relationship between the deposition rate, flow rate and sediment concentration over 2 year of the study. Therefore, other factors such as sediment and water electro-chemical properties may affect the process which further studies can answer these questions.

4.6 *References*

Andersen, T. J., Fredsoe, J., and Perjrup, M. 2007. In situ estimation of erosion and deposition thresholds by acoustic Doppler velocimeter (ADV). Estuarine, Coastal and Shelf Science, **75**: 327–336.

ASTM standard D5852. 2011. Standard Test Method for Erodibility Determination of Soil in the Field or in the Laboratory by the Jet Index Method. ASTM International, West Conshohocken, PA.

ASTM standard D3977-97. 2013. Standard Test Methods for Determining Sediment Concentration in Water Samples. ASTM International, West Conshohocken, PA.

Blanchard, R. A., Ellison, C. A., Galloway, J. M., and Evans, D. A. 2011. Sediment concentrations, loads, and particle-size distributions in the Red River of the North and selected tributaries near Fargo, North Dakota, during the 2010 spring high-flow event, U.S. Geological Survey Scientific Investigations Report. 2011-5064.

Berkhovskikh V. F., Debolsky V.K., Vishnevskaya G.N., and Zolotareva N.S. 1991, Erosion of cohesive bottom sediments: the influence of the Benthos. Journal of Hydraulic Research, **29**(2), 149-160.

Bloomquist, D., Sheppard, D. M., Schofield, s. and Crowley, R. W. 2012. The Rotating Erosion Testing Apparatus (RETA): A Laboratory Device for Measuring Erosion Rates versus Shear Stresses of Rock and Cohesive Materials. Geotechnical Testing Journal, **35**(4). Available from:

http://www.astm.org/DIGITAL_LIBRARY/JOURNALS/GEOTECH/PAGES/GTJ104221.htm

Briaud, J. L., Ting, F., Chen, H. C., Cao, Y., Han, S.-W., and Kwak, K. 2001. Erosion Function Apparatus for Scour Rate Predictions. Journal of Geotechnical and Geoenvironmental Engineering., **127**(2): 105–113.

Carr, M. L. and Rehmann, C. R. 2007. Measuring the dispersion coefficient with acoustic Doppler current profilers. Journal of Hydraulic Engineering, ASCE,**133**(8), 977–82.

Charonko, C. M. 2010. Evaluation of an in situ measurement technique for streambank critical shear stress and soil erodibility. M.Sc. thesis, Department of Biological Systems Engineering, Virginia Polytechnic Institute and State University, Blacksburg, VA.

Crowley, R. W., Bloomquist, D.B., Shah, D. F., and Holst, C. M. 2012. The Sediment Erosion Rate Flume (SERF): A New Testing Device for Measuring Soil Erosion Rate and Shear Stress. Geotechnical Testing Journal, **35**(4). Available from: http://www.astm.org/DIGITAL_LIBRARY/JOURNALS/GEOTECH/PAGES/GTJ103814.htm

Crowley R. W., Robeck C., and Thieke R. J. 2014, Computational modeling of bed material shear stresses in piston-type erosion rate testing devices. Journal of Hydraulic Engineering, ASCE, **140**(1), 24-34.

Debnath, K. and Chaudhuri, S. 2010, Cohesive sediment threshold: A review. ISH Journal of Hydraulic Engineering, **16**(1), pp. 36-56.

Deng, Z. Q., Singh, V. P., and Bengtsson, L. 2001. Longitudinal dispersion coefficient in straight rivers. Journal of Hydraulic Engineering, ASCE, **127**(11), 919-27.

DHI, 2012. MIKE 21 Flow Model advection-dispersion module scientific documentation. P.1, DHI Group.

Fernando, L., 2009. The effect of flow induced erosion on riverbank stability along the Red River in Winnipeg. M.Sc. thesis, Department of Civil Engineering, University of Manitoba, Winnipeg, MB.

Fischer, H.B., List, E.J., Koh, R. C.Y., Imberger, J., and Brooks N. H. 1979. Mixing in inland and coastal waters. Academic Press, NY.

Fugate, D. C., Friedrichs, C.T., 2002. Determining concentration and fall velocity of estuarine particle populations using ADV, OBS and LISST. Continental Shelf Research **22**, 1867-1886.

Goharrokhi, M. and Clark, S. P. 2015. Using Suspended Sediment Particle Size Distributions to Characterize Sediment Transport On the Red River. In Proceedings of the 22nd Canadian Hydrotechnical Conference. Montreal, QB. April 29- May 2.

Graham, D. I., James, P. W., Jones, T. E. R., Davies, J. M., and Delo, E. A. 1992. Measurement and Prediction of Surface Shear Stress in Annular Flume. Journal of Hydraulic Engineering, ASCE, **118**(9), 1270-1286.

Guerrero, M., Nones, M., Saurral, R., Montroull, N., and Szupiany, R. N. 2013a. Parana River morphodynamics in the context of climate change. International Journal of River Basin Management, 11(4), 423-437.

Guerrero, M., Di Federico, V., and Lamberti, A. 2013b. Calibration of a 2-D

morphodynamic using water-sediment flux map derived an ADCP recording. Journal of Hydroinformatics, 15(3), 813-828.

Guerrero, M., Latosinski, F., Nones, M., Szupiany, R. N., Re, M., and Gaeta, M. G. 2015. A sediment fluxes investigation for the 2-D modelling of large river morphodynamics. Advances in Water Resources, 81, 186-198.

Hanson, G.J. 1991. Development of a JET index to characterize erosion resistance of soils in earthen spillways. Transactions of the ASAE, **34**(5): 2015–2020.

Hanson, G. J. and Cook, K. R. 2004. Apparatus, test procedures, and analytical methods to measure soil erodibility in situ. Applied Engineering in Agriculture. **20**(4), 455-462.

Henderson, M. R. 1999. A Laboratory Method to Evaluate the Rates of Water Erosion of Natural Rock Materials. M. Sc. thesis, University of Florida, Gainesville, FL.

Houwing, E.J., van Rijn, L.C. 1997. In Situ Erosion Flume (ISEF): determination of bed-shear stress and erosion of a kaolinite bed. Journal of Sea Research, **39**, 243-253.

Huang J., Hilldale R.C., and Greimann B.P. 2006, Cohesive sediment transport. Erosion and sedimentation manual, Chapter 4, US Department of the Interior Bureau Reclamation.

Jianfar, A. 2014. Evaluation of Erosion Rates and Their Impact on Riverbank Stability. M. Sc. thesis, University of Manitoba, Winnipeg, MB.

Kashefipour, S. M. and Falconer, R.A. 2002. Longitudinal dispersion coefficients in natural channels. Water Research, **36**(6), 1596-1608.

Kerr, K. 2001. A Laboratory Apparatus and Methodology for Testing Water Erosion in Rock Materials. M. Eng. thesis, University of Florida, Gainesville, FL.

Kimiaghalam N., Goharrokhi M., Clark S.P. and Ahmari H. 2013. Riverbank erosion on the Red River in Winnipeg. The 21st Canadian Hydrotechnical Conference (CSCE), Banff, AB, May 14-17, paper: CSCE-64.

Kimiaghalam, N., Clark, S. & Ahmari, H., 2015a. An experimental study on the effects of physical, mechanical, and electrochemical properties of natural cohesive soils on critical shear stress and erosion rate. International Journal of Sediment Research, http://dx.doi.org/10.1016/j.ijsrc.2015.01.001.

Kimiaghalam, N., Goharrokhi, M., Clark, S. & Ahmari, H., 2015b. A comprehensive fluvial geomorphology study of riverbank erosion on the Red River in Winnipeg, Manitoba, Canada. Journal of Hydrology, **529**(3), 1488-1498,

http://dx.doi.org/10.1016/j.jhydrol.2015.08.033

Maa, J.-Y. and Kwon, J. -I. 2007. Using ADV for cohesive sediment settling velocity measurements. Estuarine, Coastal and Shelf Science, **73**, 351-354.

Maa, J.-Y., Sanford, L., & Halka, J. 1998. Sediment Resuspension Characteristics in Baltimore Harbor, Maryland. Marine Geology, **146**, 137-145.

Mazurek, K.A., Rajaratnam, N., and Sego, D.C. 2001. Scour of cohesive soil by submerged circular turbulent impinging jets. Journal of Hydraulic Engineering, **127**(7), 598–606.

McNeil, J., Taylor, C., and Lick, W. 1996. Measurements of Erosion of Undisturbed

Bottom Sediments with Depth. Journal of Hydraulic Engineering, **122**(6), 316–324.

Meng X.M., Jia Y.G., Shan H.X., Yang Z.N. and Zheng J.W. 2012, An experimental study on erodibility of intertidal sediments in the Yellow River delta, International Journal of Sediment Research, **27**, 240-249.

Moore, W.L., and Masch, F.D. 1962. Experiments on the scour resistance of cohesive sediments. Journal of Geophysical Research, **67**(4), 1437–1446.

Parchure, T., & Mehta, A. (198). Erosion of soft cohesive sediment deposites. Journal of Hydraulic Engineering, ASCE, **111**(10), 1308-1326.

Partheniades, E. (1965). Erosion and Deposition of Cohesive Soils. Journal of Hydraulics Engineering, ASCE, **91**(1), 105-138.

Roberts, J., Jepsen, R., Gotthard, D., and Lick, W. 1998. Effects of Particle Size and Bulk Density on Erosion of Quartz Particles. Journal of Hydraulic Engineering, **124**, 1261–1267.

Rouse, H. 1940. Criteria for Similarity in the Transportation of Sediment. In 1st Hydraulics Conference, University of Iowa, Iowa City, Ia., pp. 33–49.

Rutherford, J. C. 1994. *River mixing*. Wiley, Chichester, U.K.

Seo, I. W. and Cheong, T. S. 1998. Predicting longitudinal dispersion coefficient in natural streams. Journal of Hydraulic Engineering, ASCE, **124**(1), 25–32.

Shen, C., Niu, J., Anderson, E. J., and Phanikumar, S. M. 2010. Estimating longitudinal dispersion in rivers using Acoustic Doppler Current Profilers. Advances in Water

Resources, **33**, 615-623.

Sheppard, D. M., Bloomquist, D. B., Marin, J., and Slagle, P. 2005. Water Erosion of Florida Rock Materials. FDOT Report No. BC354 RPWO #12, Florida Department of Transportation, Tallahassee, FL.

Weidner, K. L. 2012. Eavaluation of the Jet Test Method for determining the erosional properties of cohesive soils; a numerical approach. M.Sc. thesis, Department of Civil Engineering, Virginia Polytechnic Institute and State University, Blacksburg, VA.

Winterwerp J.C., Cornelisse J.M., and Kuijper C. 1990, Parameters to characterize natural muds. In Abstract Volume, Int. Workshop on Cohesive Sediments, Brussels, KBIN Brussels, 103-105.

CHAPTER 5: MORPHODYNAMICS OF DIVERSION CHANNELS IN NORTHERN MANITOBA

A version of this chapter has been submitted for publication in Canadian Water Resources Journal:

Kimiaghalam, N. and Clark, S. P., 2016. *Morphodynamics of Diversion Channels in Northern Manitoba, Canada*. Canadian Water Resources Journal, MI: TCWR-2016-0018.

The 2-Mile and 8-Mile diversion channels in Northern Manitoba help to maintain the efficiency of Manitoba Hydro's hydroelectric generating stations located downstream on the lower Nelson River Hydro and also assist with flooding control on Lake Winnipeg. Erosion within the channels has been consistently monitored for several decades in order to better understand these processes to ensure the future performance of the channels. Morphodynamics studies in these channels are complicated due to the high variability of the bed and bank material, the effect of severe cold weather on the erodibility of the channel banks, and the effect of the surrounding lakes on the hydrodynamic conditions of these channels. The present study includes field measurements, experimental testing, and hydrodynamic and thermal numerical modelling to quantify morphological changes within the channels. Moreover, thirty years of monitoring data were analyzed to validate the results of the study.

5.1 *Introduction*

Morphodynamics of open channels have not been fully understood in part due to a high variation of channel bed and bank material behavior in different locations. Generally, sediments are categorized into two groups: (1) cohesive and (2) non-cohesive. Particle self-weight is the main resisting force against motion of non-cohesive sediment; while inter-particle bonds become significant in cohesive sediment due to the presence of an adequate amount of clay in the sediment structure (Winterwerp & Van Kesteren 2004). The presence of 10% clay in a sediment structure may change the soil behavior and cause the inter-particle bonds to govern the sediment behavior (Debnath & Chaudhuri 2010). Erosion and deposition are the most significant factors on the final geometry of a channel (Kimiaghalam et al. 2015a; Kimiaghalam et al. 2015c). It is important to investigate the channel bank and bed erosion separately due to the more complex nature of bank erosion. Applied shear stress due to current and waves, channel bank geometry, and subaerial processes such as wetting-drying and seasonal freeze-thaw are the three main factors that can cause erosion in a channel (Thorne 1982; Lawler et al. 1997; Lawler et al. 1999; Kimiaghalam et al. 2015a). Therefore, it is important to investigate the effect of these three factors on the future geomorphology of the channel.

5.1.1 *Fluvial Processes*

Fluvial processes include erosion and deposition due to the total hydraulic applied shear stress (τ_a) caused by current and waves. Generally, four modes of fluvial erosion exist (Winterwerp & Van Kesteren, 2004): (1) entrainment occurs when the soft surface of cohesive material behaves as a fluid; (2) floc erosion occurs when τ_a is slightly larger than threshold of sediment erosion (τ_c) and flocs detach from the surface; (3) surface

erosion when τ_a is larger than τ_c and small layers of surface material start to detach from the surface of the sample; (4) mass erosion when τ_a is much larger than τ_c causing large chunks of material to erode from the surface at a very high rate (Huang et al. 2006). A well-known fluvial erosion rate formula is an exponential or power form of the excess shear stress equation such as (Partheniades 1965; Arulanandan, et al., 1980):

$$E = k_d(\tau_a - \tau_c)^\alpha \quad \textbf{Equation 5-1}$$

where E [mm/h] is the erosion rate, k_d is the material dependent coefficient, and α is an empirically derived exponent that has been generally assumed to be equal to 1 (Darby et al. 2007). Therefore, the first step is to find the fluvial erodibility parameters τ_c and k_d for a study area. Several researchers have presented equations to estimate τ_c and k_d as a function of physical, mechanical, and electrochemical properties for their study reaches (Dunn, 1959; Smerdon and Beasley 1961; Carlson and Enger 1962; Owen 1975; Thorn and Parsons 1980; Otsubo and Muraoka 1988; Michener and Torfs 1996; Amos et al. 1997; Hanson and Simon 2001; Leonard and Richard 2004; Mostafa et al. 2008; Meng et al. 2012; Kimiaghalam et al., 2015b).

5.1.2 *Slope failure (mass wasting)*

Slope failure occurs when a large mass of riverbank slides due to the gravity force and depends on the soil type, pore-water pressure, and the riverbank geometry (Budhu 2011). It is important to distinguish between fluvial erosion and mass wasting while investigating a riverbank's geomorphology. Fluvial erosion changes the geometry of a riverbank and can cause slope failure (Budhu 2011); therefore, these two processes are dynamic and need to be considered together to understand the future geomorphology of a riverbank. Several researchers have conducted studies to combine fluvial erosion with

slope failure analysis over time to develop comprehensive models for predicting riverbank losses over time (Darby & Thorne 1996; Darby et al. 1996; Darby et al. 2007; Luppi et al. 2008). Generally, Equation 5-1 was used to evaluate fluvial slope change and then a coupled seepage and slope failure analysis was performed to quantify the slope safety factor and the process was repeated for a number of time steps.

5.1.3 *Effect of subaerial processes*

Subaerial processes such as freeze-thaw and wetting-drying can accelerate bank and bed material loss by affecting soil properties (Hooke 1979; Couper and Maddock 2001; Wynn et al. 2008). Due to the low variation of water surface elevation within the study areas, this study focused on the effect of freeze-thaw on the streambank erosion. Couper (2003), Yumoto et al. (2006), and Kimiaghalam et al. (2015a) studies showed that subaerial processes significantly accelerate fluvial riverbank erosion and slope failure. Several researchers have conducted studies to quantify the effect of freeze-thaw cycles and frost temperature on the critical shear stress and erosion rate of different riverbanks (Formanek et al. 1984; Van Klaveren 1987; Edwards et al. 1995; Van Klaveren and McCool 1998; Kimiaghalam et al. 2015a). Kimiaghalam et al. (2015a) showed that the number of freeze-thaw cycles reduced the critical shear stress of clay samples from the Red River bank in Winnipeg and can accelerate both fluvial and mass wasting processes by dramatic reduction of the cohesive soil cohesion.

The present study focused on quantifying morphological changes along two diversion channels in northern Manitoba in Canada that assist with maintaining adequate flow for downstream hydro-power production in northern Manitoba. The aim of the study was to investigate possible factors that can affect the channels geometry and thereby alter

channel performance. Access to these channels was difficult and only possible using waterways from the adjacent lakes; hence, transferring heavy equipment for soil sampling and measurements was not possible.

5.2 *Material and Methods*

5.2.1 *Study area, sampling, and field measurements*

2-Mile and 8-Mile channels were excavated in the 1970's in northern Manitoba to increase the winter out flow of the lakes that supply water to the Nelson River Hydro Electric Development (Gill 1973) and also assist with flooding control on Lake Winnipeg. These two channels convey water between three lakes in northern Manitoba. 2-Mile channel flows from the seventh largest lake in North America, Lake Winnipeg (561047 E, 5956165 N), into the Playgreen Lake (563119 E, 5958113 N) (Figure 5-1a). 2-Mile Channel has a bed slope of 0.02% with average side slope of 1:5. Average annual flow through the channel is 930 m^3/s with a peak flow around 2300 m^3/s and water surface elevation varies between 216.7-218.5 m. During the peak flow events the channel top width is approximately 207 m and the average water depth is 8.6 m. 8-Mile Channel conveys flow between Playgreen Lake at the upstream (546039 E, 5986436 N), and Kiskittogisu Lake at the downstream of the channel (538777 E, 5993821 N) (Figure 5-1a). 8-Mile Channel has a bed slope of 0.01% with average side slope of 1:9. Average annual flow through the channel is 772 m^3/s with a peak flow around 1900 m^3/s and a water surface elevation that varies between 217-218 m. During peak flow events, the top width varies between 207 and 1700 m and the average water depth is 7.5 m. Flow conditions in these channels are highly impacted by the flow conditions in the surrounding lakes. A surveying program was established by Manitoba Hydro since 1978

due to a concern about the effect of geomorphological changes, in particular fluvial erosion, on flow conditions in these channels and surrounding environment (Manitoba Hydro 2010). Figure 5-1b and Figure 5-bc show the locations that have been surveyed since 1978. Morphodynamics study of these channels is complicated since flow-induced erosion may occur in conjunction with the effect of significant wave action due to the large fetch length on the adjacent lakes. In particular, it is necessary to study the effect of wave and current combinations in 2-Mile Channel due to the waves generated in Lake Winnipeg.

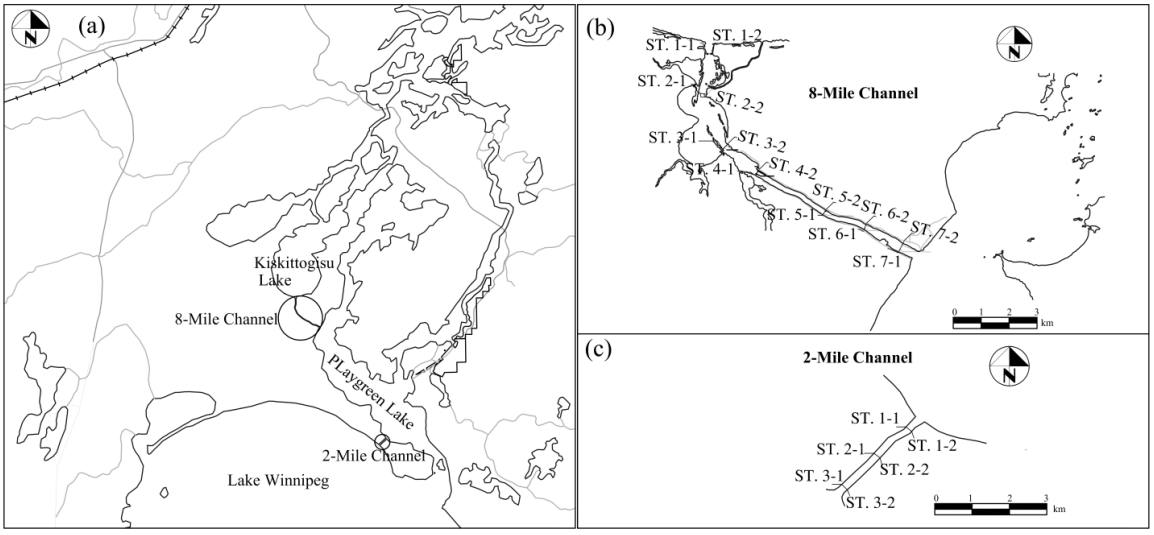

Figure 5-1 Study areas and sampling location: (a) the entire study area; (b) 8-Mile Channel sampling locations; (c) 2-Mile Channel sampling locations

A primary step to understanding the fluvial processes along the channels is to understand the behavior of the channels' bed and bank material; therefore, material samples were needed to perform soil property tests. Soil samples were taken from the channels' bank and bed at various locations along their length. ASTM standard Shelby tubes were used to take relatively undisturbed soil samples from the channel banks; undisturbed samples were necessary for measuring soil erodibility and mechanical properties. Grab soil

samples were taken to test intrinsic soil properties such as grain size distribution. Moreover, water samples were taken from several locations and different depths (surface, bottom, and middle) to test the amount of total suspended solids (TSS) in the water to understand the deposition potential due to the incoming sediment from the lakes. Soil and water samples were taken from locations close to the locations where historical bathymetric data were available (Figures 5-1b and 5-1c). Also, velocity profiles and discharge were measured several times in July 2013 at the entrance and exit of the channels using an acoustic Doppler current profiler (ADCP).

5.2.2 *Experimental setup*

To understand the primary properties of the channels material, three experiments were performed. The grain size distribution was quantified to categorize the channel material in terms of cohesive or non-cohesive. Sieve analysis and hydrometer tests were performed according to the ASTM standards D422-63 (ASTM 2007) and D2487-11 (ASTM 2011) on the grab soil samples from the bed and bank material samples to find median grain size as well as clay, silt, and sand fractions of the samples. TSS measurements according to the ASTM standard D3977-97 (ASTM, 2013) were performed to assess the possibility and importance of deposition within the channels. The third and the most important test was measuring erodibility properties of the undisturbed samples from the study areas to find critical shear stress (τ_c) and material dependent coefficient (k_d) of the undisturbed samples. For this purpose, an Erosion Measurement Device (EMD) that is a piston-type measurement device similar to Briaud et al. (2001) was used to measure these two parameters. The complete methodology and device description can be found in Kimiaghalam et al. (2015a).

5.2.3 *Hydrodynamic numerical modelling*

Hydrodynamic conditions within the study areas were simulated for four years between 2010 and 2014. Hydrodynamic numerical modelling had three main steps: (1) generating wind-waves using MIKE 21 NSW; (2) developing a coupled wave-current hydrodynamic model using MIKE 21 Flow model FM; (3) calculating applied shear stress due to a combination of waves and current.

5.2.3.1 Wave modelling using MIKE 21 NSW

In this study, the effect of wave action was only investigated on the 2-Mile channel due to its proximity to Lake Winnipeg and short channel length . The MIKE 21 NSW is a two dimensional wind-wave model based on the conservation equation for the spectral wave action density (DHI 2012a). The model solves the equations using Eulerian finite difference method to assess necessary parameters to calculate forces acting on a shoreline such as wave height, wave period, and wave direction (DHI 2012a). Therefore, this model was appropriate to find the necessary wave parameters to calculate applied shear stress on the channel. The study area bathymetry, including that of Lake Winnipeg and 2-Mile Channel was a required input for the model. Two types of boundary conditions were necessary to develop a wave model using MIKE 21 NSW: (1) offshore boundary conditions that included significant wave height (H_{m0}), mean wave period (T_m), mean wave direction (MWD), and directional standard deviation (DSD). Measured wave data between 2010-2014 at the Fisheries and Oceans Canada station C45144 (550732 E, 5898126 N) were used as boundary conditions to generate offshore waves during this period; (2) a symmetrical lateral boundary condition was used based on recommendations in the MIKE 21 manual. The last step to simulate wind-waves was to specify water

surface elevation and wind data over the study period. Wind speed and direction were obtained from the same wave measurement buoy, station C45144. The quasi-stationary simulation was run to generate waves within the study area.

5.2.3.2 Hydrodynamic modelling using MIKE 21 Flow Model FM

The MIKE 21 Flow Model FM is a two dimensional hydrodynamic model based on a solution of the shallow water Navier-Stokes equations. The model uses a flexible mesh to solve the equations using the finite volume method (DHI 2012b). The model domain included collected bathymetric data of the channels and generated mesh on these data within the channels. Upstream (entrance of the channels) discharge and downstream (exit of the channels) water surface elevation were the boundary conditions. The initial condition was defined as the average water surface elevation between the upstream and downstream boundaries on the first day of the simulation. The models were calibrated by changing the Manning number throughout the channels. The primary calibration was performed by comparing available and simulated water surface elevation as well as the measured velocity profile during a high flow event. After calibrating the models for a wide range of flow through the channels, the calibrated models were used to calculate applied shear stress.

5.2.3.3 Calculating applied shear stress using MIKE 21 Flow Model FM-MT

Several scenarios were used to calculate applied shear stress over the study areas. Since wave actions are negligible through 8-Mile Channel, pure current formulation was considered to calculate applied shear stress on the channel. MIKE 21 Flow model FM-MT uses the following equation to calculate applied shear stress in the case of a pure current condition (DHI 2012c):

$$\tau_{a,c} = \frac{1}{2}\rho f_c V^2 \quad \textbf{Equation 5-2}$$

where $\tau_{a,c}$ [Pa] is the current applied shear stress, f_c is the current friction factor, and V [m/s] is the mean current velocity. Current friction factor can be calculated using the following equation:

$$f_c = 2(2.5\left(\ln\left(\frac{30h}{k}\right) - 1\right))^{-2} \quad \textbf{Equation 5-3}$$

where h [m] is the water depth and k [m] is the bed roughness. The bed roughness can be calculated using Manning number (n) by the following equation (DHI 2012d):

$$\frac{1}{n} = \frac{25.4}{k^{1/6}} \quad \textbf{Equation 5-4}$$

For 2-Mile channel applied shear stress was calculated using Equation 5-2 for pure current condition and using the following equation for a combination of wave and current (DHI 2012c):

$$\frac{\tau_{a,max}}{\tau_{a,c} + \tau_{w,c}} = 1 + a'\left(\frac{\tau_{a,c}}{\tau_{a,c} + \tau_{w,c}}\right)^m (1 - \frac{\tau_{a,c}}{\tau_{a,c} + \tau_{w,c}})^l \quad \textbf{Equation 5-5}$$

Where $\tau_{w,c}$ [Pa] is the wave applied shear stress, $\tau_{a,max}$ [Pa] is the total maximum applied shear stress, and $a', m,$ and l are constants. Wave applied shear stress was calculated using the following equation:

$$\tau_{a,w} = \frac{1}{2}\rho f_w {U_b}^2 \quad \textbf{Equation 5-6}$$

where U_b [m/s] is the horizontal mean wave orbital velocity at the bed and f_w is the wave friction factor. Wave friction factor can be calculated using the following equation:

$$\begin{cases} f_w = 0.47 \\ f_w = \exp(5.213\left(\frac{a}{k}\right)^{-0.194} - 5.977), \ 1 < \frac{a}{k} \leq 3000 \end{cases} \quad \textbf{Equation 5-7}$$

where a [m] is the horizontal mean wave orbital motion at the boundary (DHI 2012c).

5.2.4 *Thermal modelling*

Average daily air temperature within the study areas were below the freezing point for 7 months with an average daily temperature of -21.5°C in January based on the historical temperature record between 1981-2010 at the Norway House airport weather station (Environment Canada, 2015); therefore, it was essential to understand the effect of very cold weather on the channels' bank material. The TEMP/W model from GEO-SLOPE International was used to calculate and model soil temperature for each study location. The model is a finite element software that solves the 2D heat transfer equation. The primary model inputs were the frozen and unfrozen thermal conductivity, frozen and unfrozen volumetric heat capacity, and volumetric water content which were estimated based on measured soil properties and the equations developed by Farohki (1985). The boundary condition was the soil surface temperature which was calculated using available climate data such as precipitation, air temperature, pressure, and relative humidity at the Norway House weather station. The most important result was the depth of the active layer that the bank material experienced freeze-thaw to understand the impacted zone of the riverbank by the seasonal freeze-thaw over the period of the study.

5.3 *Results*

5.3.1 *Channels material properties*

Table 5-1 shows a summary of the grain size distribution, EMD, and TSS tests on the bed and bank materials. According to the field observations the entrance and exit of 2-Mile Channel close to stations 1 and 3 contained sandy material and were categorized as non-

Table 5-1 Channel bed and bank material samples and water suspended solids

Channel	Station ID	Location	d50 (mm)	Clay %	Silt %	Sand %	τ_c (Pa)	k_d (mm/Pa.hr)	Average TSS (mg/L)
2- Mile	STATION 1-1	Bank							7
		Bed	0.0019	50	46	4			
	STATION 1-2	Bank							4
		Bed							
	STATION 2-1	Bank	0.002	42	44	14	7.8	0.67	4
		Bed							
	STATION 2-2	Bank	0.002	50	45	5	10.3	0.64	4
		Bed							
	STATION 3-1	Bank							3
		Bed	0.0019	50	38	12			
	STATION 3-2	Bank							3
		Bed	0.0087	40	13	47			
8- Mile	STATION 1-1	Bank	0.0004	94	4	2	4.9	0.33	11
		Bed							
	STATION 1-2	Bank							8
		Bed	0.0004	80	18	2			
	STATION 2-1	Bank	0.0013	65	33	2	1.6	8.67	11
		Bed							
	STATION 2-2	Bank	0.0011	60	34	6	8.6	0.9	11
		Bed							
	STATION 3-1	Bank	0.0015	56	27	17	2.7	0.98	12
		Bed	0.002	50	46	4			
	STATION 3-2	Bank	0.0017	54	45	1	2.7	0.42	10
		Bed	0.0028	44	54	2			
	STATION 4-1	Bank	0.45	17	8	75	Non-cohesive		12
		Bed	0.0033	43	54	3			
	STATION 4-2	Bank	0.17	20	9	71	Non-cohesive		10
		Bed							
	STATION 5-1	Bank	Peat and organic material						9
		Bed							
	STATION 5-2	Bank	Peat and organic material						8
		Bed							
	STATION 6-1	Bank	Peat and organic material						8
		Bed	0.004	40	57	3			
	STATION 6-2	Bank	0.02	24	37	39	1.6	6.95	5
		Bed							
	STATION 7-1	Bank	0.0074	25	50	25	0.3	3.68	11
		Bed	Peat and organic material						
	STATION 7-2	Bank							7
		Bed	0.22	0	0	100			

cohesive material; however, the middle of the channel near stations 2-1 and 2-2 contained a high amount of clay and silt material with around 50% clay in the soil samples structure

and a median grain size of 0.002 mm. Results of the EMD test showed that these samples had a high τ_c that varied between 7.8-10 Pa and a low k_d that varied between 0.64-0.67 mm/(Pa.hr). The bed materials contained more than 40% clay and were more homogeneous than the bank material along the channel. Figure 5-2 shows typical cohesive material from the 2-Mile Channel bank near stations 2-1 and 2-2. The average measured TSS in August 2013 was between 3-7 mg/L when the discharge was around 1120 m^3/s (close to the average channel annual flow of 930 m^3/s). The low TSS in the channel indicated that the incoming sediment budget in the channel was low and deposition through the channel was insignificant.

Figure 5-2 2-Mile Channel cohesive bank material sample near stations 2-1 and 2-2

8-Mile Channel bank material contained different varieties of soil and sediment. Stations 7-1 and 7-2 were near the upstream entrance of the channel. Station 7-1 had a steep slope with a high amount of silty material. Critical shear stress of the undisturbed sample was very low around 0.3 Pa and erodibility was very high. Station 7-2 was a sandy beach that contained fine sand. Bed material at this station mostly contained sand and organic material; therefore, a high amount of erosion was expected. The bank at Station 6-1 contained peat and organic material and station 6-2 bank contained peat and sandy material with around 24% clay in the soil matrix with a low τ_c around 1.6 Pa and a high

k_d around 7 mm/Pa.hr. Stations 5-1 and 5-2 contained only peat and organic material that were very soft material with high water content. Station 4-1 and 4-2 contained a high amount of sand (> 70%) and despite the presence of clay in the soil matrix, this material behaved like non-cohesive soil. Stations 3-1 and 3-2 contained silty clay with a high amount of organic material. Both stations had τ_c around 2.7 Pa and k_d of 0.42 and 0.98, respectively. Stations 2-1 and 2-2 contained same the amount of clay material at around 60% but showed very different resistance against fluvial erosion. Station 2-1 had a low τ_c of 1.6 Pa and a high k_d of 8.67 while station 2-2 had a high τ_c of 8.6 Pa and a low k_d of 0.9. Significant effect of subaerial processes was observed in the samples from station 2-1. Station 1-1 contained pure clay with τ_c of 4.9 Pa and a low k_d of 0.33. Station 1-2 was not accessible for sampling due to very shallow water. Figure 5-3 shows soil samples from these sites.

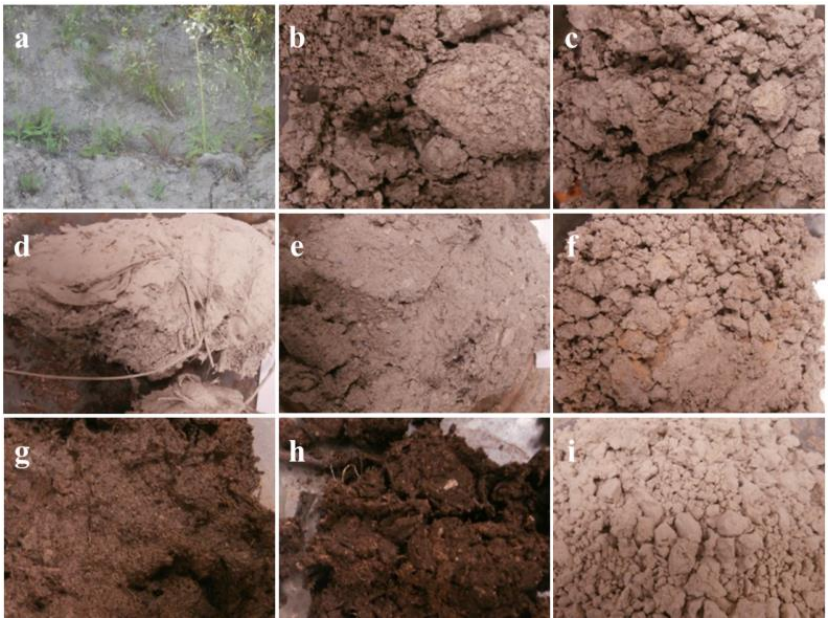

Figure 5-3 8-Mile Channel bank dry material samples: (a) Station 1-1; (b) Station 2-1; (c) Station 2-2; (d) Station 3-1; (e) Station 4-1; (f) Station 4-2; (g) Station 5-2; (h) Station 6-1; (i) Station 7-2.

5.3.2 *Historical bathymetric monitoring*

Bathymetric surveys were performed over the cross sections between 1979 and 2010. Figure 5-4 shows a cross sectional survey near the sampling location 2-1 and 2-2 in 2-Mile Channel that contained cohesive material with a high critical shear stress. The observed erosion pattern from over 32 years of erosion was in qualitative agreement with the EMD results since the bank had eroded around 0.5 m near station 2-2 and 1 m near location 2-1 while the EMD results showed that the bank material from station 2-1 had a lower critical shear stress than station 2-2 (around 2.5 Pa less than station 2-2). The part of the riverbank that experienced the most significant erosion was close to the water surface where the applied shear stress was very low; therefore, it is hypothesized that subaerial processes had a significant effect on riverbank erodibility. It is expected that the effect of seasonal freeze-thaw was more significant than wetting/drying in reducing the critical shear stress of the channel bank against fluvial erosion since the water surface elevation did not change significantly through the channel. A total of 1.1 m erosion was observed over the channel bed where the highest applied shear stress occurred.

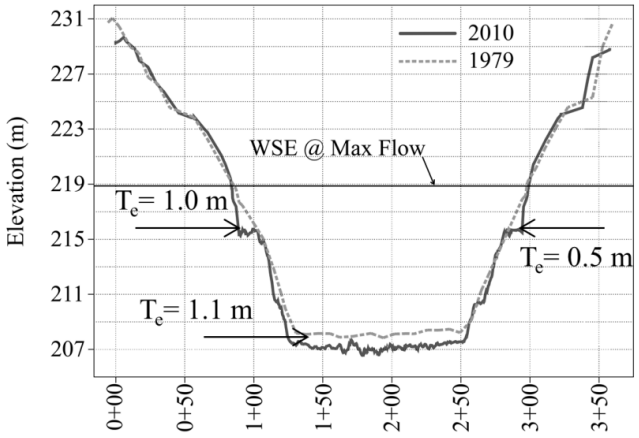

Figure 5-4 2-Mile Channel sections survey in 1979 and 2010 at locations near to stations 2-1 and 2-2 and total amount of erosion from banks and bed

Figures 5-5a-5-5g shows historical survey results over cross sections 1 to 7 within the 8-Mile Channel between 1979 and 2010. Total erosion varied significantly within cross sections which was in good agreement with the results of EMD and physical soil properties tests since according to these results the material from 8-Mile Channel had a wide range of critical shear stress (0.3-8.6 Pa) as well as a variety of different soil types (clay, silty-clay, silt, and sand). The highest bank erosion was observed near stations 4-1 (Figure 5-5d) and 1-1 (Figure 5-5a) which contained fine sands and behaved similar to non-cohesive material (Table 1). The highest amount of channel bed erosion was observed near station 7 where the bed material contained a high amount of sand.

5.3.3 *Hydrodynamic numerical models*

The 2-Mile Channel hydrodynamic model was calibrated with a Manning number of 0.029 that is equivalent to $k_s = 0.17$ m using Equation 5-4. This Manning number was a summary of the effect of intrinsic and bed roughness as well as vegetation. Figure 5-6 shows the 2-Mile Channels validation curve for three years between 2003 and 2005 with R^2 =0.86 that shows the model worked efficiently. Moreover, Figure 5-7 shows measured and simulated velocity profiles at the exit and entrance of the channel at a discharge close to the channel peak flow and confirmed that the calibrated model works well. Significant wave height and wave period were the two important wave properties for estimating wave-induced applied shear stress over the 2-Mile Channel that were obtained from the MIKE 21 NSW model. Average wave height varied between 0 - 0.15 m and wave period varied between 0.5-1.5 sec. Figure 5-10 shows variation of average applied shear stress with discharge over the channel boundary for both pure current and a combination of wave and current. This figure indicated that incoming waves from Lake Winnipeg had a

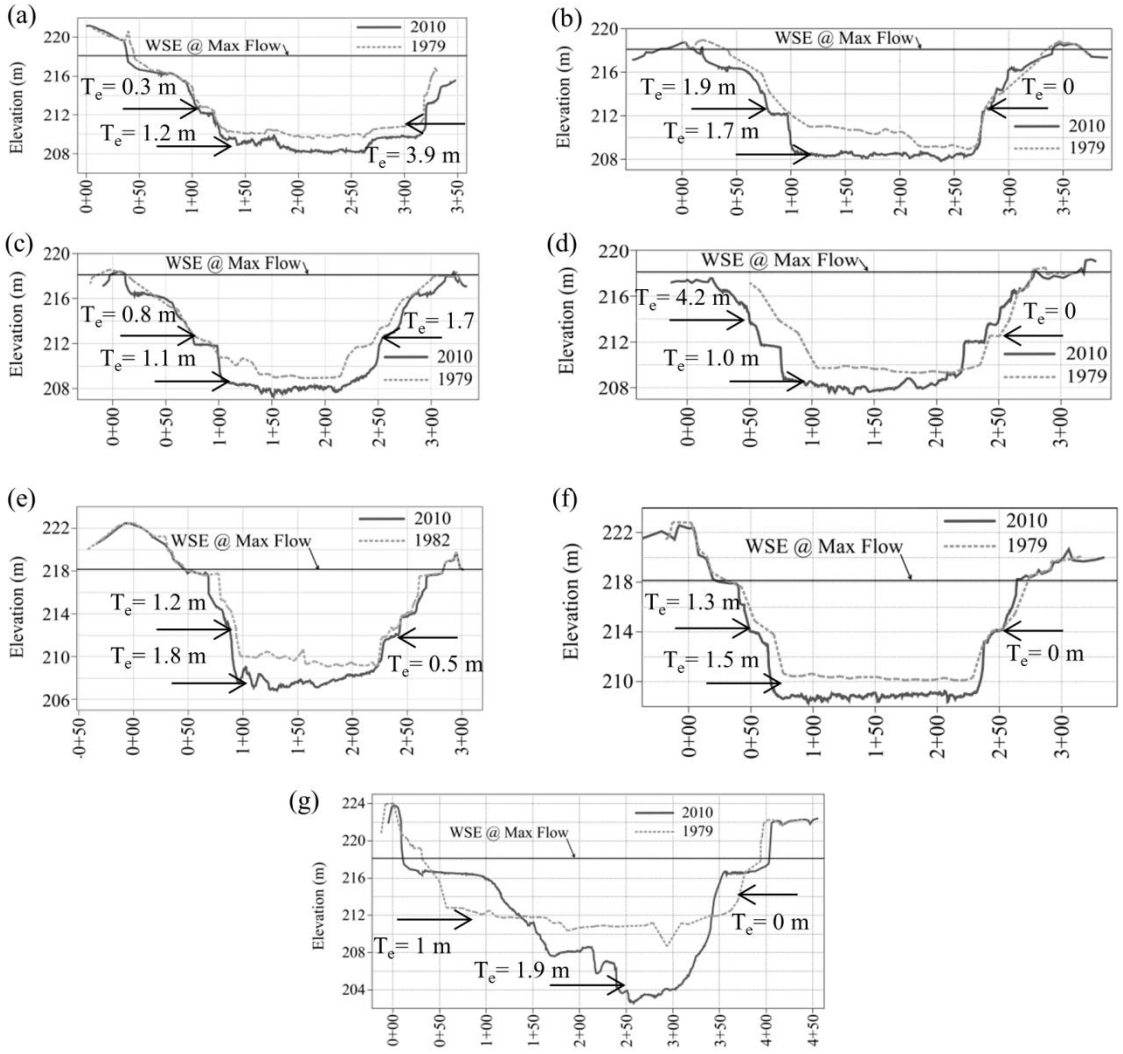

Figure 5-5 8-Mile Channel sections survey in 1979 and 2010 and total amount of erosion from banks and bed: (a) stations 1-1 and 1-2; (b) stations 2-1 and 2-2; (c) stations 3-1 and 3-2; (d) stations 4-1 and 4-2; (e) stations 5-1 and 5-2; (f) stations 6-1 and 6-2; (g) stations 7-1 and 7-2.

significant impact on the total applied shear stress when the channel flow rate was low and became insignificant with increasing flow rate. A strong linear correlation was found between the channel discharge (Q) and total average applied shear stress (τ_a) with R^2=0.98:

$$\tau_a = 0.0032Q - 1.45 \qquad \textbf{Equation 5-8}$$

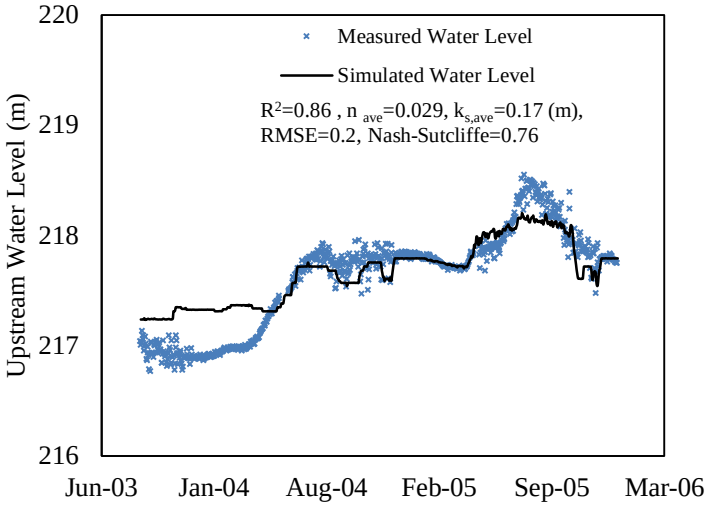

Figure 5-6 Validation curve for 2-Mile Channel entrance water level for 3 years: 2003-2006

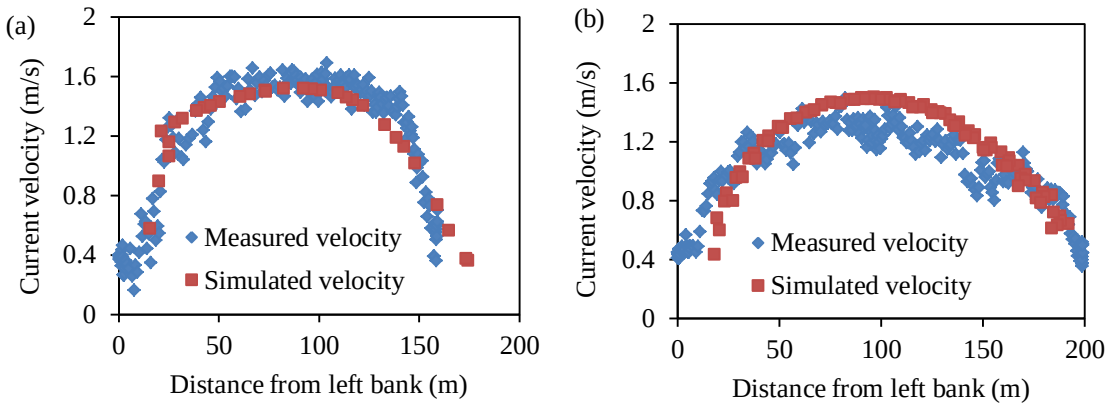

Figure 5-7 2-Mile Channel measured and simulated velocity profile at Q=1818 m3/s: (a) at the entrance of the channel; (b) at the exit of the channel

Figure 5-11 shows variation of applied shear stress with the 2-Mile Channel discharge over the channel bank, bed, and entire wetted perimeter of the channel. This figure indicated that the channel bed experienced a higher amount of applied shear stress than the riverbank.

The 8-Mile Channel hydrodynamic model was calibrated with a Manning number of 0.021 that is equivalent to $k_s = 0.02$ m using Equation 5-4. Figure 5-8 shows the 8-Mile

Channel's validation curve for two years between 2003 and 2005 with R^2 =0.64. Moreover, Figure 5-9 shows measured and simulated velocity profiles at the middle and entrance of the channel at a discharge close to the channel peak flow and confirmed that the calibrated model works well. Figure 5-12 shows the variation of average applied shear stress with discharge over the channel boundary. A strong linear correlation was found between the channel discharge (Q) and total average applied shear stress (τ_a) with R^2=0.98:

$$\tau_a = 0.0013Q - 0.48 \qquad \textbf{Equation 5-9}$$

Figure 5-13 shows the variation of applied shear stress with 8-Mile Channel discharge over the channel bank, bed, and entire wetted perimeter of the channel. This figure indicated that the channel bed experienced higher amount of applied shear stress than the riverbank and the entire channel.

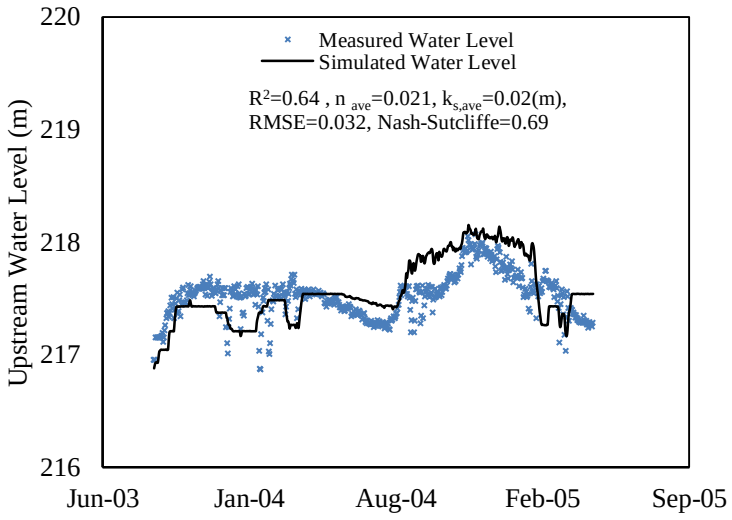

Figure 5-8 Validation curve for 8-Mile Channel entrance water level for 2 years: 2003-2005

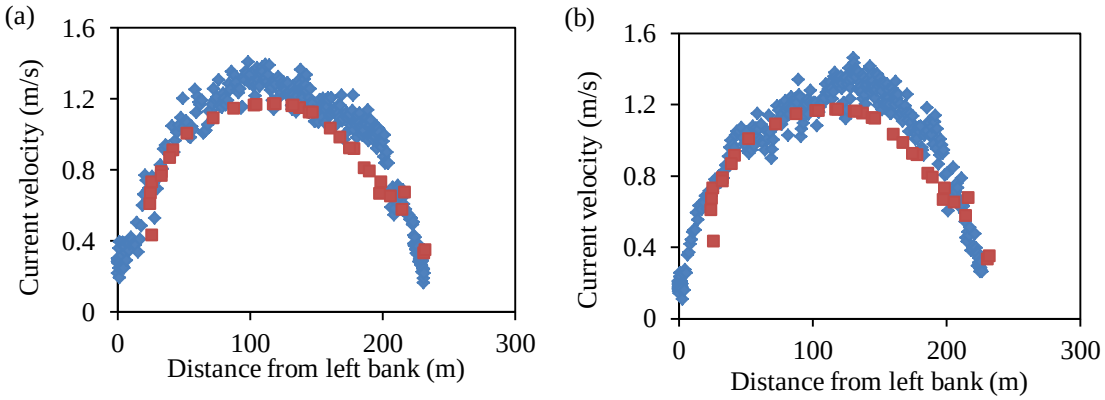

Figure 5-9 8-Mile Channel measured and simulated velocity profile at Q=1648 m3/s: (a) at the entrance of the channel; (b) at the middle of the channel

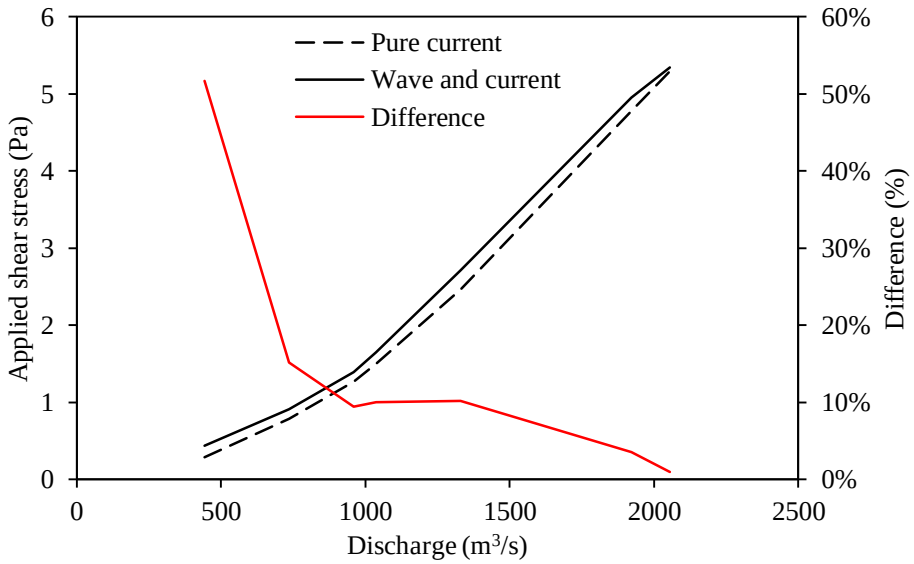

Figure 5-10 Variation of the average applied shear stress with discharge within 2-Mile Channel for pure current and a combination of wave and current

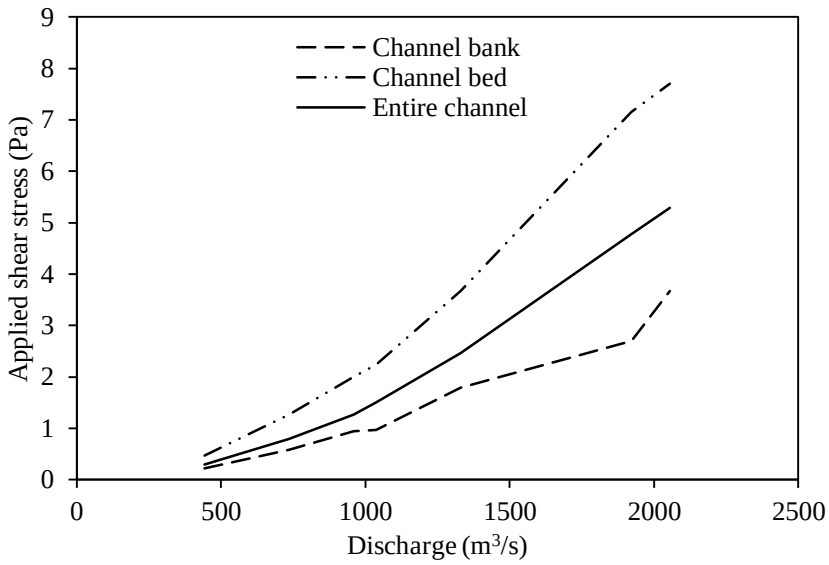

Figure 5-11 Variation of the average applied shear stress with discharge within 2-Mile Channel bank, bed, and the entire wetted perimeter

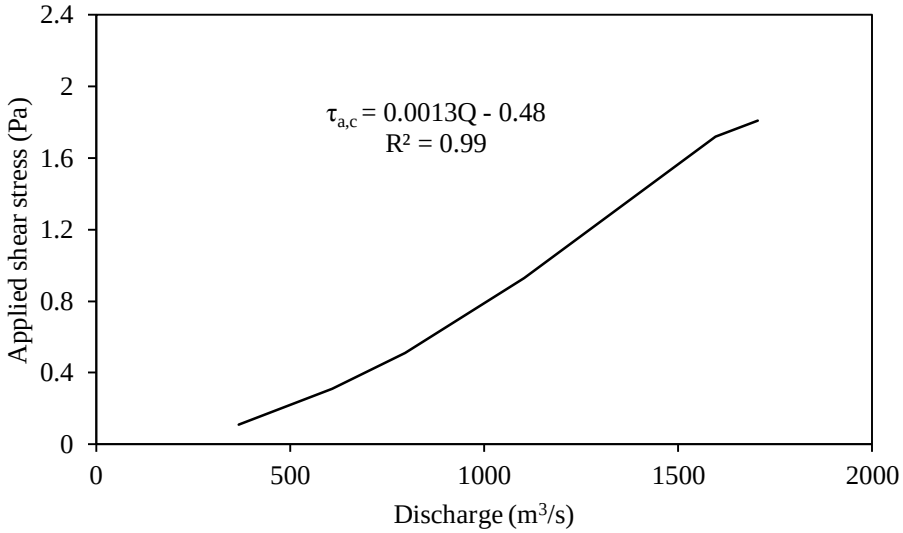

Figure 5-12 Variation of the average applied shear stress with discharge within 8-Mile Channel for pure current condition

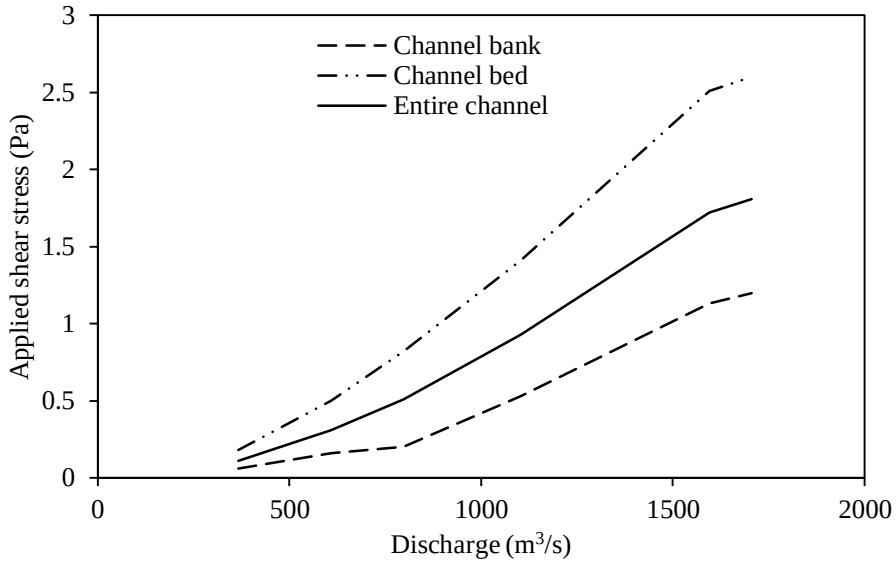

Figure 5-13 Variation of the average applied shear stress with discharge within 8-Mile Channel bank, bed, and the entire wetted perimeter

5.3.4 *Statistical analysis of flow conditions*

Historical flow rate analysis was essential to understand the effect of applied shear stress since erosion and deposition are dynamic processes. Also, in the previous section relationships were found between discharge and applied shear stress; therefore, statistical analysis on flow rates can be used to understand the occurrence duration of a specific amount of applied shear stress within the channels. Figure 5-14 and Figure 5-15 show the estimated channels' flow rate (Bijeljanin, 2013) histogram over 37 years (1977-2014) within the 2-Mile and 8-Mile channels, respectively. These figures are useful tools to understand the history of the exerted applied shear stress within the channels and also are beneficial for future prediction of fluvial processes.

5.3.5 *Thermal models*

Table 5-2 shows the result of TEMP/W thermal model for several samples from the 2-Mile and 8-Mile channels for 4 years between 2010 and 2014. The maximum depth of the

frozen soil in winter varied between 2.3-3 m near stations 2-1 and 2-2 within the 2-Mile Channel and varied between 2.6-3.5 m within the 8-Mile Channel. These numbers indicated at least 3 m of the surface soil had to be removed in order to take undisturbed samples that had not experienced freeze-thaw. This is a very time consuming and expensive process due to the difficult access to these channels. The benefit of this modeling was to define the depth that the bank material experienced seasonal freeze-thaw and show this impacted zone throughout the 4 modelled winters.

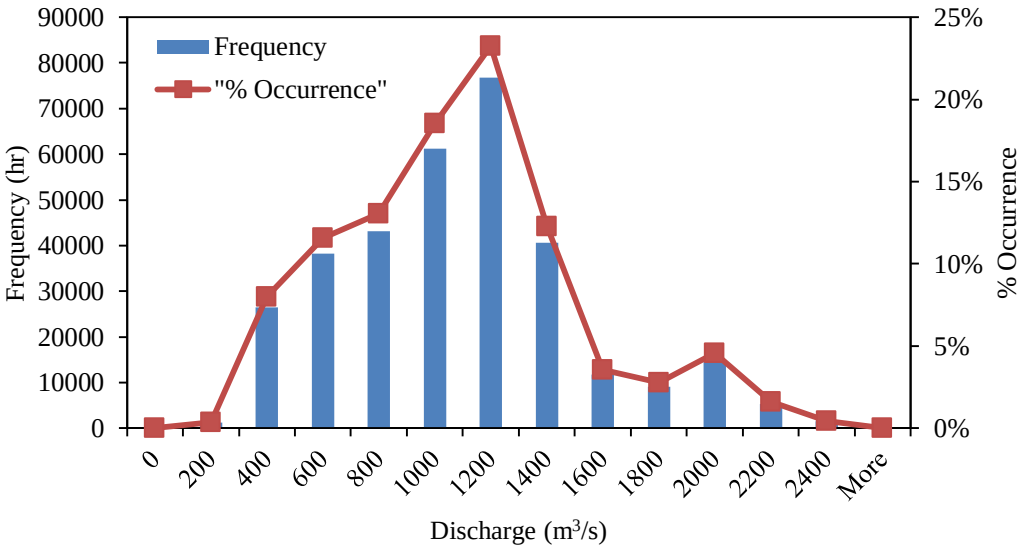

Figure 5-14 Estimated flow histogram of 2-Mile Channel flow rates between 1977-2014

Table 5-2 Active layer thickness for 2-Mile and 8-Mile channels samples based on climate data between 2010 and 2014

Sample ID	Maximum thickness of the active layer (m)			
	2010-2011	2011-2012	2012-2013	2013-2014
2M(1-1)&2M(2-2)	2.3	2.4	2.7	3
8M (1-1)	3.2	2.8	3.3	3.5
8M (2-1)	2.6	2.6	3	3.2
8M (2-2)	2.6	2.4	3	3.1
8M (3-1)	2.6	2.5	3.3	3.2
8M (3-2)	2.8	2.6	3.3	3.5
8M (6-1)	3.1	2.8	3.3	3.5
8M (7-1)	2.9	2.5	3	3.3

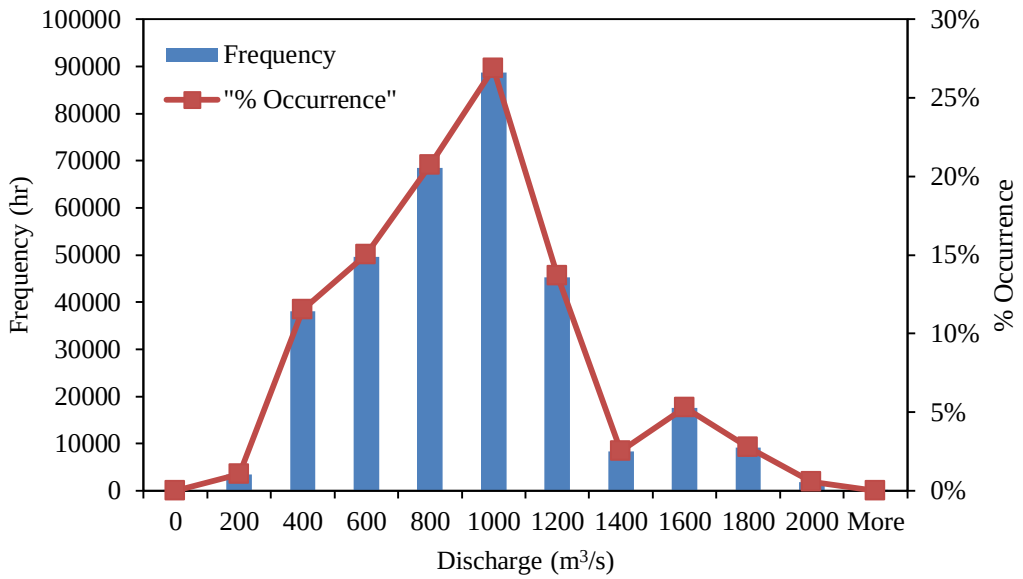

Figure 5-15 Estimated flow histogram of 8-Mile Channel flow rates between 1977-2014

5.4 *Discussion*

According to Figure 5-11, the maximum average applied shear stress over the 2-Mile channel bank was around 3.7 Pa whereas the measured critical shear stress at stations 2-1 and 2-2 varied between 7.8-10.3 Pa; therefore, it can be concluded that these locations were resistant to fluvial erosion. However, historical erosion measurement showed that around 1.10 m and 0.50 m erosion occurred at the channel bank near stations 2-1 and 2-2, respectively, over 33 years. According to Table 5-3, 42% of the erosion happened close to the water surface where the applied shear stress was very low but the channel bank material was impacted by the seasonal freeze-thaw processes. Overall, the cohesive parts of the 2-Mile Channel bank were resistant to fluvial erosion; however, the seasonally frozen section of the channel bank and toe of the bank were susceptible to fluvial erosion due to the effect seasonal freeze-thaw and high applied shear stress at the toe of the bank near the bed (Figure 5-11). Moreover, comparing measured critical shear stress and applied shear stress demonstrated that the seasonal freeze-thaw reduced critical shear

stress of the cohesive channel bank material and increased erodibility of the channel bank. Also, wave action can significantly increase the total applied shear stress when the channel has a low flow rate; although the pure current was the most dominant part of the total applied shear stress. Figure 5-11 shows that the total applied shear stress was quite higher than the channel bank applied shear stress with average applied shear stress around 7.7 Pa for the maximum discharge (twice more than the bank); therefore, it can be concluded that the bed of the channel was more susceptible to fluvial erosion where 1.1 m erosion was observed between 1979-2010. However, consistent bed erosion maintained the original design slope of the channel and with assumption of same water level in the Lake Winnipeg; the erosion would not be an issue on the total flow through the 2-Mile Channel.

Table 5-3 Contribution of the upper part of the channel banks to the total observed erosion between 1979 - 2010 by considering the result of the thermal model and active layer thickness

Channel	Station ID	Contribution of the upper part of the channels bank to the total bank erosion
2-Mile	2-1 & 2-2	42%
8-Mile	1-1 & 1-2	79%
	2-1 & 2-2	50%
	3-1 & 3-2	27%
	4-1 & 4-2	51%
	5-1 & 5-2	39%
	6-1 & 6-2	22%
	7-1 & 7-2	100%
Average		51%

The average applied shear stress on the 8-Mile Channel banks varied between 0.06 - 1.2 Pa and between 0.18-2.6 Pa at the toe of the bank. Stations 2-1 and 1-1 contained a high amount of cohesive material with higher measured critical shears stress (Table 5-1) among other parts of the channel which is in agreement with the observed historical bank

loss (Figure 5-5a, b). The highest amount of erosion happened at stations 1-2, 4-1, and 7-1 (Figure 5-a, d, g). Station 1-2 contained 65% clay but had a critical shear stress of 1.6 Pa and the highest measured k_d of 8.67 mm/(Pa.h). Station 4-1 contained non-cohesive fine sand that was highly susceptible to fluvial erosion. Station 7-1 and the bed at this location contained a high amount of silt material with a very low critical shear stress (0.3 Pa) and also had the most deformation (i.e., Net change in cross sectional shape) amongst all monitored sites both in the form of deposition and erosion. Due to a very low level of TSS in the channel, the source of the deposited material is likely Playgreen Lake since station 7 is very close to the channel entrance. Moreover, those sites that contained organic and peat material were relatively resistant to fluvial erosion processes. The measured contribution of the upper part of the bank to the total erosion was significant; especially considering the low total applied shear stress over the upper part of the bank which indicates that seasonal freeze-thaw increased erodibility of the bank. Also, the highest amount of erosion of the channel banks was at stations 1 and 7, where station 1 had high clay content and station 7 had high silt content; therefore it can be concluded that fine soil homogeneity can increase susceptibility of the soil to seasonal freeze-thaw. The 8-Mile channel bed experienced a higher amount of applied shear stress than the channel banks; hence the channel bed eroded continuously at a rate of approximately 5 cm each year. Moreover, historical erosion (Figure 5-5) and bed material distribution (fine sand and silty material upstream and cohesive clay material downstream) indicated that the upstream of the channel was more susceptible to fluvial erosion; therefore, the channel slope decreases gradually. This erosion pattern would impact the performance of the 8-Mile Channel and potentially affect the flow through the channel; thereby, further

consideration and historical monitoring would be helpful to record slope changes along the channel.

5.5 *Conclusions*

Very important regional and general results have been obtained from this study:

1) Historical bathymetric measurements complemented with soil sampling and erosion rate tests can provide the baseline information necessary to understand channel bank morphodynamics. The short term measurements in this study helped to understand the current properties of the channel bank material and comparing short and long term measurements showed that factors other than applied shear stress had significant effects on bank.

2) Seasonal freeze-thaw dramatically increased the erodibility of the upper part of the banks and had significant impact on the channel banks that had high amount of clay and silt material.

3) Wave action had significant effect on the total applied shear stress within 2-Mile Channel when the flow rate was low and could be a dominant eroding agent during the low flow events. At high flows the impacts of wave action were much less important.

4) Several equations and graphs were obtained to estimate applied shear stress within the study areas that will be beneficial for Manitoba Hydro for further protection and design purposes. This same methodology is transferrable to other stakeholders near waterways to help better understand and quantify cohesive riverbank erosion processes.

5.6 *References*

Amos C.L., Feeney T., Sutherland T.F., and Luternauer J.L. 1997, The stability of fine-grained sediment from the Frase River Delta. Estuarine, coastal and shelf science, **45**: 507-524.

Arulanandan, K., Gillogley, E. & Tully, R., 1980. Development of a quantitative method to predict critical shear stress and rate of erosion of natural undisturbed cohesive soils, Vicksburg: U.S. Army Corps of Eng., Waterways Exp. Station.

ASTM standard D422-63. 2007. Standard Test Method for Particle-Size Analysis of Soils. ASTM International, West Conshohocken, PA.

ASTM standard D2487-11. 2011. Standard practice for classification of soils for engineering purposes (unified soil classification system). ASTM International, West Conshohocken, PA.

ASTM standard D3977-97. 2013. Standard test methods for determining sediment concentration in water samples. ASTM International, West Conshohocken, PA.

Bijeljanin, M., 2013. Application of CRISSP-2D finite element modelling in predicting ice formation processes upstream of the Jenpeg Generating Station. M.Sc. thesis, University of Manitoba, Winnipeg, MB.

Briaud, J. L., Ting, F., Chen, H. C., Cao, Y., Han, S.-W., and Kwak, K. 2001. Erosion Function Apparatus for Scour Rate Predictions. Journal of Geotechnical and Geoenvironmental Engineering., **127(2)**: 105–113.

Budhu, M., 2011. Soil mechanics and foundations. 3rd ed. John Wiely & Sons, Inc., New York, NY.

Carlson E.J. and Enger P.F. 1962, Studies of tractive forces of cohesive soils in earth canals. US Department of the Interior Bureau of Reclamation, Denver, USA, Report N0. Hyd-504.

Couper, P. R. & Maddock A. P. 2001. Subaerial river bank erosion processes and their interaction with other bank erosion mechanisms on the river arrow, warwickshire, uk. Earth Surface Processes and Landforms, **26**: 631-646.

Couper, P., 2003. Effects of silt-clay content on the susceptibility of river banks to subaerial erosion. Geomorphology, 56: 95-108.

Environment Canada, 2015. Weather.gc.ca. Available at: http://climate.weather.gc.ca/climate_normals/results_1981_2010_e.html?stnID=3868&lang=e&StationName=norway+house&SearchType=Contains&stnNameSubmit=go&dCode=4&dispBack=1

Darby, S. E., and Thorne, C. R., 1996. Numerical simulation of widening and bed deformation of straight sand-bed rivers. I: model development. Journal of Hydraulic Engineering, **122**: 184-193.

Darby, S. E., Throne, C. R., and Simon, A., 1996. Numerical simulation of widening and bed deformation of straight sand-bed rivers. II: model evaluation. Journal of Hydraulic Engineering, **122**: 194-202.

Darby, S. E., Rinaldi, M., and Dapporto, S., 2007. Coupled simulations of fluvial erosion and mass wasting for cohesive river banks. Journal of Geophysical Research, **112**: 1-15.

Debnath, K., and Chaudhuri, S., 2010. Cohesive sediment threshold: a review. ISH

Journal of Hydraulic Engineering, **16(1)**: 36-56.

DHI, 2012a. MIKE Nearshore Spectral Wind-Wave Module scientific documentation. P.1-2, DHI Group.

DHI, 2012b. MIKE 21 & MIKE 3 Flow Model FM Hydrodynamic and Transport Module scientific documentation. P.1, DHI Group.

DHI, 2012c. MIKE 21 & MIKE 3 Flow Model FM Mud Transport Module scientific documentation. P.27-28, DHI Group.

DHI, 2012d. MIKE 21 & 3 FLOW Model FM Hydrodynamic and transport module scientific documentation. P. 17: DHI Group.

Dunn I. S. 1959, Tractive resistance of cohesive channels. Journal of Soil Mechanics and Foundations, **85**: 1-24.

Edwards, L., Burney, J. R. & Frame, P. A., 1995. Rill sediment transport on a prince Edward Island (Canada) fine sandy loam. Soil Technology, **8**: 127-138.

Farouki, O. T., 1985. Ground Thermal Properties. ASCE, New York, NW.

Formanek, G., McCool, D. & Papendick, R., 1984. Freeze-thaw and consolidation effects on strength. Transactions of the ASAE, **27(6)**: 1749-1752.

Gill, D. G., 1973. Morphology of the 8-Mile Channel Lake Winnipeg Regulation. M.Sc. thesis, Winnipeg: University of Manitoba.

Hanson G.J. and Simon A. 2001, Erodibility of cohesive streambed in the loess area of the midwestern USA. Hydrological Processes, **15**: 23-38.

Hooke, J. m., 1979. An analysis of the processes of river bank erosion. Journal of Hydrology, **42**: 39-62.

Huang J., Hilldale R.C., and Greimann B.P. 2006, Cohesive sediment transport. Erosion and sedimentation manual, Chapter 4, US Department of the Interior Bureau Reclamation.

Kimiaghalam, N., Goharrokhi, M., Clark, S. and Ahmari, H., 2015a. A comprehensive fluvial geomorphology study of riverbank erosion on the Red River in Winnipeg, Manitoba, Canada. Journal of Hydrology, **529(3)**: 1488-1498. Doi: 10.1016/j.jhydrol.2015.08.033.

Kimiaghalam, N., Clark, S. and Ahmari, H., 2015b. An experimental study on the effects of physical, mechanical, and electrochemical properties of natural cohesive soils on critical shear stress and erosion rate. International Journal of Sediment Research, Doi: 10.1016/j.ijsrc.2015.01.001.

Kimiaghalam, N., Goharrokhi, and M., Clark, S., 2015c. Estimating cohesive sediment erosion and deposition rates in wide rivers. Canadian Journal of Civil Engineering, **43(2)**: 164-172. Doi: 10.1139/cjce-2015-0361.

Manitoba Hydro, 2010. Lake Winnipeg regulation project; assessment of 2-Mile & 8-Mile channel surveys, Winnipeg, MB.

Meng X.M., Jia Y.G., Shan H.X., Yang Z.N. and Zheng J.W. 2012, An experimental study on erodibility of intertidal sediments in the Yellow River delta, International Journal of Sediment Research, **27**: 240-249.

Mitchener H, and Torfs H. 1996, Erosion of mud/sand mixtures. Coastal Engineering, **29**: 1-25.

Mostafa T.S., Imran J., Chaudhry M.H. and Khan I.B. 2008, Erosion resistance of cohesive soils. Journal of Hydraulics Research, **46(6)**: 777-787.

Otsubo K,and Muraoka K. 1988, Critical shear stress of cohesive bottom sediments. Journal of Hydraulics Engineering, **114(10)**: 1241-1256.

Owen, M.W. 1975. Erosion of Avonmouthmud. Report No. INT150. Wallingford, UK: Hydraulic Research Station.

Lawler, D.M., 1993. Needle ice processes and sediment mobilization on river banks — the River Ilston, West-Glamorgan, UK. Journal of Hydrology, **150**: 81–114.

Lawler, D.M., Thorne, C.R., Hooke, J.M., 1997. Bank erosion and instability. In: Thorne, C.R., Hey, R.D., Newson, M.D. (Eds.), Applied Fluvial Geomorphology for River Engineering and Management. John Wiley & Sons, New York, pp. 137–172.

Lawler D. M., Grove J.R., Couperthwaite J.S., & Leeks G. J. L. 1999. Downstream change in river bank erosion rates in the Swale–Ouse system, northern England. Hydrological Processes, **13**: 977–992.

Leonard L. and Richard G. 2004, Estimation of runoff critical shear stress for soil erosion from soil shear strength, Catena, **57**: 233-249.

Luppi, L., Rinaldi, M., Teruggi, L. B., Darby, S. E., and Nardi, L., 2008. Monitoring and numerical modelling of riverbank erosion processes: a case study along the Cecina River (central Italy). Earth Surface Processes and Landforms, **34(4)**: 530-546.

Partheniades, E., 1965. Erosion and deposition of cohesive soils. Journal of Hydraulics

Engineering, **91(1)**: 105-138.

Smerdon E.T., and Beasley R.P. 1961, Critical tractive forces in cohesive soils. Agricultural Engineering, **42**: pp. 26-29.

Thorn M.F.C, and Parsons J.G. 1980, Erosion of cohesive sediments in estuaries: an engineering guide. Proc 3rd International Symposium on Dredging Technology. Bedford: BHRA, 349-358.

Thorne, C.R., 1982. Processes and mechanisms for river bank erosion.In: Hey, R.D., Bathurst, J.C., Thorne, C.R. (Eds.), Gravel-Bed Rivers: Fluvial Processes, Engineering, and Management. John Wiley & Sons, New York, pp. 227–259.

Van Klaveren, and R. W., 1987. Hydraulic erosion resistance of thawing soil. PhD dissertation. Washington State University.

Van Klaveren, R. and McCool, D., 1998. Erodibility and critical shear of a previously frozen soil. Transactions of the ASAE, **41(5)**: 1315-1321.

Winterwerp, J. C. and Van Kesteren, W. G., 2004. Introduction to the Physics of Cohesive Sediment in the Marine Environment. Elsevier, Amsterdam.

Wynn, T. M., Henderson, M. B., and Vaughan, D. H. 2008. Change in streambank erodibility and critical shear stress due to subaerial processes along a headwater stream, southwestern Virginia, USA. Geomorphology, **97**: 260-273.

Yumoto, M., Ogata, T., Matsuoka, N., and Matsumoto , E. 2006. Riverbank freeze–thaw erosion along a small mountain stream, Nikko Volcanic Area, Central Japan. Permafrost and Periglacial Processes, **17**: 325–339.

CHAPTER 6: CONCLUSIONS AND RECOMMENDATIONS

6.1 *Conclusions*

This field, experimental, and numerical study evaluated the effects of applied shear stress on the erodibility of cohesive riverbanks. The effects of seasonal freeze-thaw as one of the major subaerial processes affecting erodibility were also evaluated in this study. A new methodology was suggested to improve measurement of erosion and deposition rate in wide rivers. Empirical equations were presented to predict the erodibility parameters and applied shear stress within the study areas in Manitoba.

This thesis focused more on the practical aspects of fluvial geomorphology by providing simplified results in the form of convenient equations and graphs, thereby simplifying these complicated processes into useful and understandable methodologies. For example, for the Red River study area which is a wide meandering stream, the 2-D Navier-Stokes equations with a horizontal turbulence model were used to develop the hydrodynamic model of the river rather than using a time consuming 3-D model to completely model

the effect of secondary flows, in particular, helical flow within and downstream of channel bends. Several velocity profile measurements within the Red River bends showed that there was a good agreement between the 2-D model results and measurements, in particular, measured and simulated applied shear stress distribution.

Each chapter includes regional and general useful information to quantify the effect of applied shear stress on geomorphological changes within open channels. The second chapter discussed the effects of several soil properties on the erodibility parameters within the study areas that help the readers to understand the complicated behavior of cohesive riverbanks in general and also, to gain a better understanding the study areas soil and sediment behavior. The third chapter focused on fluvial processes within the Red River to understand the river hydrodynamic conditions, local soil erodibility parameters at several locations, and the effect of subaerial processes on this complicated phenomenon. Although this chapter includes regional results for the Red River, it also suggests a general methodology to perform a fluvial geomorphological assessment on any river. Moreover, for the first time a methodology has been suggested to quantitatively include the effects of freeze-thaw into erosion predictions. Findings from the second chapter can be combined with the results of this chapter to understand the Red River soil samples behavior under different hydrodynamic conditions and severe freeze-thaw. For example based on the result of the erodibility test, it was found that local, site specific erosion can be initiated when the Red River flow rate exceeds $600 m^3/s$. The fourth chapter presented a general new methodology to estimate net erosion-deposition for an entire study area rather than a local area (local scour) that is useful to look at a water body as a more general and broad picture. For instance, despite having local erosion at

some sites within the Red River study area when flow rate exceeds 600m^3/s, net deposition may be the overall dominant fluvial process for even higher flow rates (>600m^3/s) when considering the entire study area. The exact flow rate that causes net erosion throughout the entire study section on the Red River will depend on the flow rate as well as the sediment budget. The necessity of this methodology becomes more understandable when one looks at the complex behavior of the Red River morphodynamic conditions through reading the previous chapters. The last chapter includes a regional study on two important diversion channels in Manitoba with complicated hydrodynamic conditions. Findings from the previous chapters were used to quantify morphodynamic conditions of these two diversion channels. This chapter highlighted the role of the historical bathymetric measurements and possible wave action within an open channel. Moreover, this chapter includes very important regional information for practical purposes such as estimating applied shear stress distribution over time and space and gives an idea about the channel's erodibility characteristics. The major contributions of this research are listed below, followed by recommendations.

6.1.1 *Effects of Soil Properties on the Erodibility Parameters*

The primary step for this study was to understand the effects of several cohesive soil properties on critical shear stress and erosion rate within the study areas. Thirteen main soil properties were selected and measured to evaluate and find the most significant parameters on the erodibility.

1. Statistical analysis showed that cohesive soil cohesion (*C*) had a strong linear correlation with critical shear stress. This result concluded that in-situ conditions

can alter the soil erodibility since cohesion is highly impacted by in-situ conditions such as stress history and subaerial processes.

2. The study showed that previous suggested equations in the literature cannot be used to estimate critical shear stress and erosion rate of cohesive riverbanks within the study areas.
3. Statistical analysis showed that the material independent coefficient (k_d) had a strong correlation with SAR. Despite several previous studies, k_d was not found to have a strong correlation with the other soil properties.
4. Empirical equations were suggested to estimate critical shear stress and erosion rate of the cohesive riverbanks within the study areas. These equations can reduce the cost and time of the erodibility tests. Also, average measured critical shear stress and erosion rate can be used for design and further research.

6.1.2 *Effects of Seasonal Freeze-Thaw on the Erodibility*

Another major contribution of this study was to examine the effects of seasonal freeze-thaw on the erodibility parameters and also present a methodology to include this process into riverbank erosion studies:

1. Experiments showed that seasonal freeze-thaw had a significant impact on critical shear stress.
2. The first freeze-thaw cycle could reduce the critical shear stress up to 80% while after the first cycle the reductions were moderate.
3. Critical shear stress was not affected by the frost temperature and only the number of freeze-thaw cycle had a dominant impact on critical shear stress.

4. Direct shear test results showed that seasonal freeze-thaw could reduce the soil cohesion to zero after the fifth cycle; therefore, the study results suggest that one could neglect the cohesion in riverbank stability analysis within the study areas. Also, soil friction angle was not impacted by the freeze-thaw processes.
5. A thermal numerical model was used to estimate the number of freeze-thaw cycle and thickness of the impacted soil layer by the seasonal freeze-thaw. This was the first study that suggested a methodology to quantitatively contribute the effects of freeze-thaw in the fluvial geomorphology analysis.
6. Field observations and numerical modelling showed that the seasonal freeze-thaw as a subaerial process can be a dominant eroding agent in low gradient rivers such as the Red River in Winnipeg.

6.1.3 *Estimating Erosion and Deposition Rate using In-Situ Measurements*

Field observations and measurements showed that in low gradient rivers such as the Red River, the deposition process can be as important as erosion. Moreover, the available devices and methods are not reliable to estimate both erosion and deposition rate for a major study area. Therefore, a novel methodology was proposed based on ADCP measurements, water sampling, and numerical modelling to estimate both erosion and deposition rate in wide rivers.

1. An equation was suggested to estimate the Red River streamwise dispersion coefficient as a function of the river discharge. This result is beneficial for future research and design purposes.

2. Red River in Winnipeg was used as a case study to test the methodology and it was found that the deposition rate is not only a function of applied shear stress but it is a function of both sediment concentration and discharge.
3. Deposition was the common process through the Red River based on the result of the methodology as well as field measurements.

6.1.4 *Estimating Applied Shear Stress within Study Areas*

Hydrodynamic numerical models were developed based on extensive field measurements and using available record of flow within the study areas. Valuable results were obtained during the modelling process.

1. Average Manning number and bed roughness were found for each study area that can be useful for engineering design and future research.
4. Simple equations and graphs were suggested to estimate average applied shear stress within the study areas as a function of river discharge or water surface elevation.
5. Frequency analysis was conducted on historical flow records to understand occurrence probability of each shear stress range over time and space.
6. Wave action due to the adjacent lakes can be a major portion of the total applied shear stress under low flow rates within channels. Also, this effect can be more significant at the entrance of the channels.

6.2 *Recommendations*

This research showed that the subaerial processes can be a dominant factor that can dramatically reduce riverbank resistance against fluvial erosion. Effects of seasonal

freeze-thaw were studied in this project; however, wetting-drying processes can have significant effects on erodibility of the riverbanks, in particular, through the Red River due to a high water level variation. Therefore, my first recommendation for future research is to investigate the effects of wetting-drying on the erodibility parameters. This can be done by designing similar experimental setup that I presented in this study.

This research was done on fully saturated soil samples that were taken close to the water level. Also, all tests were conducted on saturated soil samples. My second recommendation for future work is to investigate the effect of natural water content on unsaturated soil samples erodibility parameters.

To better understand geomorphological changes along natural streams such as the Red River, fluvial processes, geotechnical failure, and underground processes such as seepage erosion must be coupled together. Hence, my third recommendation is to investigate the possibility of developing a comprehensive geomorphological model to include all these processes into one package.